SPACE RESEARCH IN SLOVAKIA

2020 – 2021

SLOVAK ACADEMY OF SCIENCES

COSPAR

SLOVAK NATIONAL COMMITTEE

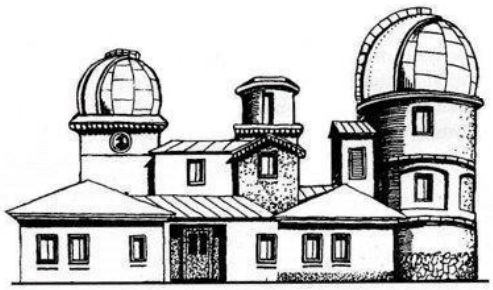

Slovak Central Observatory Hurbanovo

APRIL 2022

Slovak Central Observatory, Hurbanovo, April 2022
Editors: Ivan Dorotovič and Ján Feranec
ISBN: 978-80-89998-24-1

CONTENTS

1. EXPERIMENTS FOR MEASUREMENTS IN SPACE 5
   J. Baláž, I. Strhárský, Š. Mackovjak, M. Musilová

2. SPACE PHYSICS, GEOPHYSICS AND ASTRONOMY..... 13
   J. Baláž, P. Bobík, I. Dorotovič, L. Kornoš, Š. Mackovjak, M. Revallo, J. Rybák, J. Šilha, J. Tóth

3. LIFE SCIENCES 35
   M. Musilová

4. MATERIAL RESEARCH IN SPACE 39
   J. Lapin

5. REMOTE SENSING..... 41
   Ľ. Balažovič, I. Barka, T. Bucha, J. Feranec, Z. Fulmeková, M. Gallay, T. Goga, J. Hofierka, M. Kopecká, K. Onačilová, P. Pastorek, R. Pazúr, M. Rusnák, I. Sačkov, M. Sedliak, M. Sviček, D. Szatmári, A. Zverková

6. SPACE METEOROLOGY..... 67
   J. Kaňák, Ľ. Okon, L. Méri, M. Jurašek

7. INSTITUTIONS PARTICIPATING IN SPACE RESEARCH IN SLOVAKIA. NATIONAL COMMITTEE OF COSPAR 79

1. EXPERIMENTS FOR MEASUREMENTS IN SPACE

J. Baláž, I. Strhárský, Š. Mackovjak

Experiment SERENA/PICAM on mission ESA-BepiColombo

IEP SAS contributed to ESA-BepiColombo mission to planet Mercury in the frame of scientific-technical collaboration with Space Technology Ireland (*STIL*) and Institute for Space Research of Austrian Academy of Sciences (*IWF-ÖAW*). The delivery involved the mechanical structures of the PICAM (*Planetary Ion Camera*) an ion mass spectrometer, that were manufactured in Slovakia (mechanical stress simulations and mechanical components manufacture on 5-axis centre of Q-Products, Bratislava, space-qualified processing and integration and testing at IEP-SAS, Košice).

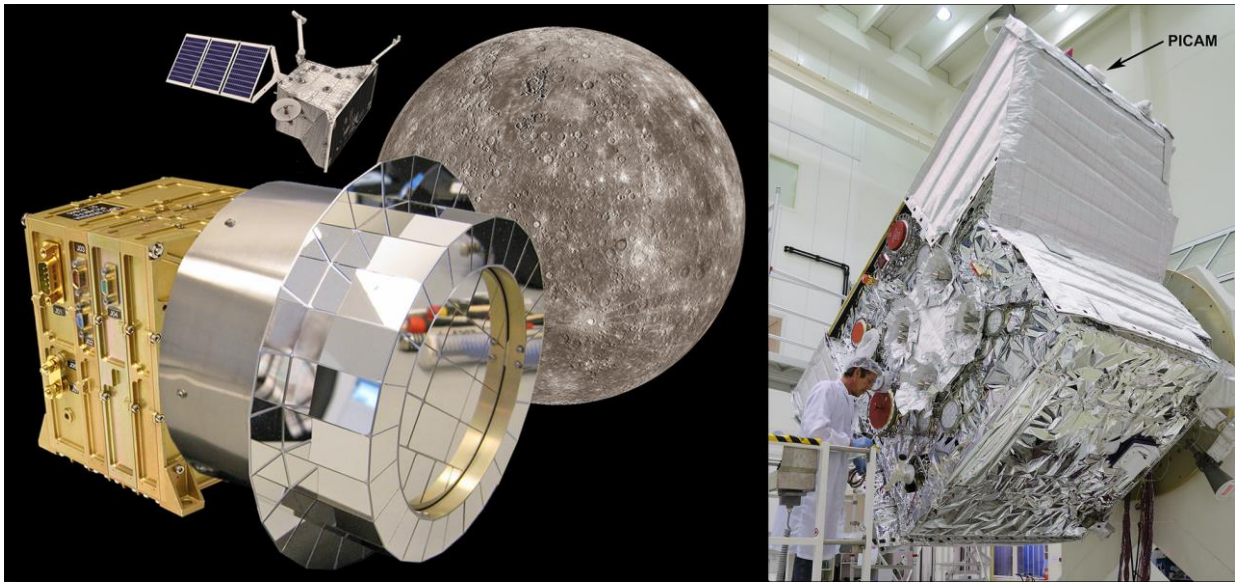

Figure 1.1. *SERENA / PICAM and Mercury planetary orbiter (MPO) of BepiColombo mission.*

PICAM is a part of a complex space science suite SERENA (*Search for Exospheric Refilling and Emitted Natural Abundances*) for particle detection at planet Mercury. The detailed description of SERENA, its scientific background and objectives are provided in [1] and [2].

Launch of the mission was on 20-OCT-2018 and the space probe is progressing to Mercury in good health. Up to date, four gravitational assistances were performed: Earth on 13-APR-2020, Venus on 16-OCT-2020, Venus on 11-AUG-2021 and Mercury on 1-OCT-2021. The arrival to Mercury is scheduled in December 2025.

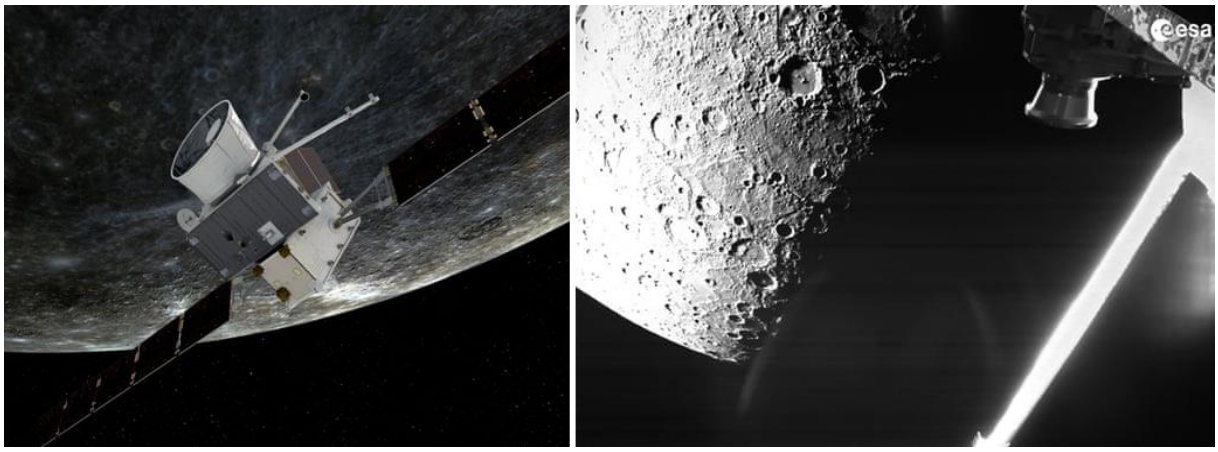

Figure 1.2. *(Left) BepiColombo at Mercury / artist view. (Right) BepiColombo at Mercury on 1-OCT-2021 at 23:41:12 UTC – a real record by camera of the BC transfer module.*

The first results from the Mercury flyby on 1-OCT-2021 (Orsini et al.) *First observations of Mercury's inner southern magnetosphere by BepiColombo/SERENA ion sensors*) is presently submitted for publication.

Experiment PEP/JDC for mission ESA-JUICE

Experiment PEP (*Particle Environment Package*) will provide comprehensive detection and analysis of the plasma and particle environment in the system of planet Jupiter and its Galilean moons Europa, Calisto and Ganymede. PEP will measure density and flux of positive and negative ions, electrons, exospheric neutral gas, thermal plasma and energetic neutral atoms in the energy range from <0.001 eV to >1 MeV with full angular coverage. The PEP suite includes six sensors (JDC, JEI, JoEE, NIM, JNA and JENI) that are under development at several EU and US institutions led by Swedish Institute for Space Physics (IRF, P.I. prof. S. Barabash). Based on invitation from IRF, the IEP-SAS contributes to development and construction of anti-coincidence particle detection system for JDC sensor (*Jovian plasma Dynamics and Composition*) of the PEP suite. The anti-coincidence system will improve the plasma particles detection efficiency on the background of penetrating electron radiation from Jovian radiation belts. The system consists from silicon solid state detector (SSD) and dedicated processing electronic unit (ANU).

The JUICE mission including the PEP science suite details is described in [3], the JDC sensor is in details described in [4].

The participation of IEP SAS to JUICE mission is supported by Slovak PECS (*Plan for European Cooperating States*) project named: *"Slovak contribution to ESA-JUICE mission: Development of Anti-Coincidence Module ACM for Particle Environment Package PEP".*

The ACM/EM (engineering model), ACM/FM (flight model) and ACM/FS (flight spare model) were built from the space-qualified components, calibrated by mono-energetic particles, environmentally tested at IEP SAS Kosice and delivered to IRF Kiruna for integration to respective PEP/JDC systems. The PEP/JDC unit with ACM integrated is already installed on the board of the JUICE probe.

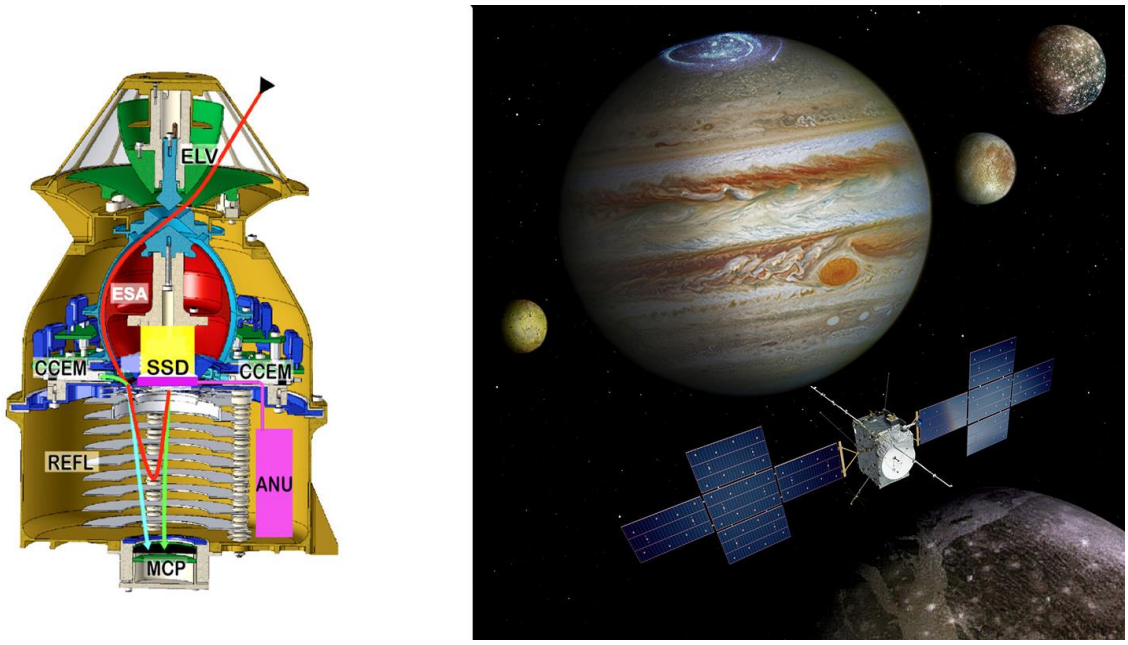

Figure 1.3. *(Left) JDC sensor of the PEP science suite with the ACM, consisting of solid state detector SSD and analog electronic unit ANU. (Right) JUICE spacecraft orbiting in the system of Jupiter and its Galilean moons.*

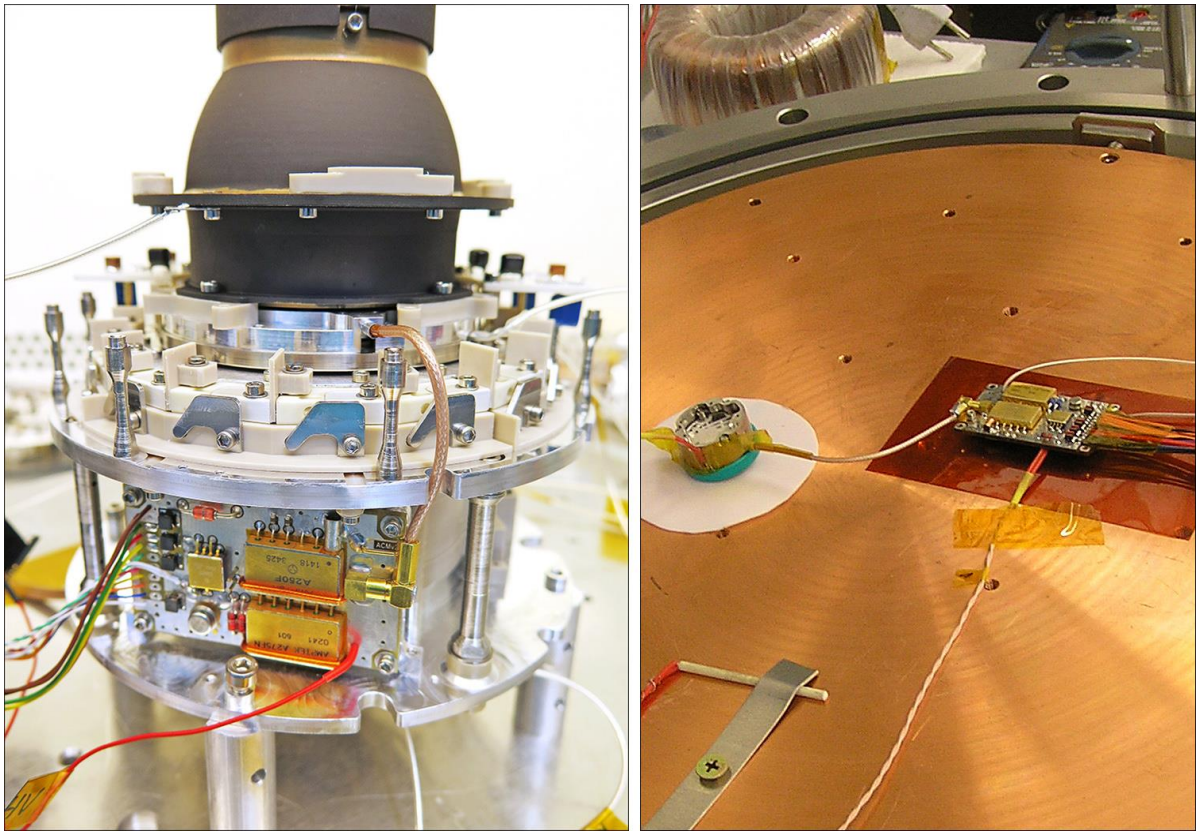

Figure 1.4. *(Left) ACM subsystem on integration to JDC at IRF Kiruna. (Right) ACM under thermal-vacuum test in SPACEVAC space environment simulator at IEP-SAS Košice.*

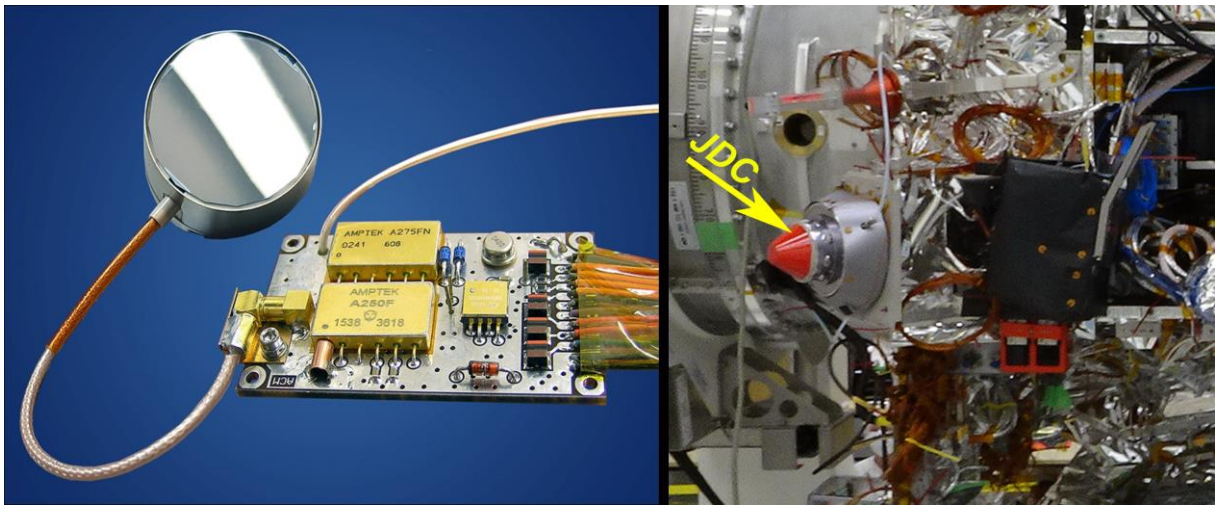

Figure 1.5. *(Left) ACM consisting of solid state detector and signal processing electronic unit. (Right) PEP/JDC unit with integrated ACM on board of JUICE spacecraft.*

Experiment JEM-EUSO

The activities related to international collaboration JEM-EUSO (*Joint Experiment Missions for Extreme Universe Space Observatory*) consist of the contribution to the missions within the NASA program. The results of the theoretical studies dedicated to the natural UV radiation of the night-time Earth's atmosphere has been utilized in data analysis from stratospheric mission EUSO-SPB1 [5] and in preparatory activities of space-based mission POEMMA (*Probe of Extreme Multi-Messenger Astrophysics*, [6]). The participation on mission EUSO-SPB2 (*Super-Pressure Balloon*), with a planned launch in Q2/2023, consists of the design, development, construction and environmental qualifications of the photo-detectors prepared according to the requirements of the mission's principal investigator. Specifically, the hardware and software of four EMON (Euso MONitor) instruments have been prepared. The EMONs will control light conditions inside the EUSO telescopes (Cherenkov and Fluorescence) and so it will protect the main detectors from the harmful intensive light. Thanks to EMON's high sensitivity, effective operation, and low demands it should overcome problems reported during the previous mission EUSO-SPB1.

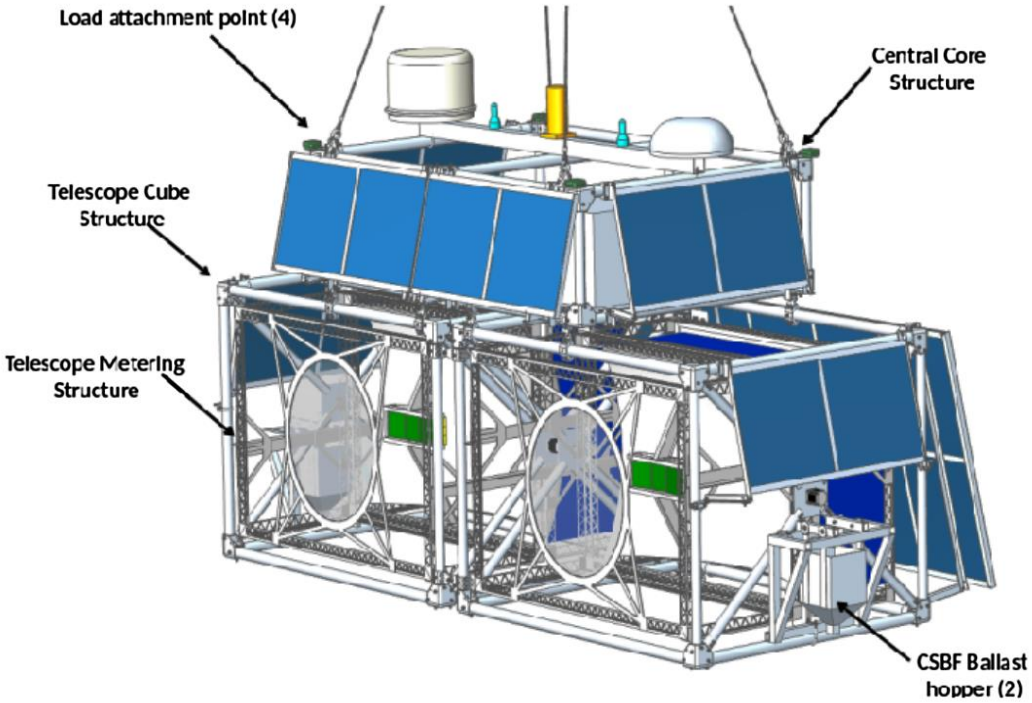

Figure 1.6. *Gondola of the NASA-SPB2 mission.*

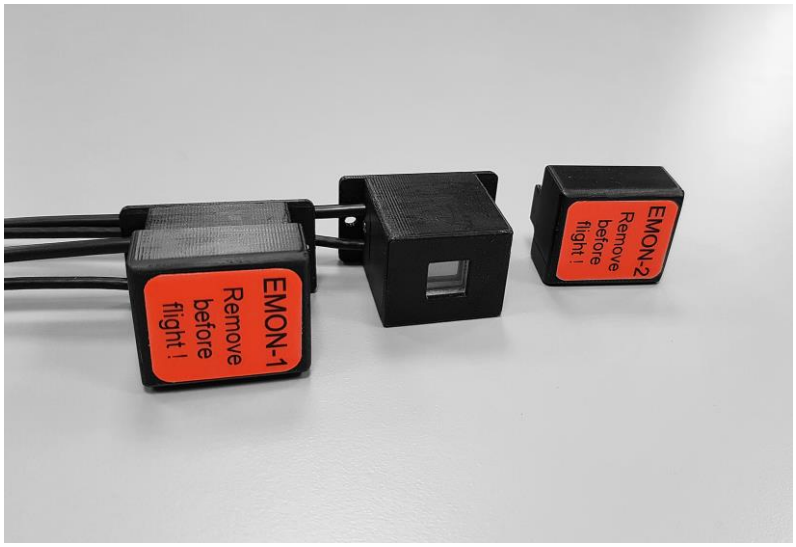

Figure 1.7. *A pair of the EMON photo-detectors developed at IEP SAS for NASA-SPB2 mission.*

Information regarding the CubeSat gamma-ray measurements and the SchoolSat project

The long duration GRB 210807A (Swift-BAT detection; [7]) was detected by the GRBAlpha 1U CubeSat ([8]). This is the first time that a GRB was observed by a 1U CubeSat dedicated to gamma-ray burst observations. The data acquisition started at 10:05:14 UT and the tail part of the prompt emission, which consists of multiple peaks, was observed with a duration of about 80 sec. The 7.3 sigma detection significance was confirmed at around 10:06:00 UT. The light curve obtained by GRBAlpha is available here:
https://grbalpha.konkoly.hu/static/share/GRB210807A.pdf

GRBAlpha is a demonstration mission for a future CubeSats constellation ([9]). The detector of GRBAlpha consists of a 75 x 75 x 5 mm3 CsI scintillator read out by a SiPM array, covering the energy range from ~50 keV to ~1000 keV. GRBAlpha was launched on 2021 March 22 from Baikonur. After its commissioning phase, the scientific observations are now under way. To increase the duty cycle and the downlink rate, the upgrade of the on-board data acquisition software stack is in progress. The ground segment is also supported by the radio amateur community and it takes advantage of the SatNOGS network for increased data downlink volume; https://gcn.gsfc.nasa.gov/gcn3/30624.gcn3,
https://www.om3ksi.sk/en/2021/03/17/grbalpha-mission-basic-facts/

In 2021, SOSA (Slovak Organisation for Space Activities) began the development of the educational platform SchoolSAT, on which it cooperated together with the Hungarian Astronautical Society and the Valašské Meziříčí Observatory with the financial support of the Visegrad Fund. The result is a functional model of a cubesat satellite measuring 10x10x10cm, which teaches students the basics of soldering and mechanical composition of a small satellite and work from preparation, assembly to data collection. It also gives them real experience with space hardware, while SchoolSAT is fully open to its own development of programs, electronics and entire experiments. This project attracted the attention of secondary and higher education institutions in Slovakia, Hungary and the Czech Republic, and more than 700 students took part in related presentation workshops; http://sosa.sk/sk/projekty/projekty-schoolsat/

References:

[1] ORSINI, S. - LIVI, S. - ... - BALAZ, J. - KUDELA, K., et al.: SERENA: A suite of four instruments (ELENA, STROFIO, PICAM and MIPA) on board BepiColombo-MPO for particle detection in the Hermean environment. Planetary and Space Science 58 (2010), 166-181, https://doi.org/10.1016/j.pss.2008.09.012

[2] ORSINI, S. - LIVI, S - ... - BALAZ, J., et al.: SERENA: Particle Instrument Suite for Determining the Sun-Mercury Interaction from BepiColombo. Space Sci Rev (2021) 217:11, https://doi.org/10.1007/s11214-020-00787-3

[3] JUICE, JUpiter ICy moons Explorer, Exploring the emergence of habitable worlds around gas giants. ESA/SRE(2014)1. September 2014.
https://sci.esa.int/documents/33960/35865/1567260128466-JUICE_Red_Book_i1.0.pdf

[4] STUDE, J.: Advanced Plasma Analyzer for Measurements in the Magnetosphere of Jupiter. Doctoral Thesis. Swedish Institute of Space Physics and Umeå University, 2016. https://www.diva-portal.org/smash/get/diva2:926416/FULLTEXT01.pdf

[5] ADAMS, J.H. - ALLEN, L. - ... - MACKOVJAK, Š., et al.: 2021, Extreme Universe Space Observatory on a Super Pressure Balloon 1 calibration: from the laboratory to the desert, Experimental Astronomy, 52, 125 https://doi.org/10.1007/s10686-020-09689-2

[6] OLINTO, A.V. - KRIZMANIC, J.F. - ... - MACKOVJAK, Š., et al.: 2021, The POEMMA (Probe of Extreme Multi-Messenger Astrophysics) observatory, Journal of Cosmology and Astroparticle Physics, 06, 007, 66 https://doi.org/10.1088/1475-7516/2021/06/007

[7] LIEN, A.Y. - GRONWALL, C. - GROPP, J.D. - KLINGER, N.J. - PAGE, K.L. - PALMER, D.M.: (2001) GRB 210807A: Swift detection of a burst with an optical counterpart. GCN CIRCULAR 30600.

[8] PÁL, A. - OHNO, M. - MÉSZÁROS, L. - WERNER, N. - RIPA, J. - FRAJT, M. - HIRADE, N. - HUDEC, J. - KAPUŠ, J. - KODELA, M. - LASZLO, R. - LIPOVSKÝ, P. - MATAKE, H. - ŠMELKO, M. - UCHIDA, N. - CSÁK, B. - ENOTO, T. - FREI, Z. - FUKAZAWA, Y. - GALGÓCZI, G. - HIROSE, K. HISADOMI, S. - ICHINOHE, Y. - KISS, L.L. - MIZUNO, T. - NAKAZAWA, K. - ODAKA, H. - TAKAHASHI, H. - TORIGOE, K.: (2020) GRBAlpha: a 1U CubeSat mission for validating timing-based gamma-ray burst localization. Proc. SPIE 11444, Space Telescopes and Instrumentation 2020: Ultraviolet to Gamma Ray, 114444V (13 December 2020); https://doi.org/10.1117/12.2561351

[9] WERNER, N. - ŘÍPA, J. - PÁL, A. - OHNO, M. - TARCAI, N. - TORIGOE, K. - TANAKA, K. - UCHIDA, N. - MÉSZÁROS, L. - GALGÓCZI, G. - FUKAZAWA, Y. - MIZUNO, T. - TAKAHASHI, H. - NAKAZAWA, K. - VÁRHEGYI, Z. - ENOTO, T. - ODAKA, H. - ICHINOHE, Y. - FREI, Z. - KISS, L.: (2018) CAMELOT: Cubesats Applied for MEasuring and LOcalising Transients mission overview. Society of Photo-Optical Instrumentation Engineers (SPIE) Conference Series 10699, 106992P.

2. SPACE PHYSICS, GEOPHYSICS AND ASTRONOMY

J. Baláž, P. Bobík, I. Dorotovič, L. Kornoš, Š. Mackovjak,
M. Revallo, J. Rybák, J. Šilha, J. Tóth

The Department of Space Physics, ***Institute of Experimental Physics, SAS, Košice*** (http://space.saske.sk) in collaboration with the laboratories in abroad continued studies of the dynamics of low energy cosmic rays (CR) and of suprathermal cosmic particles, as well as high energy cosmic rays based on measurements in space and on the ground.

In the field of cosmic ray (CR) modulation in the heliosphere, research was focused on the modulation of CR at very high energies of 50, 100, 150, and 200 GeV per 1 au. The results obtained by two independent numerical and one analytical method show that even at such high energies the modulation per 1 au is in the order of a few percent ([1]). Mentioned research is the application of AI method further developed and presented in [2] and other numerical methods developed at Institute of Experimental Physics SAS devoted to CR in heliosphere physics.

The actual space weather studies are focused on research by state-of-the-art machine learning techniques. They are mainly dedicated to the understanding of airglow variation in the thermosphere-ionosphere system. Data-driven modeling of atomic oxygen airglow over a period of three solar cycles has been presented in [3]. There was an assumption that this data-driven approach might be even more precise if new data, that are not commonly available, is involved. For this reason, the SCSS-Net has been developed. It is a model for solar corona structures segmentation based on deep neural networks ([4]) and it provides an automatic characterization of solar activity with high temporal and spatial resolution. The airglow can be affected also by the discharges in the lower atmosphere. Therefore methods for automatic detection of tweek atmospherics ([5]) and Transient Luminous Events ([6]) has been also developed.

References:

[1] BOBIK, P. – PUTIS, M. - KOLESNYK, Y.L. – SHAKHOV, B.A.: 2021, Estimation of the modulation level of cosmic rays at high energies, Monthly Notices of the Royal Astronomical Society 503, 3386–3393, doi: 10.1093/mnras/stab597

[2] KOLESNYK, Y. L. – SHAKHOV, B. A. – BOBIK, P. – PUTIS, M.: 2020, An exact solution of cosmic ray modulation problem in a stationary composite heliosphere model, Monthly Notices of the Royal Astronomical Society, Volume 491, Issue 4, p.5826-5842, doi: 10.1093/mnras/stz3343

[3] MACKOVJAK, Š. – VARGA, M. – HRIVŇÁK, S. – PALKOCI, O. – DIDEBULIDZE, G. G.: 2021, Data-Driven Modeling of Atomic Oxygen Airglow over a Period of Three Solar Cycles, JGR Space Physics, 126, 3 (https://doi.org/10.1029/2020JA028991)

[4] MACKOVJAK, Š. – HAMRAN, M. – MASLEJ-KREŠŇÁKOVÁ, V. – Butka, P.: 2021, SCSS-Net: Solar corona structures segmentation by deep learning, Monthly Notices of the Royal Astronomical Society, 508, 3, 3111-3124 (https://doi.org/10.1093/mnras/stab2536)

[5] MASLEJ-KREŠŇÁKOVÁ, V. – KUNDRÁT, A. – MACKOVJAK, Š. – BUTKA, P. – JAŠČUR, S. – KOLMAŠOVÁ, I. – SANTOLÍK, O.: 2021, Automatic detection of atmospherics and tweek atmospherics in radio spectrograms based on a deep learning approach, Earth and Space Science, 8, 11 (https://doi.org/10.1029/2021EA002007)

[6] AMRICH, S. – MACKOVJAK, Š. – STRHÁRSKÝ, I. – BALÁŽ, J. – HANČIKOVSKÝ, M.: 2021, Design and construction of hardware and software for autonomous observations of Transient Luminous Events, Journal of Instrumentation, 16, T12016 (https://doi.org/10.1088/1748-0221/16/12/T12016)

The ***Faculty of Mathematics, Physics and Informatics, Comenius University, Bratislava*** was involved in the following directions of research as listed below.

Meteor observations and analyses by AMOS global meteor network

In 2020-21 continued the monitoring of meteor activity above the Central Europe in Slovakia, Canary Islands, Atacama Desert in Chile, Hawaii and Australia by All-sky Meteor Orbit System (AMOS) and AMOS-Spec systems (Fig. 2.1.). AMOS systems work as autonomous intensified video observatory for detection of meteors and other transient events on the sky. Hardware and software of AMOS have been developed and constructed at Faculty of Mathematics, Physics and Informatics of Comenius University in Bratislava.

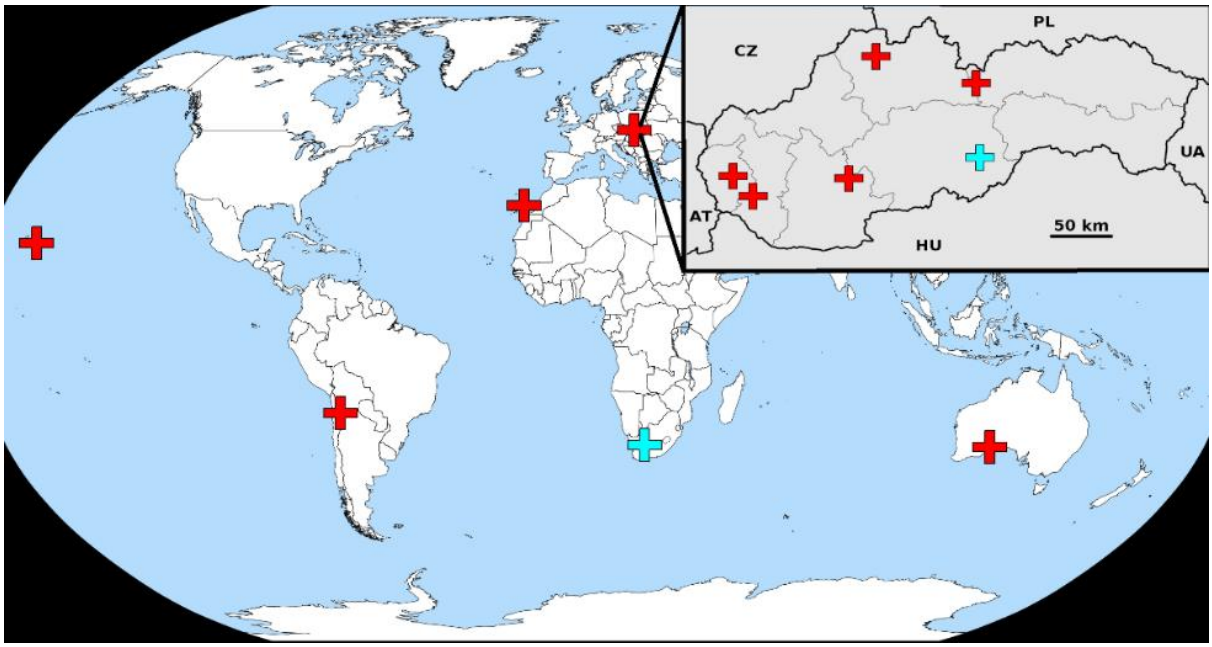

Figure 2.1. *AMOS global meteor network. Red crosses are active location (2-3 AMOS systems) and blue crosses are planned location in 2022.*

We have demonstrated the capability of the updated All-Sky Meteor Orbit System (AMOS and AMOS-Spec) to provide complex characterization of meteoroids. Spectral observations allow us to measure emission lines intensities of meteoric elements and thus provide compositional characterization even for minor meteoroid streams such as the June epsilon Ophiuchids ([1]). The meteoroid trajectories and pre-atmospheric orbits are independently measured from data collected by the AMOS network and combined with spectral data allows us to find links between meteoroids and their parent bodies, from both dynamical and physical side. In this case, we have presented analysis of 22 JEO meteors and provided comparison to other major streams based on the determined mean spectral classification reflecting different abundances of main compositional species (Fig. 2.2.).

We also lead an international ESA PECS project MetSpec focused on simulated ablation of meteorites in plasma wind tunnel of IRS University of Stuttgart, aimed to improve our methods for studying meteoroid composition from meteor spectra observations ([2]).

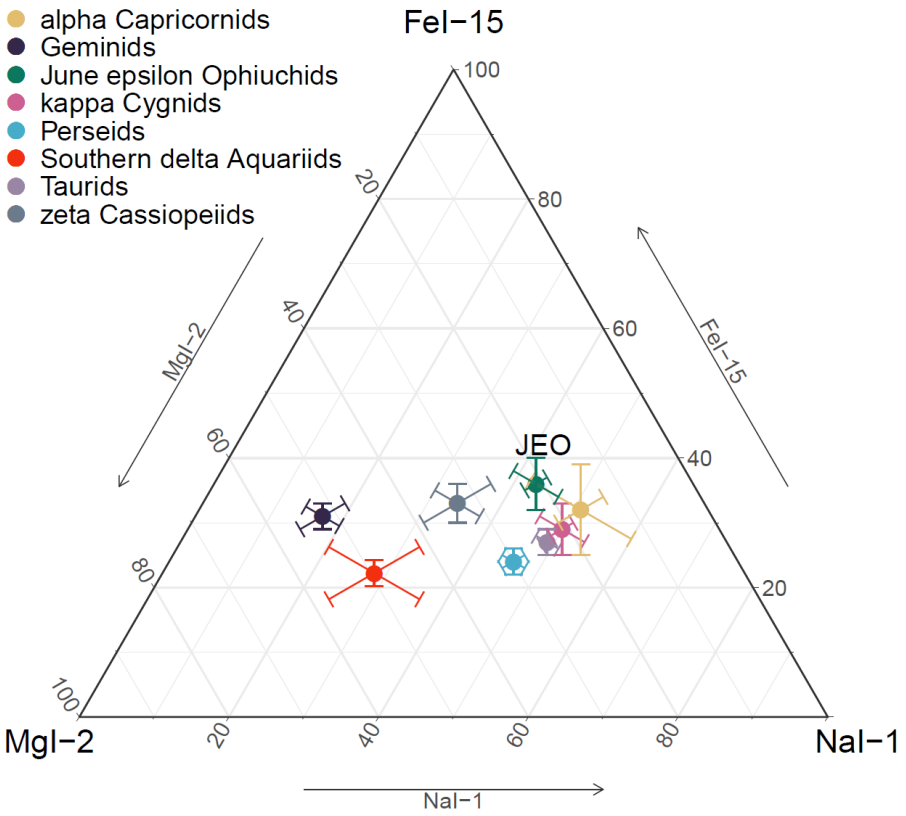

Figure 2.2. *Mean spectral classification (mean Na I/Mg I/Fe I intensity ratios and standard error of the mean) of JEO meteoroids and comparison to other major meteoroids streams from Matlovič et al. (2019).*

Photometric observations and research of asteroids using a 60-cm telescope

With our targeted long-term photometric observations of a number of asteroids of taxonomic type V, being located either in the Vesta family or outside it, at different phase angles and different geometric conditions, we determine along with rotation periods and amplitudes of the lightcurve also the values of the slope parameters and absolute magnitudes. In addition, for a part of the examined bodies we gradually obtain valuable material for determination of their approximate shape and sense of rotation. In 2020 and 2021 we significantly contributed to two papers published with colleagues from several observatories around the world.

In [3] we analyzed all available rotational periods for spectrally confirmed V-types, putative V-types, and Vesta family members and we found that the population of V-types outside the Vesta family shows a significant excess of fast rotators compared to the Vesta family. We hypothesized that the objects that evolved from the Vesta family though the Yarkovsky drift were also more susceptible to the YORP effect. We also showed for the first time that the spin barrier for the V-type asteroids exceeds the critical density of 2.0 g.cm^{-3}.

In [4] we presented well determined phase curves for 20 V-type asteroids for the first time. Their phase curve parameters are consistent with those for moderate and high albedo asteroids. In contrast to polarimetric studies we have not found substantial evidence for any clustering into distinct phase curve parameters groups yet, though one of studied objects showed different behavior than the rest.

Space debris photometry research with 70-cm telescope

The Faculty of Mathematics, Physics and Informatics of Comenius University in Bratislava, Slovakia (FMPI) operates its own 0.7-m Newtonian telescope (AGO70) dedicated to the space surveillance tracking and research, with an emphasis on space debris. The observation planning focuses on objects on geosynchronous (GEO), eccentric (GTO and Molniya) and global navigation satellite system (GNSS) orbits. To verify the system's capabilities, we conducted an observation campaign in 2017, 2018 and 2019 focused on astrometric and photometric measurements. In last four years we have built up a light curve catalogue of space debris which is now freely available to the scientific community (www.sdlcd.space-debris.sk) ([5]). Catalogue can be used for further scientific applications such as support of active debris removal missions, rotation axis determination, BVRI photometry, object's shape and albedo estimation, etc. We report periodic signals extracted from more than 285 light curves of 226 individual objects situated on highly eccentric and geosynchronous orbits (Fig. 2.3.). We analyzed the object's rotation properties (Fig. 2.4.) and we constructed phase diagrams for 153 light curves for which we obtained apparent rotation periods and amplitudes. Majority of the observed objects showed rotational behavior within the 20 minutes duration of data acquisition.

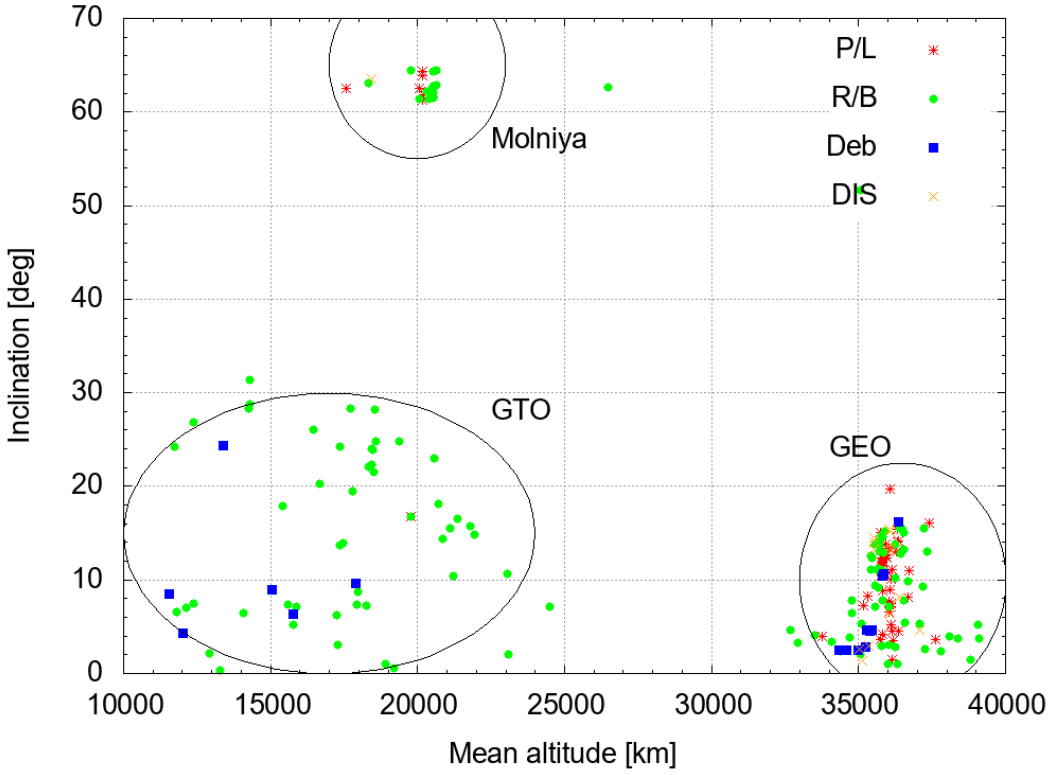

Figure 2.3. *Distribution of 226 objects observed for photometry by AGO70 system in years 2017 to 2019 according to their orbital properties.*

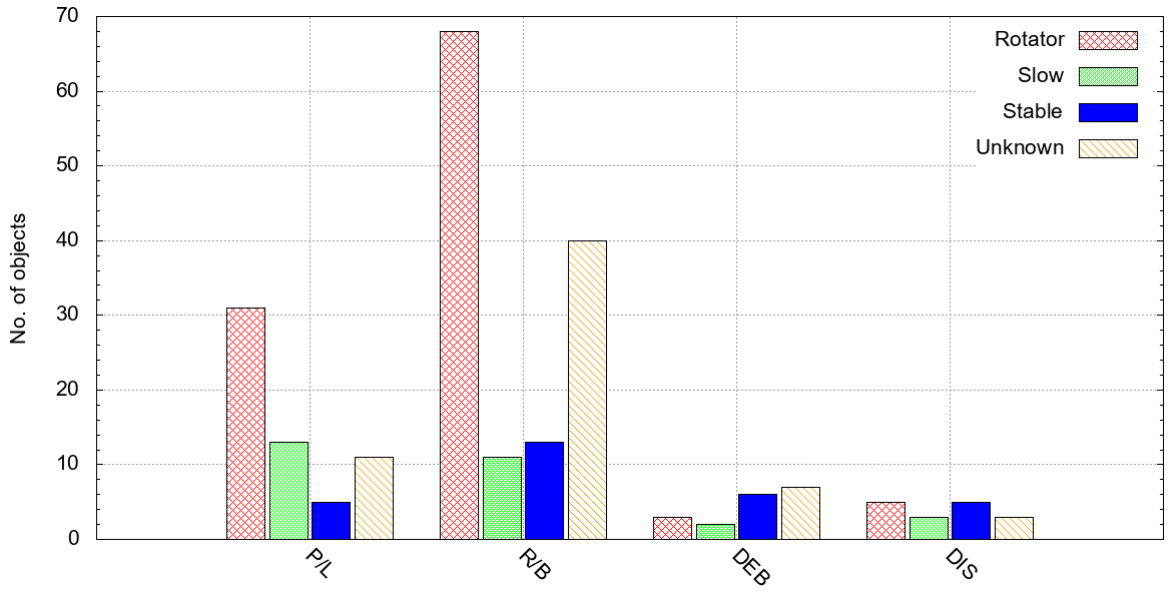

Figure 2.4. *Distribution of 226 objects observed by AGO70 system in years 2017 to 2019 according to their rotation properties and type. Plotted are rotators, slow rotators, stable objects and objects for which the light curve could not be processed.*

Study of the Milky Way galaxy using astrometric data from Gaia mission

The division of astronomy and astrophysics of FMPI CU is also involved in the research of the structure of the Milky Way galaxy. In collaboration with Instituto de Astrofísica de Canarias (IAC) in Spain, we studied the special distribution of stars in the remote regions of the Galaxy, since the structure of outer disc of our Galaxy is still not well described, and many features need to be better understood. We also explored the kinematics and dynamics of the Galactic disc ([6]). We make use of the Gaia data, which provide an excellent opportunity to probe Galactic disc at large distances and study structural features in the outskirts of Milky Way. We calculate the stellar density using star counts obtained from Gaia DR2 up to a Galactocentric distance R = 20 kpc with a deconvolution technique for the parallax errors. Then we analyzed the density in order to study the structure of the outer Galactic disc. We have focused on constrain their warp (warping of the plane of the Galaxy) and flare (thickening of the Galactic disc with increasing Galactocentric distance) ([7]). We calculated the average elevation of the plane and fitted it with different warp models. We found a small south-north asymmetry: the northern warp reaches an amplitude approx. 0.5 kpc and the southern warp reaches approx. 0.4 kpc (Fig. 2.5.). The analysis was also carried out for very luminous stars alone ($M_G < -2$), which on average represents a younger population. We concluded that the maximum amplitude of the warp is 20-30% larger than with the whole population. The north-south asymmetry is maintained.

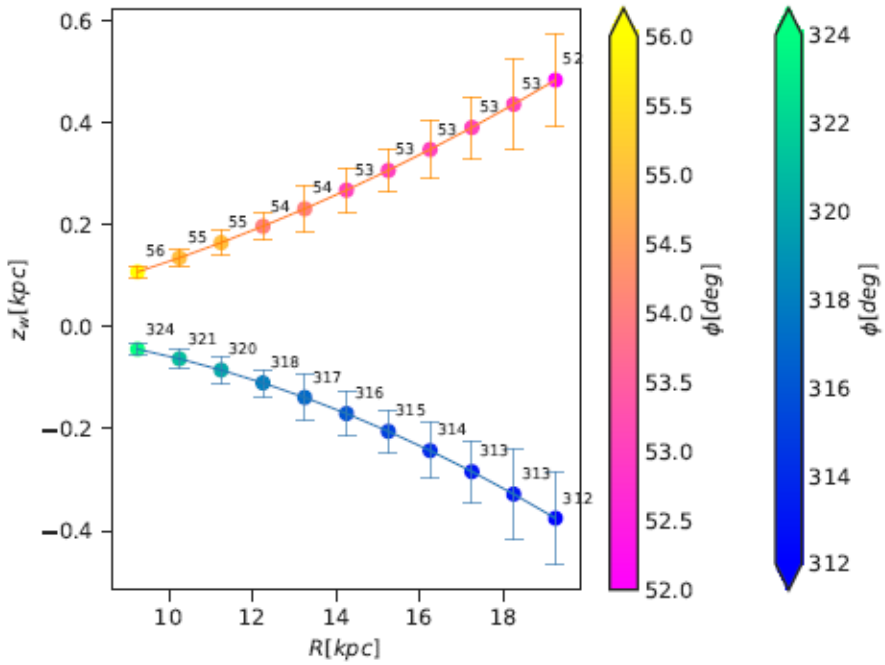

Figure 2.5. *Minimum and maximum of the average elevation of the plane as a function of Galactocentric distance. The colors code the azimuth of the minimum and maximum of the warp fit, and the error bars represent the uncertainty in the deconvolution method. The whole dataset was considered.*

References:

[1] MATLOVIČ, P. – KORNOŠ, L. – KOVÁČOVÁ, M. – TÓTH, J. – LICANDRO, J.: Characterization of the June epsilon Ophiuchids meteoroid stream and the comet 300P/Catalina, Astronomy & Astrophysics 636, A122 (2020).

[2] RAVICHANDRAN, R. – LEISER, D. – ZANDER, F. – LÖHLE, S. – MATLOVIČ, P. – TÓTH, J. – FERRIÈRE, L.: High frame rate emission spectroscopy for ablation tests in plasma wind tunnel, Review of Scientific Instruments, 92, 033101, (2021).

[3] OSZKIEWICZ, D. – TROIANSKYI, V. – FÖHRING, D. – GALÁD, A. – KWIATKOWSKI, T. – MARCINIAK, A. – SKIFF, B. – GEIER, S. – BORCZYK, W. – MOSKOWITZ, N. A. – KANKIEWICZ, P. – GAJDOŠ, S. – VILÁGI, J. – POLCIC, L. – KLUWAK, T. – WILAWER, E. – KASHUBA, V. – UDOVICHENKO, S. – KEIR, L. – KAMINSKI, K. – DEVOGELE, M. – GUSTAFSSON, A.: Spin rates of V-type asteroids. Astronomy&Astrophysics, 2020, Vol 643, A117.

[4] OSZKIEWICZ, D. – WILAWER, E. – PODLEWSKA-GACA, E. – KRYSZCZYNSKA, A. – KWIATKOWSKI, T. – TROIANSKYI, V. – KOLENCZUK, P. – FÖHRING, D. – GALÁD, A. – SKIFF, B. A. – GEIER, S. – BORCZYK, W. – MOSKOVITZ, N. A. – GAJDOŠ, Š. – VILÁGI, J. – POLCIC, L. – KASHUBA, V. – BENISHEK, V. – SHEVCHENKO, V.: First survey of phase curves of V-type asteroids. Icarus, 2021, Volume 357, 114158.

[5] ŠILHA, J. – KRAJČOVIČ, S. – ZIGO, M. – TÓTH, J. – ŽILKOVÁ, D. – ZIGO, P. – KORNOŠ, L. – ŠIMON, J. – SCHILDKNECHT, T. – CORDELLI, E. – VANANTI, A. – KAUR MANN, H. – RACHMAN, A. – PACCOLAT, C. – FLOHRER, T.: Space debris observations with the Slovak AGO70 telescope: Astrometry and light curves, Advances in Space Research 65 (8), (2020).

[6] LÓPEZ-CORREDOIRA, M. – GARZÓN, F. – WANG, H.-F. – SYLOS LABINI, F. – NAGY, R. – CHROBÁKOVÁ, Z. – CHANG, J. – VILLARROEL, B.: Gaia -DR2.

[7] CHROBÁKOVÁ, Ž. – NAGY, R. – LÓPEZ-CORREDOIRA, M.: Structure of the outer Galactic disc with Gaia DR2. Astronomy and Astrophysics, 2020, Volume 637, A96.

In the ***Earth Science Institute of the Slovak Academy of Sciences, Bratislava and Hurbanovo***, a number of issues concerning space weather modeling and forecasting were investigated and ground magnetic field measurements were performed.

Theoretical research was particularly focused on the analysis of historical geomagnetic records obtained long time before the space age at the Clementinum Observatory in Prague. Reliable long time series of geomagnetic records are needed for studying the long-term behavior of the Earth's magnetic field, in particular its secular variation. It is therefore desirable to have high-quality measurements of the geomagnetic field covering as long a time span as possible. Historical geomagnetic records can be useful for dealing with this task, however, they are often heterogeneous, incomplete, or consist of corrupted data. Their processing should involve several steps like digitization, conversion from the originally adopted scale units (i.e. divisions of the instrument scale) to proper physical units, dealing with inaccuracies or missing data, searching for accompanying information like auroral records, etc. Also, the knowledge on development of the historical magnetic instrumentation and observatory methods is necessary for proper understanding and interpretation of old geomagnetic data.

The work in [3] and [4] presents the first comprehensive review of the historical magnetic data recorded at the Clementinum observatory in Prague during the 19th century. The magnetic observatory Clementinum operated in Prague from 1839 to 1926. Historical data from the printed yearbooks, which have previously been digitized, were subsequently converted into the physical units of SI. Introducing a database of geomagnetic data from this historical source is a part of the study. Some controversial data were also analyzed. In the original historical sources, an error in using the physical units was identified. It was probably introduced by the observers determining the temperature coefficient of the so-called bifilar apparatus. By recalculating the values in the records, some missing values were added; for instance, the temperature coefficients for the bifilar magnetometer, the baselines, and the annual averages for the horizontal intensity in the first years of observations were redetermined. The values of absolute measurements of the declination in 1852, which could not be found in the original sources, were also estimated. The reconstructed time series for the horizontal intensity and magnetic declination are provided in Fig. 2.6. and Fig. 2.7., respectively. The main contribution of the study rests in critically reviewed information about the magnetic observations in Prague, which is, so far, more complete than any other.

In addition to regular daily observations at Clementinum with a typical 2-hr time step, two categories of data with a higher cadence were provided in the first decade. These unique data were studied in [5] and were provided in digital form in online database PANGAEA in [6]. The first category of the data captures 73 magnetic storms with their magnitude being of at least a moderate level (Fig. 2.8.). The second category is the dense observations during the days that had been agreed for joint measurements by the observatories organized in the Göttingen Magnetic Union (GMU), these measurements being known as term-day observations. Whereas four terms per year were set by GMU, many observatories agreed to carry out additional observations in the eight remaining months. The term-day observations also continued being performed for several years after the end of the GMU activities in 1841. Data of 120 term days from January 1840 to December 1849 were published. The declination was observed using the magnetic compass principle, while a bifilar apparatus was used to measure the horizontal intensity. When converting the data to the physical units of the SI, it was possible to achieve the consistency of these high cadence data with previously published regular hourly observations of the geomagnetic field. This requirement was also met by considering the temperature dependence of measurements by the bifilar apparatus in determining the absolute values of horizontal intensity. Revealing the historical observations of the geomagnetic field can serve as a valuable material for studying the space weather in the past and may also contribute to the refinement of global field modelling.

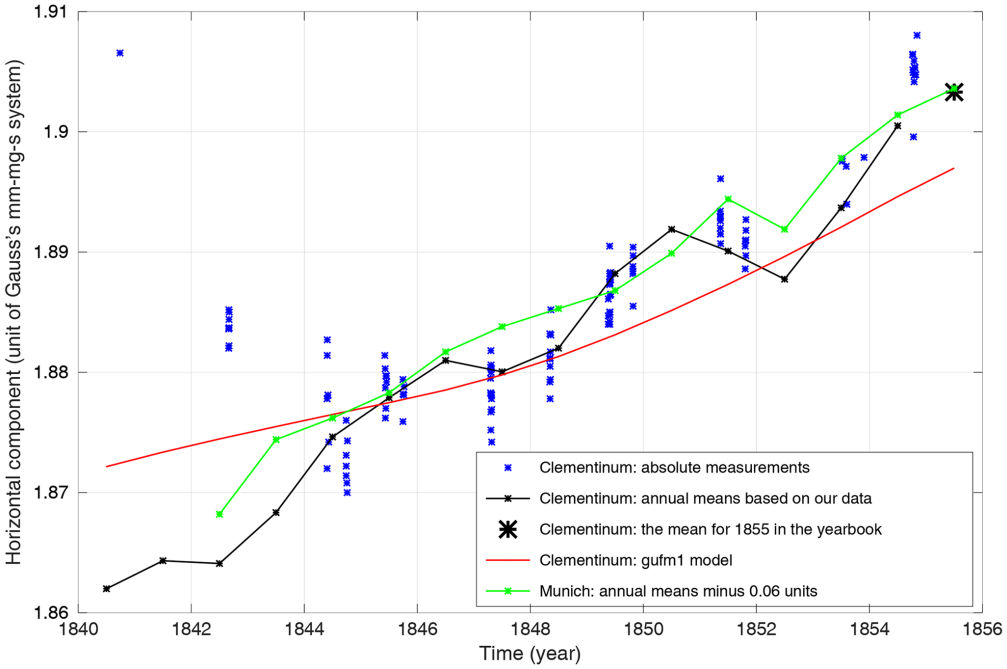

Figure 2.6. *The comparison of the absolute values of the horizontal intensity observed at Clementinum (absolute measurements – blue; annual means calculated in [3] – black curve; the annual mean for 1855 taken from the yearbook – black asterisk) with the annual means of the horizontal intensity in Munich reduced by 600 nT (i.e., 0.06 absolute units in mm–mg–s). The red curve is the horizontal intensity for Prague provided by the so-called gufm1 model, which is based on a compilation of all suitable historical observations.*

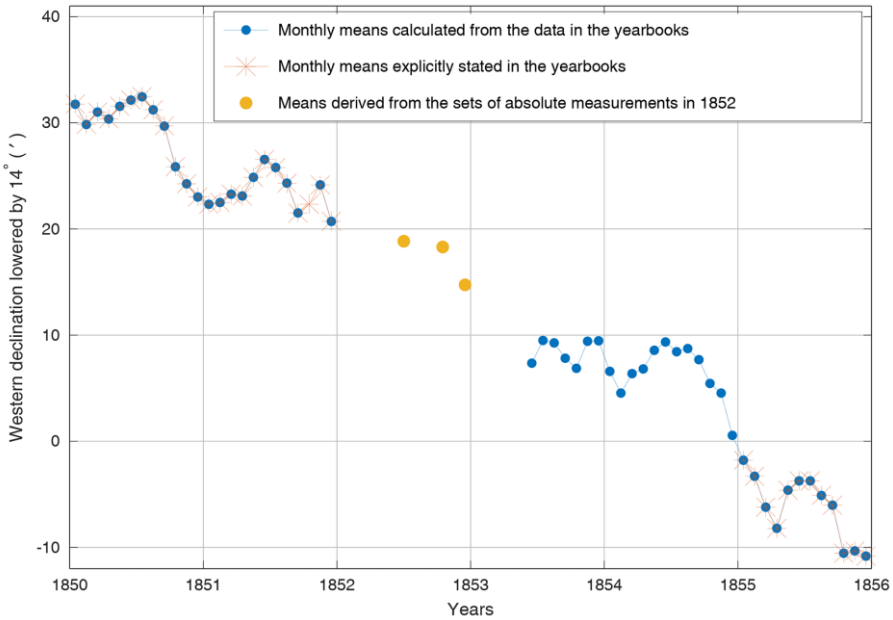

Figure 2.7. *Time series of monthly averages of declination (western), which was observed between 1850 and 1855 at the Clementinum observatory in Prague at 22:00 Göttingen civic time. The yellow dots supplement the back-calculated results in [3] of the absolute measurements for 1852 at about the time of the summer solstice, the autumn equinox, and the winter solstice.*

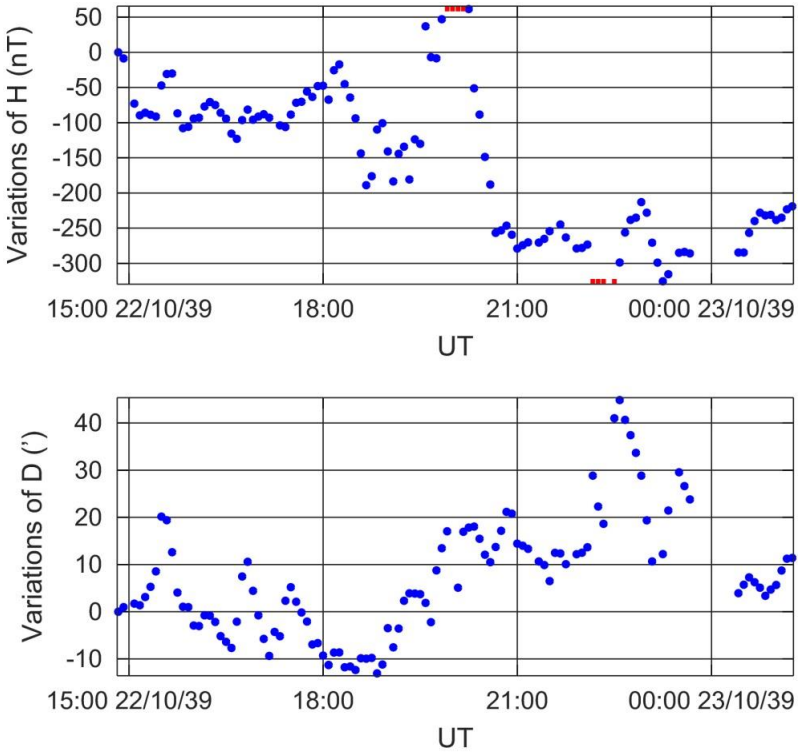

***Figure 2.8**. An example of a remarkable strong magnetic storm (the horizontal intensity H and the declination D) in the database presented in [6]. The event occurred on 22 October 1839. The red symbols in the time series of the horizontal intensity mark the instances when the bifilar device went off the scale.*

The collection of historical geomagnetic data from the presented database [6] can provide information about historical magnetic storms from the period when the network of geomagnetic observatories was still sparse. The importance of these data is all the greater because in geomagnetic disturbances, it is necessary to study both their global and local manifestations. It is believed that this kind of research may stimulate future collaborative research in the collection and analysis of hitherto unknown historical geomagnetic data.

In order to make the basic scientific knowledge about magnetic storms available to broader community, a study textbook [1] was published. It is a unique book in Slovak with a focus on the physical principles of magnetic storms. Although the prerequisites for studying this book are elementary skills in higher mathematics, the physical knowledge needed to understand the material comes more from the apparatus of well-mastered high school physics. The author explains the necessary more advanced physics, which is usually the subject of university courses, directly in this book. This book is intended for those interested in the issue of geomagnetic activity and solar-terrestrial relations, who wish to gain deeper insight into the physical nature of phenomena and processes related to the Earth's magnetic field disturbances. The book is written from the perspective of geomagnetism and cosmic geophysics, but due to the complexity of the issue, it also has an ambition to address experts in the field of solar astrophysics, cosmic magnetic fields and planetary magnetospheres. The book also takes a historical look at measuring the Earth's magnetic field and touches on current issues in the space weather, such as the mechanisms of magnetic substorms and the prediction of magnetic disturbances.

In 2020, we commemorated the 120th anniversary of the establishment of the Hurbanovo Geomagnetic Observatory of the Earth Science Institute SAS. The observatory was officially founded on September 30, 1900, by Dr. Miklós Konkoly-Thege – local noble, renowned scholar,

and director of the State Institute for Meteorology and Earth Magnetism in Budapest. On the occasion of this anniversary, a review article [2] in Slovak was prepared within the framework of outreach activities. This article concisely maps the history and present of the Hurbanovo Observatory and points on its role in the field of contemporary geoscience research.

In addition to the theoretical focus of the research work, there are observatory measurements of the geomagnetic field performed at the Hurbanovo Geomagnetic Observatory of the Earth Science Institute of the SAS. The Hurbanovo Observatory is located at geographical latitude 47.87° and geographical longitude 18.18°. It performs continuous monitoring and registration of the geomagnetic field components. The one-minute mean values of all components of the geomagnetic field as well as the records acquired with the one-second sampling interval are available. K-indexes characterising the geomagnetic activity in the middle latitudes are computed regularly. Main equipment of the observatory includes the digital variometer station TPM made in Poland (1996) and magnetoregistration device DI-fluxgate Magson gained on the co-operation bases with Geo Forshung Zentrum Potsdam and VW Stiftung. For absolute geomagnetic measurements, the DI-fluxgate magnetometer and proton precession magnetometer ELSEC are employed. The magnetovariational data in the one-minute step are supplied via the internet to the INTERMAGNET centre. The data are sent to World Data Centers in Edinburgh and Paris, from where they are available for the whole geomagnetic and space weather community. The data are published also on the CD-ROMs prepared in the frame of INTERMAGNET. That is because the Hurbanovo Geomagnetic Observatory of the Earth Science Institute of the SAS is a member of INTERMAGNET, the international network of world first order magnetic observatories. Information about the geomagnetic activity is also published on the web site of the observatory, www.geomag.sk. The level of the geomagnetic activity is reported to public media (TV), too.

The members of the Hurbanovo Geomagnetic Observatory staff regularly perform field measurements at the observation points of the national magnetic repeat station network, which is a part of the European repeat station network. The measurements are coordinated by the MagNetE Group. Measurements of the magnetic declination are performed regularly at selected Slovak airports. The knowledge of the distribution of the geomagnetic field elements over a country is important for many practical as well as scientific purposes. Such distributions result from magnetic surveys. The surveys need to be repeated periodically. Two-year period has been agreed for repeat stations by the MagNetE Group. This periodicity enables to find out information about the magnetic secular variations.

References:

[1] VALACH, F. Magnetické búrky. Fyzikálne základy. Hurbanovo, 2020. 240 s. ISBN 978-80-89998-11-1 (in Slovak).

[2] REVALLO, M. - VOZÁR, J. - VALACH, F. - VÁCZYOVÁ, M. - GUBA, P. Zem ako veľký magnet. In Quark: magazín pre vedu a techniku, 2020, roč. 26, č. 11, s. 7-11. ISSN 1335-4000. https://www.quark.sk/zem_ako_velky_magnet/ (in Slovak).

[3] HEJDA, P. - VALACH, F. - REVALLO, M. The geomagnetic data of the Clementinum observatory in Prague since 1839. In Annales Geophysicae, 2021, vol. 39, no. 3, p. 439-454. ISSN 0992-7689. https://doi.org/10.5194/angeo-39-439-2021.

[4] VALACH, F. - HEJDA, P. - REVALLO, M. Prague-Clementinum Geomagnetic Observations from 1839 to 1926. In IAGA-IASPEI 2021, 21-27 august 2021: abstracts: symposium: J9 Analogique data for the future preservation and present-day utilization of historical data in the geoscienes, Sr no: 111. - Hyderabad, India: CSIR-National Geophysical Research Institute, 2021, p. 93. (IAGA-IASPEI 2021).

[5] HEJDA, P. - REVALLO, M. - VALACH, F. Magnetic storm and term-day observations at the Prague observatory Clementinum in the mid-19th century. In Geoscience Data Journal, 2021. https://doi.org/10.1002/gdj3.141

[6] HEJDA, P. - REVALLO, M. - VALACH, F. Data of magnetic storms and term-day observations from the Prague-Clementinum observatory (1839-1849). PANGAEA, 2021. https://doi.org/10.1594/PANGAEA.936921

In the ***Slovak Central Observatory*** **(SCO)** in Hurbanovo (http://www.suh.sk/) a number of activities related to space research were performed. We observed sunspots (the Wolf number data were submitted to the SILSO in Brussels, Belgium and to the SONNE Netz in Germany) and prominences (images are published at the website of the Observatory). We performed also spectrographic observations of the solar spectrum (variations of selected spectral lines during a solar activity cycle) using a horizontal solar telescope with spectrograph, we registered solar radio bursts using a solar radio spectrometer CALLISTO. The research activities comprise study of the differential rotation of the solar corona.

One researcher from the SCO is the national ISWI (International Space Weather Initiative, http://iswi-secretariat.org) coordinator for the Slovak Republic and since September 2014 he is also as a Scientific Discipline Representative of the SCOSTEP for the field of solar physics. He is member of the National Committee of the SCOSTEP and chair and representative to the COSPAR.

We continued to publish at the website of the SCO data on the modified coronal index (MCI) and the modified homogeneous data set (MHDS) of coronal intensities based on satellite EUV measurements as a replacement of ground-based coronagraphic observations at Lomnický Štít. Both the MCI and the MHDS data sets can be used further for studies of the coronal solar activity and its cycle. These data are available at http://www.suh.sk/online-data/modifikovany-koronalny-index and http://www.suh.sk/online-data/modifikovany-homogenny-rad, respectively.

In the Computer Intelligence Group (CA3) of the CTS/UNINOVA (Caparica, Portugal) has been developed in previous years various software tool for automatic tracking of solar activity features (sunspots and coronal bright points - CBPs) using a hybrid algorithm combining PSO (Particle Swarm Optimization) and Snake algorithms, and an image segmentation algorithm, respectively, for detecting and tracking of a feature, and determining the differential rotation of the Sun. Another segmentation algorithm for automatic detection of CBPs was developed using SunPy and OpenCV in Python. An automatic tool to detect coronal holes (CHs) and to determine solar differential rotation using CBPs inside and outside the CHs, respectively, is being developed in the CTS/UNINOVA-CA3 group.

In collaboration with the Observatório Geofísico e Astronómico da Universidade de Coimbra (OGAUC, Coimbra, Portugal) we developed in recent zears algorithms to detect and track solar activity features, chromospheric plages as test features. The Ca II K3 spectroheliograms registered in the OGAUC were used to investigate the evolution of the chromospheric plages activity during the 24th solar cycle. Research team of the OGAUC created a special tool based on the segmentation by watershed method combined with other mathematic morphological operators to detect automatically and analyze the plages and/or other solar features.

In the SCO we developed also an alternative software tool to estimate the solar rotational profile based on cross-correlation (CC) method. Rotational velocity was calculated for each day in the years 2011 – 2020 from CC maxima of two consecutive SDO/AIA images with a cadence of 30 minutes taken through the 21.1 nm filter, in a window of 6° in heliographic longitude and 69° in heliographic latitude (241 x 2761 pxs). It was performed only in the rows where the CC maximum was higher than 0.5. The calculation of ω was repeated separately for rows that intersect a CBP and for rows without the contribution of a CBP, respectively. We call these background rows BCGs. In a current study we investigated eventual relationship between the coronal rotational rate and the phase of a solar cycle [1]. Time series graph of monthly averages of ω_n including cubic parabola approximation and a sinusoidal approximation is presented in Fig. 2.9.

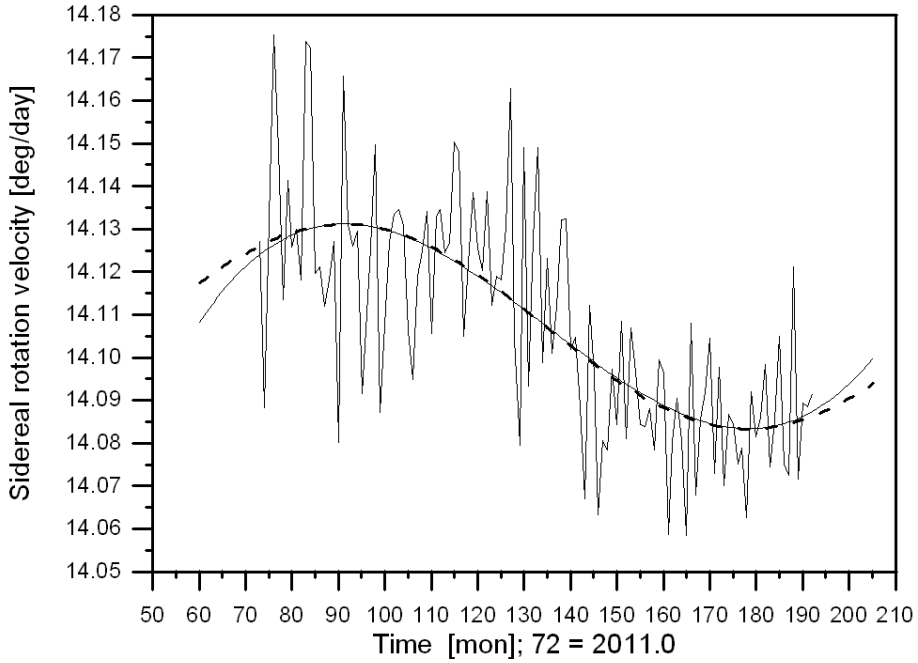

Figure 2.9. *Time series graph of monthly averages of ω_n; cubic parabola approximation (thin solid line): $y = 14.123 + 8.93.10^{-4}\ t - 2.73.10^{-5}\ t^2 + 1.45.10^{-7}\ t^3$, where t is time in months; sinusoidal approximation (thick dashed line): $y = 14{,}1072 + 0{,}02388.\sin((t + 24).2\pi/173{,}8)$.*

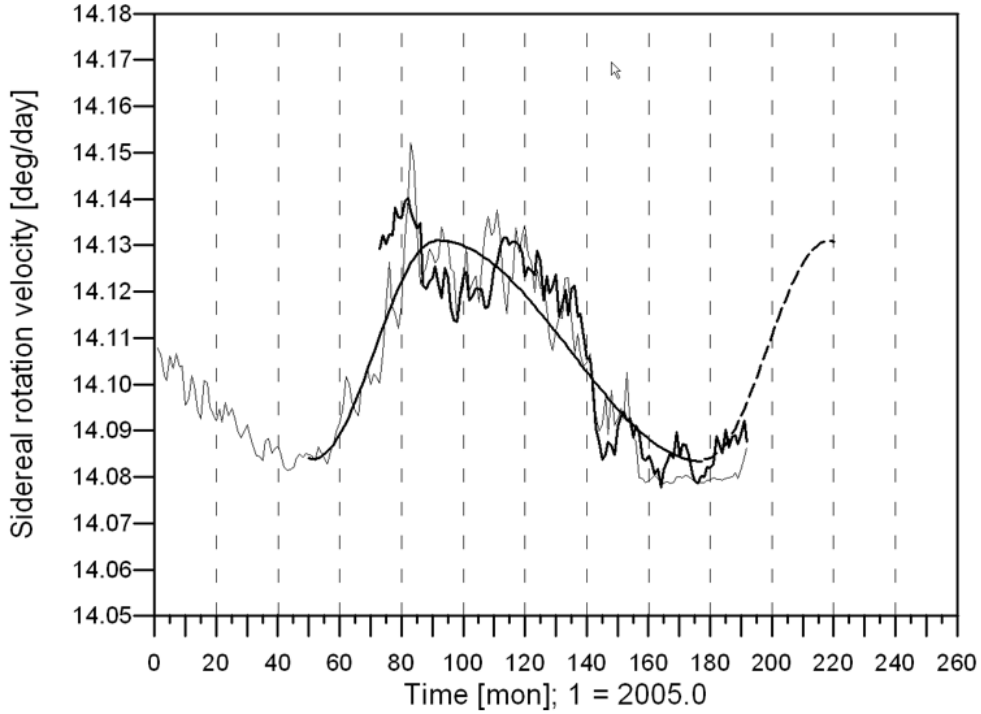

Figure 2.10. *Graphs of monthly averages of CI (thin gray line), running mean of monthly averages of ω_n (thick black solid line) and model of solar activity cycle according to the sinusoidal approximation of evolution of the rotational speed of the solar corona (solid+dashed line).*

The SCO organised in the year 2020 the 25th National Solar Physics Meeting with participation from abroad. Due to the pandemic situation it was a virtual online meeting. The goal of the Meeting was to present new results of solar physics and from the field of the space weather (Sun-Earth connections), to provide overview of present status in selected fields of solar physics, geophysics, meteorology, and climatology. A separate space was devoted to the presentation of research results of undergraduate and PhD students of university and academic departments and also to results of scientific and popularisation activities of Astronomical Observatories in the Slovak Republic and the Czech Republic. Invited talks, short contributions and posters covered the following fields: physical phenomena in the solar atmosphere, solar activity, total solar eclipses, space weather, geoactivity, meteorological events with solar forcing.

References:

[1] RYBANSKÝ M. - DOROTOVIČ I. (2021). Rotational velocity of the solar corona versus solar activity. Poster at the 16th European Solar Physics Meeting (ESPM-16), https://indico.ict.inaf.it/event/794/contributions/9544/

The activities of the ***Astronomical Institute of the Slovak Academy of Sciences (AISAS)***, Tatranská Lomnica (http://www.astro.sk/), related to COSPAR, were devoted to research in stellar, solar, and interplanetary physics using different satellite observations, mainly in the UV, XUV and X-ray spectral regions. Stellar data of the Swift, XMM-Newton, MOST, TESS, CHEOPS, and Kepler satellites, including the HST were used for research of various variable stars and start hosting exoplanets [1,3,12]. Data of the current SDO, IRIS, STEREO, ACE, Hinode, Wind, SORCE/SOLSTICE and other satellites were used for solar research. In common, these data were used with the simultaneously acquired data by the ground-based solar telescopes [2,4,5,6,8,11]. Topic of the interstellar particles has been also addressed [7, 9, 10]. Hereby we present some examples of the results obtained by the AISAS staff.

We used observations carried out with The Neil Gehrels Swift Observatory (Swift) to explore the outburst on the white dwarf surface in newly discovered symbiotic binary HBHA 1704-05 in the constellation of Sagittae that suddenly brightened at the beginning of August 2018 [12]. Using the X-Ray Telescope on the board of the Swift satellite allowed us to measure the increase of the X-ray counts within the 0.3-10 keV band, whereas its UltraViolet-Optical Telescope (UVOT) recorded significant brightening within its ultraviolet filters UVW2 (λ = 1928 Å), UVM2 (λ = 2246 Å), and UVW1 (λ = 2600 Å). On the basis on the UVOT observations, supplemented by simultaneous optical measurements, we reconstructed and modeled the spectral energy distribution (SED) during the outburst of HBHA 1704-05 (now called as V426 Sagittae). Example of the SED is shown in Figure 2.11. Our analysis revealed that V426 Sge experienced the so-called Z And-type outburst of a symbiotic binary that is caused by an abrupt increase of the mass-accretion rate onto the white dwarf. V426 Sagittae (HBHA 1704-05) became a classical symbiotic star.

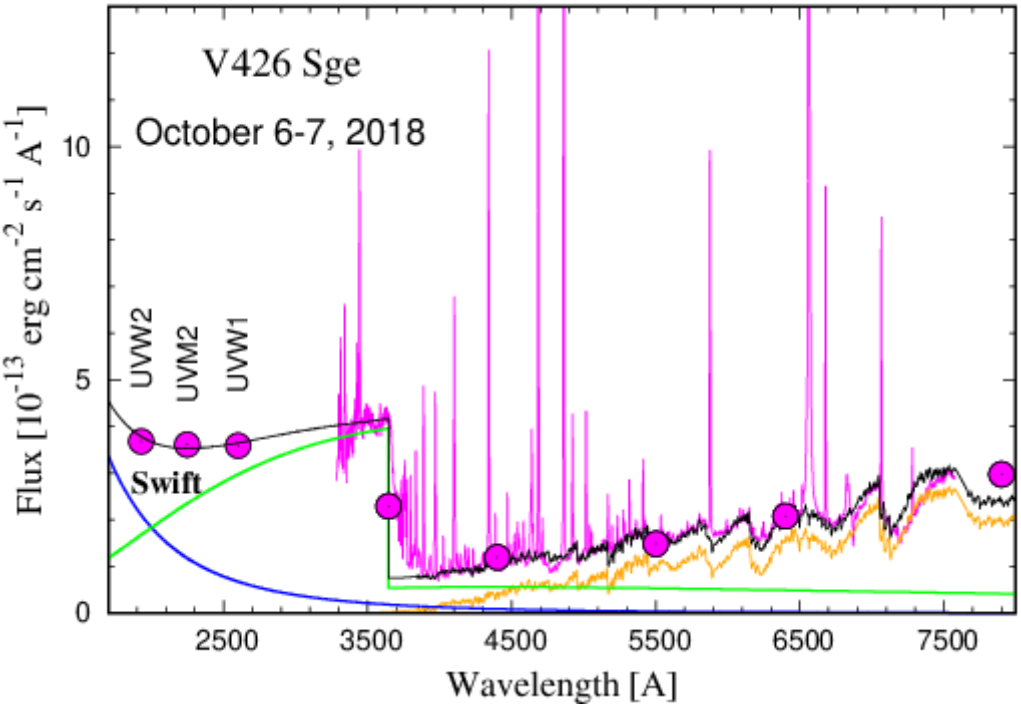

Figure 2.11. *Example of the observed (in magenta) and modeled (black line) SEDs of V426 Sge during its 2018 outburst. The blue, green and orange lines denote components of radiation from the nuclear-burning white dwarf, ionized material ejected during the explosion and giant, respectively. Circles (from left to right) represent Swift-UVOT fluxes and the optical flux-points given by the multicolor UBVRI photometry.*

A joint multi-instrument campaign involving a suite of space-borne and ground-based observatories was carried out in 2017 September 20 - 30 aimed, besides other targets, at coronal holes [11]. Out of leading ground-based telescopes (GREGOR, Vacuum Tower Telescope, ChroTel), the following spacecraft contributed to the coronal hole study: Solar Dynamics Observatory, Hinode, Advanced Composition Explorer, and Wind. The study was focused at a very extended non-polar coronal hole (Figure 2.12.). On 2017 September 24, the coronal hole developed patches of flux emergence, which contributed to the decrease of its overall area. These flux emergence patches erode the coronal hole and transform the area into a more quiet-Sun-like area. Conversely, flux cancellation leads to the reduction of opposite-polarity magnetic fields and to an increase in the area of the coronal hole. Other global coronal hole characteristics, including the evolution of the associated magnetic flux and the aforementioned area evolution in the EUV, are studied using data of the Helioseismic and Magnetic Imager and Atmospheric Imaging Assembly onboard the Solar Dynamics Observatory. The interplanetary medium parameters of the solar wind, measured in site by the Advanced Composition Explorer and Wind spacecraft, display values compatible with the presence of the coronal hole. Furthermore, a particular transient is found in those parameters.

We derived high-precision reference profiles of the Mg II h and k lines that represent the quiet Sun during a minimum of the solar activity [4]. To do so, we used the broad catalog of full-Sun mosaics obtained by the Interface Region Imaging Spectrograph (IRIS). To minimize the influence of the local variations due to the on-disk solar features and to achieve low levels of uncertainties, we used 12 IRIS full-Sun mosaics without sunspots or other significant signs of solar activity (Figure 2.13., left panel). These mosaics were obtained between 2019 April and 2020 September in the near-ultraviolet spectral range. In this study, we present the disk-averaged reference profiles of Mg ii h and Mg ii k lines, together with a series of reference

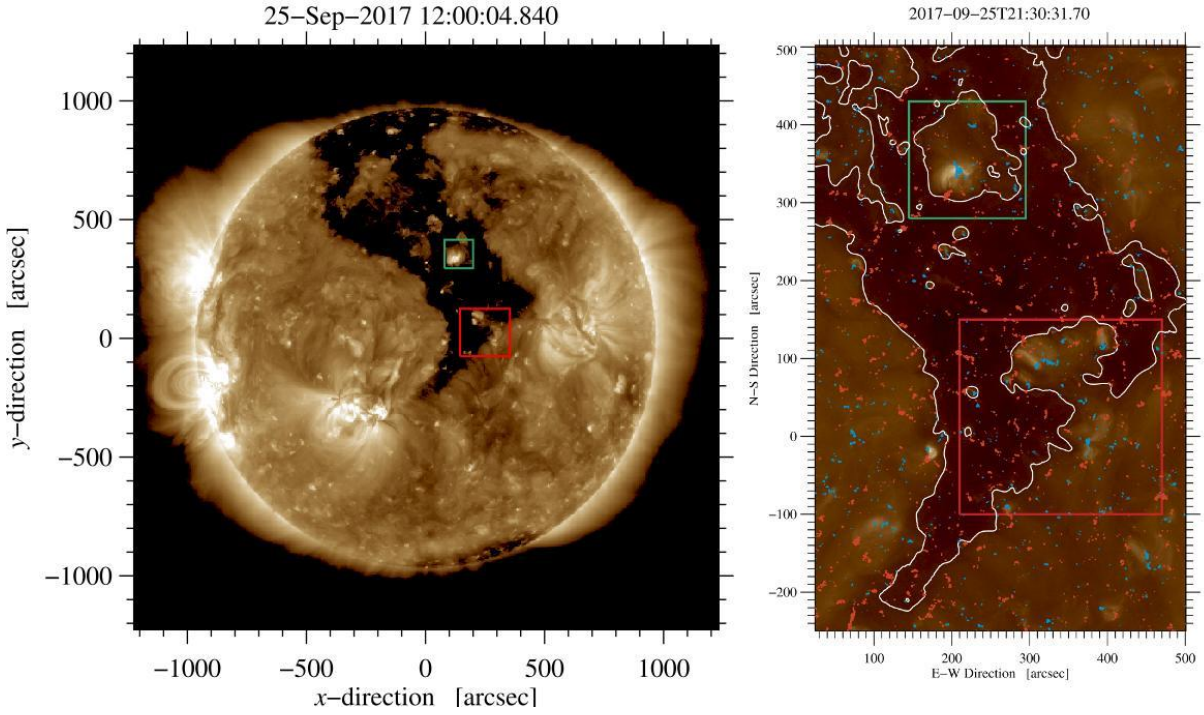

Figure 2.12. *Left: AIA EUV 193 Å images of non-polar coronal hole on 25 September 2017. The green and red boxes refer to regions of interest studied in detail. The coronal hole boundary is outlined by white contours (right). Positive and negative polarities derived from HMI magnetograms are displayed in red and blue, respectively.*

profiles spanning the distance between the disk center and the solar limb. These series of profiles offer a detailed representation of the center-to-limb variation of both Mg II h and Mg II k lines. The reference Mg II h and k line profiles provided in this study can be used as the incident radiation boundary condition for radiative-transfer modeling of prominences, spicules, and other coronal and chromospheric structures.

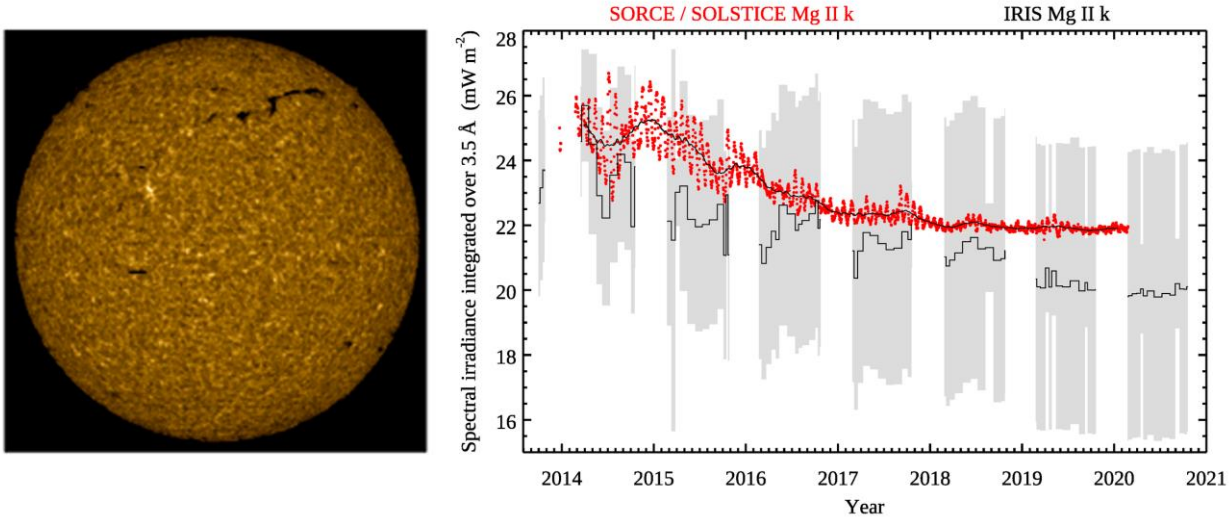

Figure 2.13. *Left: the IRIS full-Sun mosaic obtained in the Mg II k line center on 2019 May 27, i.e., before the end of the solar cycle 24 on 2019 December. Right: spectral irradiances integrated over the interval of 3.5 Å in the Mg II k line observed by the SORCE/SOLSTICE (red dots overlaid with the black curve) and IRIS (black histogram-like curve). The gray areas indicate the uncertainties of IRIS measurements.*

Among the many avenues of research currently being explored is the laboratory processing of astrophysical ice analogues. Such research involves the synthesis of an ice of specific morphology and chemical composition at temperatures and pressures relevant to a selected astrophysical setting - such as the interstellar medium, the surfaces of icy moons, or cometary nuclei. The in-situ changes in ice morphology and chemistry occurring during such processing (see Figure 2.14.) are often monitored via spectroscopic or spectrometric techniques.

In the work [7] we present a new high-vacuum laboratory end station: The Ice Chamber for Astrophysics–Astrochemistry (ICA) located at the Institute for Nuclear Research (Atomki) in Debrecen, Hungary. The ICA has been specifically designed for the study of the physico-chemical properties of astrophysical ice analogues and their chemical evolution when subjected to ionizing radiation and thermal processing. Ices pre-prepared in the ICA may be processed in a variety of ways. A 2 MV Tandetron accelerator is capable of delivering a wide variety of high-energy ions into the ICA, which simulates ice processing by cosmic rays, solar wind, or magnetospheric ions. The ICA is also equipped with an electron gun that may be used for electron impact radiolysis of ices. Thermal processing (20-300K) of both deposited and processed ices may be monitored by means of both FTIR spectroscopy and quadrupole mass spectrometry. A detailed description of the ICA setup as well as an overview of the preliminary results obtained and future plans is presented in the paper [7]. In the paper [9], we are focusing on characterising of the electron beams used for electron impact studies, as well as reporting the preliminary results obtained during electron irradiation and thermal processing of selected ices.

Sulfur is the tenth most abundant element in the universe and is known to play a significant role in biological systems. Accordingly, in recent years there has been increased interest in the role of sulfur in astrochemical reactions and planetary geology and geochemistry. In the paper [10], we have reviewed the results of laboratory investigations concerned with sulfur chemistry

in several astrophysical ice analogues. Potential future studies in the field of solid phase sulfur astrochemistry are also discussed in the context of forthcoming space missions, such as the NASA James Webb Space Telescope and the ESA Jupiter Icy Moons Explorer mission.

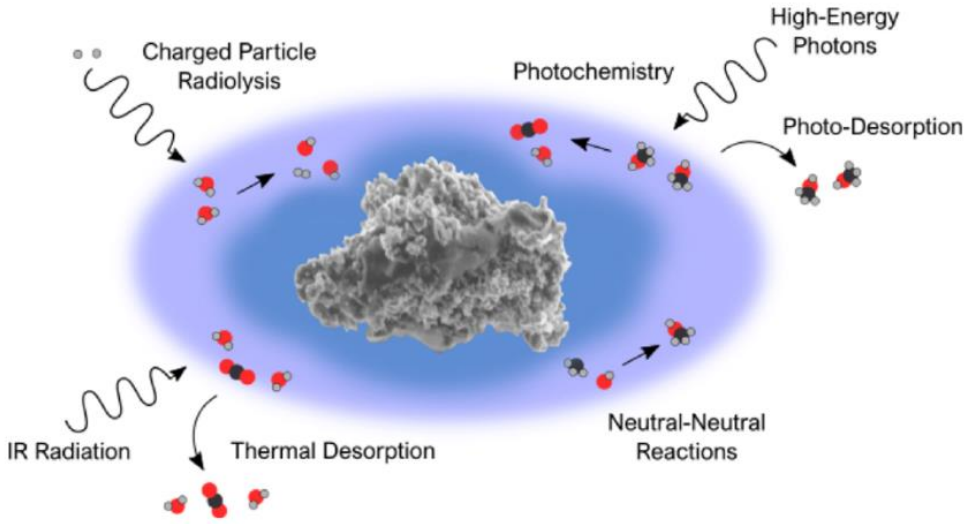

Figure 2.14. *Illustrative summary of the chemical processes that may occur in the icy mantles of interstellar dust grains.*

Besides of this, the AISAS staff was involved (or leading) in the last two years in 3 coordinated observing campaigns supporting individual Parker Solar Probe encounters to the Sun by the ground-based observations of the AISAS owned CoMP-S instrument at the Lomnicky Stit Observatory.

References:

[1] BORSATO, L. – PIOTTO, G. – GANDOLFI, D. – NASCIMBENI, V. – LACEDELLI, G. – MARZARI, F. – BILLOT, N. – MAXTED, P. – SOUSA, S. – CAMERON, A. C. – BONFANTI, A. – WILSON, T. G. – SERRANO, L. M. – GARAI, Z. – ALIBERT, Y. – ALONSO, Roi – ASQUIER, J. – BÁRCZY, T. – BANDY, T. – BARRADO, D. – BARROS, S. C. C. – BAUMJOHANN, W. – BECK, M. – BECK, T. – BENZ, W. – BONFILS, X. – BRANDEKER, A. – BROEG, C. – CABRERA, J. – CHARNOZ, S. – CSIZMADIA, S. – DAVIES, M. B. – DELEUIL, M. – DELREZ, L. – DEMANGEON, O. – DEMORY, B.-O. – DES ETANGS, A. L. – EHRENREICH, D. – ERIKSON, A. – ESCUDÉ, G. A. – FORTIER, A. – FOSSATI, L. – FRIDLUND, M. – GILLON, M. – GUEDEL, M. – HASIBA, J. – HENG, K. – HOYER, S. – ISAAK, Kate – KISS, L. L. – KOPP, E. – LASKAR, J. – LENDL, M. – LOVIS, Ch. – MAGRIN, D. – MUNARI, M. – OLOFSSON, G. – OTTENSAMER, Roland – PAGANO, I. – PALLÉ, E. – PETER, G. – POLLACCO, Don – QUELOZ, D. – RAGAZZONI, R. – RANDO, N. – RAUER, H. – RIBAS, I. – SÉGRANSAN, D. – SANTOS, N. – SCANDARIATO, G. – SIMON, A. – SMITH, A. M. S. – STELLER, M. – SZABO, Gy. M. – THOMAS, N. – UDRY, S. – VAN GROOTEL, V. – WALTON, N. Exploiting timing capabilities of the CHEOPS mission with warm-Jupiter planets. In Monthly Notices of the Royal Astronomical Society, 2021, vol. 506, no. 3, p. 3810-3830.

[2] DUDÍK, J. – DEL ZANNA, G. – RYBÁK, J. – LORINČÍK, J. – DZIFČÁKOVÁ, E. –

MASON, H. E. – TOMCZYK, S. – GALLOY, M., Electron densities in the solar corona measured simultaneously in the extreme ultraviolet and infrared. In The Astrophysical Journal, 2021, vol. 906, no. 2, article no. 118, p. 1-16

[3] GARAI, Z. – PRIBULLA, Th. – PARVIAINEN, H. – PALLÉ, E. – CLARET, A. – SZIGETI, L. – BÉJAR, V. J. S. – CASASAYAS-BARRIS, N. – CROUZET, N. – FUKUI, A. – CHEN, G. – KAWAUCHI, K. – KLAGYIVIK, P. – KURITA, S. – KUSAKABE, N. – DE LEON, J. – LIVINGSTON, J. – LUQUE, R. – MORI, M. – MURGAS, F. – NARITA, N. – NISHIUMI, T. – OSHAGH, M. – SZABÓ, Gy. M. – TAMURA, M. – TERADA, Y. – WATANABE, N. Is the orbit of the exoplanet WASP-43b really decaying? TESS and MuSCAT2 observations confirm no detection. In Monthly Notices of the Royal Astronomical Society, 2021, vol. 508, no. 4, p. 5514-5523.

[4] GUNÁR, S. – KOZA, J. – SCHWARTZ, P. – HEINZEL, P. – LIU, W., Quiet-Sun Mg II h and k line profiles derived from IRIS full-Sun mosaics. I. Reference profiles and center-to-limb variation. In The Astrophysical Journal Supplement Series, 2021, vol. 255 no. 1, article no. 16, p. 1-20.

[5] GUNÁR, S. – SCHWARTZ, P. – KOZA, J. – HEINZEL, P. Quiet-Sun hydrogen Lyman-alpha line profile derived from SOHO/SUMER solar-disk observations. In Astronomy and Astrophysics, 2020, vol. 644, article no. A109, p. 1-16.

[6] HEINZEL, P. – SCHWARTZ, P. – LORINČÍK, J. – KOZA, J. – JEJČIČ, S. – KURIDZE, D. Signatures of helium continuum in cool flare loops observed by SDO/AIA. In The Astrophysical Journal Letters, 2020, vol. 896, no. 2, article no. L35, p. 1-7.

[7] HERCZKU, P. – MIFSUD, D. V.** – IOPPOLO, S. – JUHÁSZ, Z. – KAŇUCHOVÁ, Z. – KOVÁCS, S. T. S. – TRASPAS MUIŇA, A. – HAILEY, P. A. – RAJTA, I. – VAJDA, I. – MASON, N. – MCCULLOUGH, R. W. – PARIPÁS, B. – SULIK, B. The Ice Chamber for Astrophysics-Astrochemistry (ICA): A new experimental facility for ion impact studies of astrophysical ice analogs. In Review of Scientific Instruments, 2021, vol. 92, no. 8, article no. 084501, p. 1-12.

[8] KURIDZE, D. – MATHIOUDAKIS, M. – HEINZEL, P. – KOZA, J. – MORGAN, H. – OLIVER, R. – KOWALSKI, A. F. – ALLRED, J. C. Spectral characteristics and formation height of off-limb flare ribbons. In The Astrophysical Journal, 2020, vol. 896, no. 2, article no. 120, p. 1-14.

[9] MIFSUD, D. V. – JUHÁSZ, Z.** – HERCZKU, P. – KOVÁCS, S. T. S. – IOPPOLO, S. – KAŇUCHOVÁ, Z. – CZENTYE, M. – HAILEY, P. A. – TRASPAS MUIŇA, A. – MASON, N. – MCCULLOUGH, R. W. – PARIPÁS, B. – SULIK, B. Electron irradiation and thermal chemistry studies of interstellar and planetary ice analogues at the ICA astrochemistry facility. In European Physical Journal D, 2021, vol. 75, no. 6, article no. 182, p. 1-9.

[10] MIFSUD, D. V. – KAŇUCHOVÁ, Z. – HERCZKU, P. – IOPPOLO, S. – JUHÁSZ, Z. – KOVÁCS, S. T. S. – MASON, N. – MCCULLOUGH, R. W. – SULIK, B. Sulfur ice astrochemistry: A review of laboratory studies. In Space Science Reviews, 2021, vol. 217, no. 1, article no. 14, p. 1-34.

[11] PALACIOS, J. – UTZ, D. – HOFMEISTER, S. – KRIKOVA, K. – GÖMÖRY, P. – KUCKEIN, Ch. – DENKER, C. – VERMA, M. – GONZÁLEZ MANRIQUE, S. J. – CAMPOS ROZO, J. I. – KOZA, J. – TEMMER, M. – VERONIG, A. – DIERCKE, A. – KONTOGIANNIS, I. – CID, C. Magnetic flux emergence in a coronal hole. In Solar Physics, 2020, vol. 295, article no. 64, p. 1-23.

[12] SKOPAL, A. – SHUGAROV, S. – MUNARI, U. – MASETTI, N. – MARCHESINI, E. –

KOMŽÍK, R. – KUNDRA, E. – SHAGATOVA, N. – TARASOVA, T. N. – BUIL, Ch. – BOUSSIN, C. – SHENAVRIN, V. I. – HAMBSCH, F.-J. – DALLAPORTA, S. – FRIGO, A. – GARDE, O. – ZUBAREVA, A. M. – DUBOVSKÝ, P. – KROLL, P. The path to Z And-type outbursts: The case of V426 Sagittae (HBHA 1704-05). In Astronomy and Astrophysics, 2020, vol. 636, article no. A77, p. 1-18. (2019).

3. LIFE SCIENCES

M. Musilová

Currently, space-related life sciences research in Slovakia is primarily performed through the Faculty of Electrical Engineering and Information Technology of the Slovak University of Technology in Bratislava (FEI STU), in collaboration with multiple Slovak and international partners. It is focused on astrobiology and human space exploration. A visiting professor at FEI STU is working with teams from NASA Goddard Space Flight Center, NASA Headquarters, University of Maryland, Georgetown University, Hawaii - Space Exploration Analog and Simulation (HI-SEAS), space companies (such as Honeybee Robotics) and others on these projects. They involve collecting biochemical, microbiological and geological samples from unique lava caves on the volcano Mauna Loa in Hawaii. The researchers are trying to understand what lifeforms can survive in these cave systems and whether similar extreme lifeforms could potentially survive in similar caves on Mars. Data suggests that lava caves most likely exist on Mars and they are considered some of the most promising places to look for Martian extra-terrestrial life. The teams have presented their results at multiple space conferences worldwide and they are currently preparing several peer-reviewed publications from the results of their research.

The human space exploration research is performed mostly at HI-SEAS, which is run by the aforementioned visiting professor at FEI STU. Almost 20 simulated missions to the Moon and Mars have been performed at HI-SEAS over the past couple of years. They were performed in collaboration with NASA, ESA and numerous other space organizations and companies from around the world. HI-SEAS is an analog space research facility located at 2,500 meters in elevation on the active volcano Mauna Loa, on the Big Island of Hawaii. It is used for a variety of research projects, which include astrobiology, geology, engineering, psychology, physiology, botany, education, in situ resource utilization and other experiments. The goal of the analog space missions is to field-test scientific and technological initiatives aimed to help humans return to the Moon and explore Mars one day. The missions can last from several weeks up to a whole year, depending on the research goals of the mission. A mission involves a crew of six people living as if they were on the Moon or Mars, while performing various scientific and engineering projects. This means that they are subject to time delays when communicating with the Mission Control Centre on “Earth”, they eat freeze-dried astronaut-like food and they have to survive on their own with very limited supplies of all the materials they bring with them. They are also isolated from the rest of the world, as if they were truly on another planet. Moreover, the visiting professor from FEI STU has also brought several Slovak technologies to HI-SEAS to be tested during simulated lunar and Martian missions. These include environmental sensors from the company HB Reavis and a rover developed by the company RoboTech Vision.

FEI STU representatives regularly present about these varied research projects worldwide at multiple international conferences, including the International Astronautical Congress (IAC) run by the International Astronautical Federation (IAF), American Geophysical Union (AGU), European Geophysical Union (EGU), Europlanet Science Congress (EPSC), Lunar and Planetary Science Conference (LPSC), various NASA workshops and forums, COSPAR Scientific Assembly and others. The visiting professor at FEI STU is also a reviewer for the NASA Planetary Protection Research Program and many other grant programs and research journals in space life sciences, such as Astrobiology and the National Science Foundation. They are a Global Faculty of the International Space University as well, where they lecture and organise workshops in astrobiology, and the robotic and human exploration of the Moon and Mars.

Figure 3.1. *An analog astronaut performing biochemical sampling for astrobiology research in a lava cave during a simulated Martian mission at HI-SEAS (Photo credit: Michaela Musilova).*

Figure 3.2. *Two analog astronauts using a Honeybee Robotics drill to collect geological and biological samples for astrobiology research in a lava cave during a simulated lunar mission at HI-SEAS (Photo credit: Michaela Musilova).*

References:

[1] MUSILOVÁ, M. – McADAM, A. C. – SETO, E.P. – BOWER, D. M. – MILLAN, M. – FISHMAN, C. (2021) Lessons learned from human lava tube exploration and research during simulated lunar and Martian missions at the HI-SEAS space research station. *Proceedings of the 72nd International Astronautical Congress (IAC) by the International Astronautical Federation (IAF)*, 25-29 October 2021, Dubai, UAE. Paper IAC-21,A5,2,13,x66867

[2] MUSILOVÁ, M. – OJEDA, O. – FISCHER, J. – BROWN, E. – EDWARDS, B. – Maxwell, Z. (2021) Selene III: Challenges and lessons learned during an analog lunar mission at the HI-SEAS research station. *Proceedings of the 72nd International Astronautical Congress (IAC) by the International Astronautical Federation (IAF)*, 25-29 October 2021, Dubai, UAE. Paper IAC-21, A5,1,12,x66971

[3] NEIDLINGER, K. – MUSILOVÁ, M. (2021) Algae Textile and Bioplastic Kit for Space Travel and Sustainable Living Applications. *Proceedings of the 72nd International Astronautical Congress (IAC) by the International Astronautical Federation (IAF)*, 25-29 October 2021, Dubai, UAE. Paper IAC-21,D4,2,8,x66977

[4] McADAM, A. C. – ACHILLES, C. – BOWER, D. M. – FISHMAN, C. – MILLAN, M. – JOHNSON, S. – NAPOLEONI, M. – KNUDSON, C. A. – WENG, M. – BLEACHER, J. E. – AREVALO, R. D. – MUSILOVÁ, M. – YOUNG, K. (2021) Investigation of a Mars-Analog Basaltic Subsurface Lava Tube Environment. *Workshop on Terrestrial Analogs for Planetary Exploration 2021*, Online, 16-18 June 2021, LPI Contribution No.2595, 8074.pdf

[5] CROWELL, C. – MUSILOVÁ, M. – BURNS, B. (2021) Determination of Iron Concentration in Volcanic Soil Around the HI-SEAS Analog Habitat. *Workshop on Terrestrial Analogs for Planetary Exploration 2021*, Online, 16-18 June 2021, LPI Contribution No.2595, 8120.pdf

[6] MUSILOVÁ, M. – FOING, B. – ROGERS, H. (2021) International MoonBase Alliance Campaigns at HI-SEAS. *Global Space Exploration Conference 2021*, 14-18 June, 2021, paper ID: 62387

[7] MUSILOVÁ, M. – FOING, B. – ROGERS, H. (2021) Simulating Lava Tube Exploration and Research during Analog Lunar and Martian Missions at HI-SEAS in Hawaii. *EGU General Assembly 2021*, 19–30 April 2021, EGU21-14600

[8] MUSILOVÁ, M. – McADAM, A. C. – RICHARDSON, J. A. – YOUNG, K. – BLEACHER, J. E. – ACHILLES, C. – BOWER, D. M. – FISHMAN, C. – JOHNSON, S. – MILLAN, M. – NAPOLEONI, M. – KNUDSON, C. A. WAGNER, N. Y. – SCHMERR, N. C. – SHIRO, B. – ROGERS, H. (2021) Lunar and Martian lava tube research simulation at HI-SEAS. *LPSC 52 Virtual Conference*, 15-19 March 2021, LPI contrib.no. 2548, 2600.pdf

[9] SETO, E.P. – ZACNY, K. – MUSILOVÁ, M. (2021) Astronaut drilling simulation for sign of life. *LPSC 52 Virtual Conference*, 15-19 March 2021, LPI Contrib.no. 2548, 1738.pdf

[10] ROMO, R. – ANDERSEN, C. – EDISON, K. – MUSILOVÁ, M. (2021) Analog Field Sites on Hawai'i Island. *Earth & Space 2021*, Earth and Space 2021: Space Exploration, Utilization, Engineering, and Construction in Extreme Environments, pp. 577 – 589, ISBN: 9780784483374

[11] MUSILOVÁ, M., FOING, B. – ROGERS, H. (2021). International Moonbase Alliance campaigns at HI-SEAS - Preparing for Future Moon & Mars Human Exploration. *43rd COSPAR Scientific Assembly*, Virtual Conference, 28 January – 4 February, 2021, id.156.

[12] MUSILOVÁ, M. – McADAM, A. C. – RICHARDSON, J. A. – YOUNG, K. – BLEA-

CHER, J. E. – ACHILLES, C. – BOWER, D. M. – FISHMAN, C. – JOHNSON, S. – MILLAN, M. – NAPOLEONI, M. – KNUDSON, C. A. – WAGNER, N. Y. – SCHMERR, N. C. – SHIRO, B. – ROGERS, H. (2020) Lunar and Martian lava tube research simulation at HI-SEAS. *American Geophysical Union Fall Meeting*, Online, 1-17 December 2020

[13] FISHMAN, C. – JOHNSON, S. – WAGNER, Y. Y. – ACHILLES, C. – BOWER, D. M. – BEVILACQUA, J. G. – HAHN, A. – VANDERWILT, M. – MILLAN, M. – MEIQI WENG, M. – GADSON, O.M. – BLEACHER, J. E. – YOUNG, K. – MUSILOVÁ, M. – McADAM, A. (2020) Microbial Life in Mauna Loa Lava Tubes as a Martian Analog. *American Geophysical Union Fall Meeting*, Online, 1-17 December 2020

[14] MILLAN, M. – NAPOLEONI, M. – McADAM, A. C. – BOWER, D. M. – KNUDSON, C. A. – ACHILLES, C. – FISHMAN, C. – BLEACHER, J. E. – YOUNG, K. – MUSILOVÁ, M. – JONHSON, S., (2020) Organic Characterization of Mauna Loa Lava Tubes, Hawaii, as Analogs for Mars: Implications for Martian Habitability and Exploration. *American Geophysical Union Fall Meeting*, Online, 1-17 December 2020

[15] MUSILOVÁ, M. – Rogers, H. – FOING, B.: International MoonBase Alliance analog space missions at HISEAS – preparing for the human exploration of the Moon & Mars (2020) *Proceedings of the 71st International Astronautical Congress (IAC) by the International Astronautical Federation (IAF)*, 12-14 October 2020, CyberSpace Edition. Paper IAC-20,A3,2B,16,x59758

[16] NEIDLINGER, K. – MUSILOVÁ, M. – FOING, B. (2020) Extimacy - Expressive Biofeedback for Personal Wellbeing and Intercultural Collaboration in Human Space Flight. *Proceedings of the 71st International Astronautical Congress (IAC) by the International Astronautical Federation (IAF)*, 12-14 October 2020, CyberSpace Edition. Paper IAC-20,A5,1.15

[17] MUSILOVÁ, M. – ROGERS, H. – FOING, B.: International MoonBase Alliance missions at HISEAS (2020) *Europlanet Science Congress 2020*, 21 September–9 Oct 2020, EPSC2020-1035, https://doi.org/10.5194/epsc2020-1035

[18] MUSILOVÁ, M. – NUNES, A. – KERBER, S. – POUWELS, C. – WANSKE, A. – D'ANGELO, J. – FOING, B. – ROGERS, H.: The Second EuroMoonMars IMA at HI-SEAS Field Campaign: An Overview of the EMMIHS-II Analog Mission to the Moon, *Europlanet Science Congress 2020*, 21 September–9 Oct 2020, EPSC2020-1020, https://doi.org/10.5194/epsc2020-1020, 2020

[19] MUSILOVÁ, M. – FOING, B. – ROGERS, H. (2020) Astrobiology research at the HI-SEAS Moon and Mars analog station. *European Astrobiology Network Association* 2020, 27-28 August, 2020

[20] MUSILOVÁ, M. – FOING, B. – ROGERS, H. – THANGAVELU, M. (2020) HI-SEAS lunar simulations: plans and progress. *7th annual NASA Exploration Science Forum 2020*, 8-10 July, 2020

[21] MUSILOVÁ, M. – FOING, B. – BENIEST, A. – ROGERS, H. (2020) Lunar and Mars analogue research performed at the HI-SEAS research station in Hawaii, part of the EuroMoonMars - IMA - HI-SEAS campaigns. *EGU General Assembly 2020*, 4–8 May 2020, EGU2020-13646

[22] MUSILOVÁ, M. – FOING, B. – BENIEST, A. – ROGERS, H. (2020) EuroMoonMars IMA at HI-SEAS Campaigns in 2019: An Overview of the Analog Missions, Upgrades to the Mission Operations and Protocols. *LPSC 51 Virtual Conference*, March 16–20, 2020, LPI contrib.no. 2893

4. MATERIALS RESEARCH IN SPACE

J. Lapin

Project-funded activities in the field of materials research in space at the ***Institute of Materials and Machine Mechanics of the Slovak Academy of Sciences*** (IMMS SAS) has not been performed during the reported period of 2020 – 2021.

5. REMOTE SENSING

Ľ. Balažovič, I. Barka, T. Bucha, J. Feranec, Z. Fulmeková, M. Gallay, T. Goga, J. Hofierka, M. Kopecká, K. Onačilová, P. Pastorek, R. Pazúr, M. Rusnák, I. Sačkov, M. Sedliak, M. Sviček, D. Szatmári, A. Zverková

Selected activities of six institutions are included in this report (2020-2021):

Institute of Geography, Slovak Academy of Sciences (IG SAS) in Bratislava

The role of field survey in abandoned agricultural land identification in Slovakia using Sentinel-2 data

The result was obtained within the solution of the ESA PECS project: ***Advanced Techniques for Biomass Mapping in Abandoned Agriculture Land Using Novel Combination of Optical and Radar Remote Sensing Sensors (ATBIOMAP)***, No. 4000123812/18/NL/SC (2018-2020): National Forest Centre (prime contractor), Zvolen, IG SAS (subcontractor).

Abandonment of agricultural land is a dynamic process characterised by both significant spectral variability and spectral similarity with areas of agricultural land. The identification of abandoned agricultural land (AAL) based on remote sensing data must be preceded by field surveys focused on the acquisition of the physiognomic characteristics (the composition of species, heights of vegetation, textures, and clustering into patterns) of these areas. This result documents the physiognomic and spectral differences between the AAL and other land cover/land use classes in Slovakia. The Normalised Difference Vegetation Index (NDVI), derived from Sentinel-2 time series for vegetation over April to September 2018, was applied.

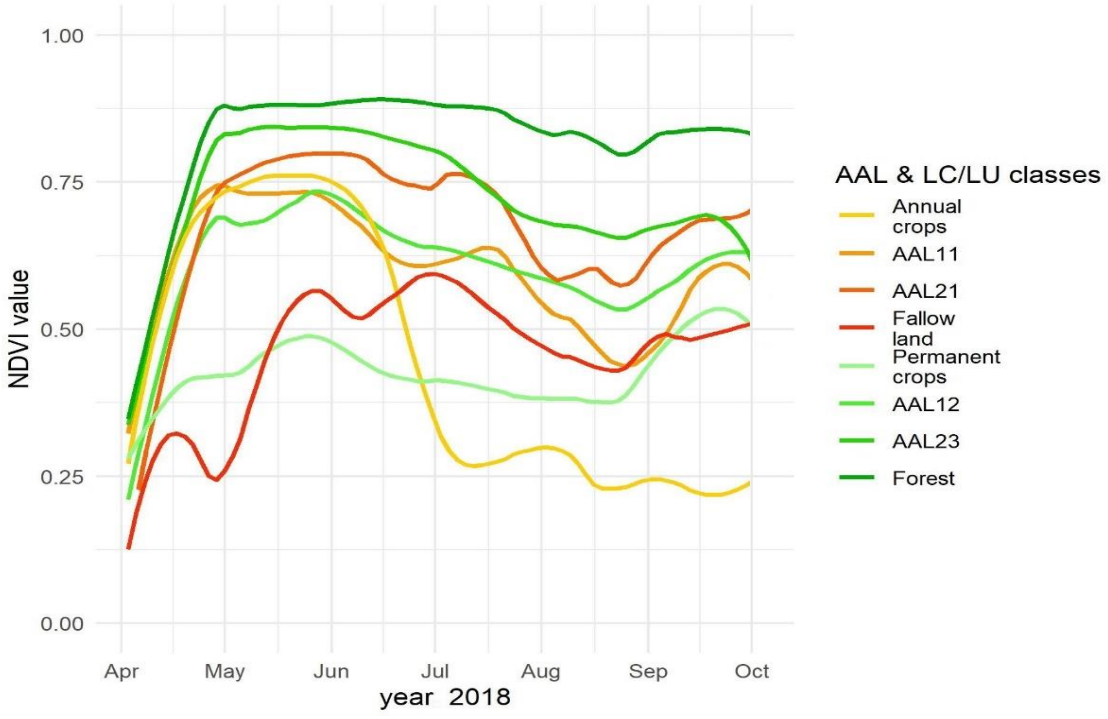

Figure 5.1. *NDVI values for homogeneous samples in study are 1.*

NDVI values were calculated for each Sentinel-2 scene. NDVI profiles for selected samples were used to create phenological profiles for each AAL and land cover/land use class. The dispersion in the NDVI values for these classes, their median, and the root mean square error between NDVI data show that overgrowth by herbaceous plants is characterised by more significant dynamics (0.40–0.75), resulting in better spectral discriminability than classes overgrown by shrubs and trees (0.70–0.80). Field research data are a fundamental prerequisite for the correct explanation of the discriminability of these AAL classes.

Abandonment of agricultural landscape assessed on remote sensing data [dissertation thesis]

The result was obtained within the solution of the ESA PECS project: ***Advanced Techniques for Biomass Mapping in Abandoned Agriculture Land Using Novel Combination of Optical and Radar Remote Sensing Sensors (ATBIOMAP)***, No. 4000123812/18/NL/SC (2018-2020): National Forest Centre (prime contractor), Zvolen, IG SAS (subcontractor) and Slovak Scientific Grant Agency VEGA under Grant (2/0023/19): ***Land cover dynamics as indicator of changes in landscape***.

Satellite data provide the possibility of a relatively fast and reliable evaluation of the state and dynamics of this process, which is a fundamental prerequisite for taking measures to eliminate it. In this context, the development of new methods for the identification and classification of running agricultural areas based on remote sensing data is desirable. The dissertation aimed to propose a methodological procedure for identifying and classifying abandoned agricultural land (AAL) using available satellite data.

The dissertation thesis analysed current trends used in the process of AAL identification and presented the definitions of AAL classes optimised for the geographical conditions of the Slovak Republic with emphasis on the physiognomic properties of the overgrown vegetation. Three AAL classes and their corresponding subclasses were identified within the two areas of interest (AOI) – Podunajská nížina (PN) and Zvolenská kotlina (ZK). AAL classes were analysed and evaluated based on their spectral and physiognomic characteristics. The field survey enabled a qualitative and quantitative evaluation of the mentioned characteristics.

Two types of AAL classification were implemented: i) using object-based methods with the machine learning algorithm – Random Forest with the overall accuracy of 74% and 75%, respectively ($\mathcal{F}1$ score 73% and 78%, respectively); ii) using a pixel-based approach using the deep learning algorithm – Deep Neural Network with the overall accuracy of 92.45% and 91.93%, respectively ($\mathcal{F}1$ score 92.46% and 91.94%, respectively).

Classification of AAL classes using deep learning methods estimated the extent of abandoned agriculture approximately at 6900 hectares in PN AOI (~11% of total AOI area) and approximately at 1000 hectares in ZK AOI (~8% of total AOI area).

Nevertheless, further research activities for automated AAL classification must be implemented focusing on deep learning algorithms, cloud computing techniques and distinguishing AAL classes from other land cover classes (Fig. 5.2). Cooperation between the research organisations with upcoming activities dealing with deep learning methods could be conducive.

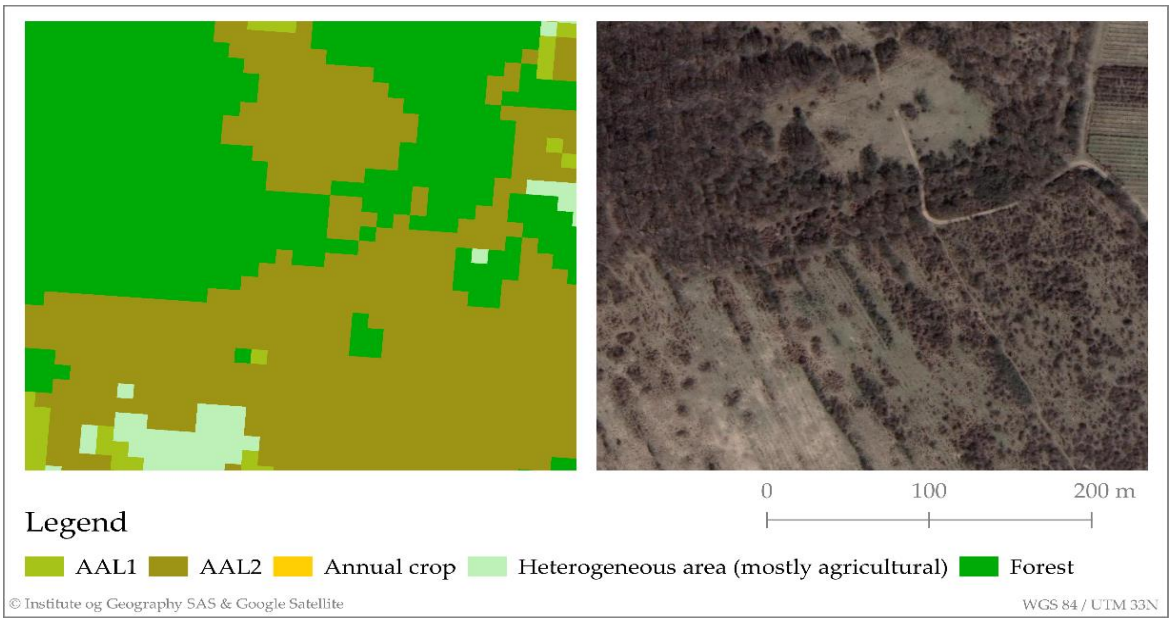

Figure 5.2. *Forest class overestimation at the expense of* ***a****bandoned* ***a****griculture* ***l****and overgrown by tree formations (AAL3).*

Automatic detection of vegetation dynamics by remote sensing in riparian zone of braided-wandering river system

The dynamics of the braided-wandering river system of the Belá River was assessed by automated supervised classification of aerial images 2012, 2015, 2018, SkySat2018 and Sentinel-2 data (2015-2019) within the project ESA TPM project ID59474. Three main vegetation classes expressed successional stages in the study area were identified using multiresolution hierarchical classification: grass, shrubs, and riparian forest. Spatial distribution of vegetation and moisture indices (NDVI, GRVI, GCI, SIPI, MNDWI, NDWI, MSI) was used for ecologic assessment of the negative human intervention to hydromorphological continuity.

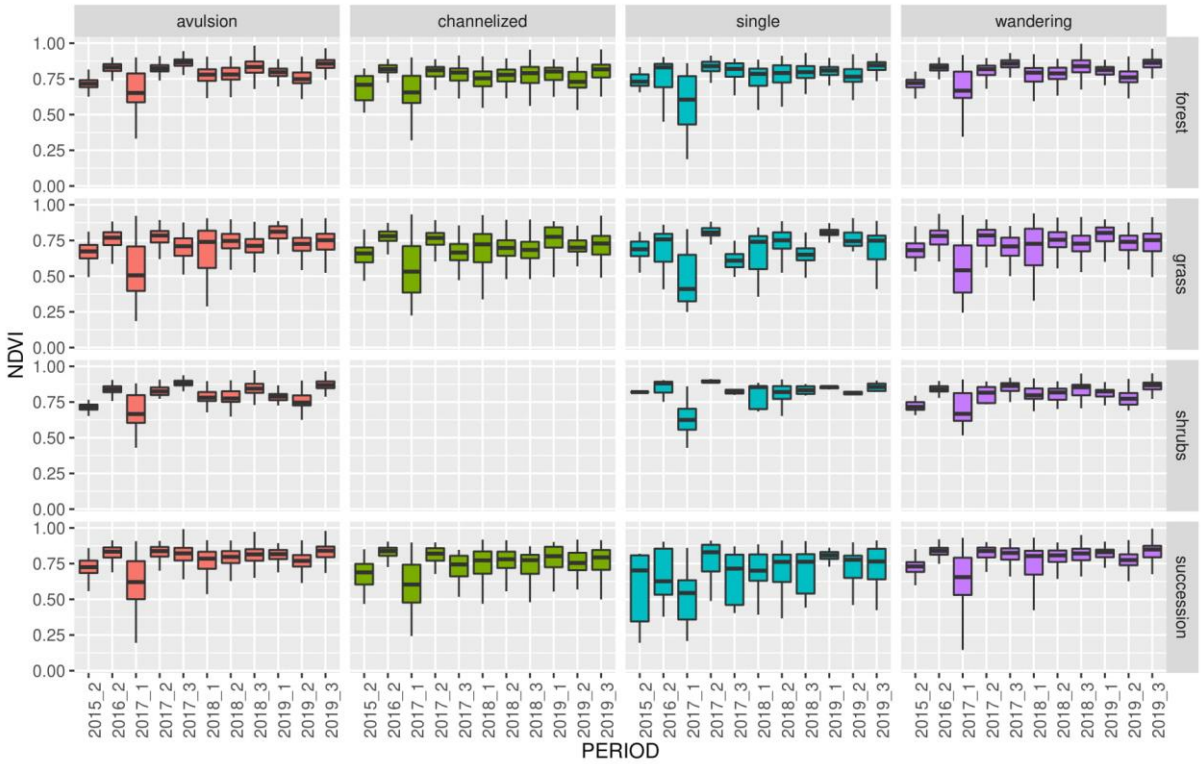

Figure 5.3. *Temporal variation of NDVI values for different vegetation classes and channel pattern types.*

Institute of Geography, Faculty of Science, Pavol Jozef Šafárik University in Košice

Project: ***Extension of the operational "Space Emergency System" towards monitoring of dangerous natural and man-made geo-processes in the HU-SK-RO-UA cross-border region*** –HUSKROUA/1702/8.1/0065/GeoSES

This project is supervised by the Uzhorod National University in Ukraine, and partners: involves Pavol Jozef Šafárik University in Košice (Slovakia), Technical University Cluj-Napoca (Romania), Technical and Economic University in Budapest (Hungary), Self-government of Szabolcs-Szatmár-Bereg county (Hungary). The project focuses on overall analysis of the recent surface deformations to obtain detailed knowledge about the current situation as well as to be able to identify the areas to assess the risks associated with surface deformation (i.e. landslides, uplift, subsidence). The work involves use of SAR interferometry, GNSS, laser scanning to reach this goal. The overall is to reduce social and economic losses and risks to human health and life caused by natural disasters in this area. GeoSES will be provide information and services that help identify danger of emergencies and will alert population about for their emergence. More details: https://www.uzhnu.edu.ua/en/cat/projects-huskroua , https://www.geoses.science.upjs.sk/?lang=en

Project: ***APVV/SK-CN-RD-18-0015: Key Technologies on the Integration of Multi-GNSS, LiDAR and Oblique Photogrammetry in 3D High-Quality Reconstruction of Smart City (3DSMARTCITY)***

The projects involved a bilateral collaboration with China University of Mining Technology in Xuzhou and our Institute. There were original contributions generated in 4 areas focusing on research and development of new methods in:

1. 3D spatial data acquisition with terrestrial and airborne LiDAR/oblique photogrammetry and GNSS with high efficiency and precision, in urban landscape and integration of the data [14].
2. Generating virtual 3D city models from the multi-source data and integration of the models in GIS (Geographical Information Systems) within the Smart City concept.
3. Precise positioning by multi-frequency and multi-mode GNSS under the condition of the limited satellite signal in the urban sheltered area [15].
4. Modeling various phenomena of the urban landscape with 3D data to assess the life quality of citizens and contribute to the SmartCity concept. [7, 8, 13] (Figs. 5.4. – 5.7.).

Aim 1 and Aim 2 were achieved by developing new methods of noise reduction in multisource 3D data and integration of the various kinds of 3D data in a GIS. A 3D geodatabase is another result of the research integrating the various kinds of multisource high-resolution 3D data of urban landscapes. Furthermore, the new university textbook contributes to up-todate teaching of global navigation satellite systems (GNSS).

• The results addressing Aim 3 concern the new approach for fusion of data recorded by an inertial navigation system (INS) and (GNSS) by adopting the robust cubature Kalman filtering. The method can be applied for improving the accuracy of reconstructing the trajectory of a moving platform for autonomous piloted aerial and ground vehicles used for remote sensing with LiDAR or photogrammetry.

• Addressing the Aim 4, the developed methods and 3D geodatabase were applied in the design of innovative approaches for modeling solar energy income and land surface temperature in high resolution. We also participated in the calculation of carbon dioxide emissions and carbon sequestration in Košice for the City Council.

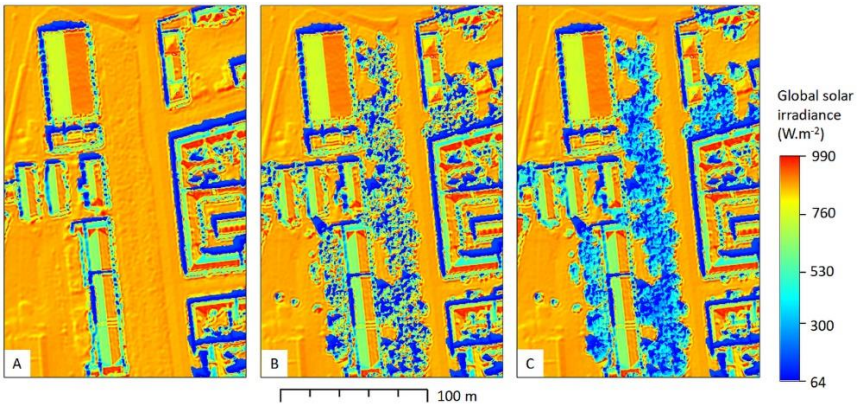

Figure 5.4. *Global solar irradiance (W.m-2) of a digital lidar-based surface model calculated by the r.sun model for June 30 at 10:20 zonal time for the smaller site as (A) without vegetation, (B) with non-transparent trees, (C) with transparent trees* [8].

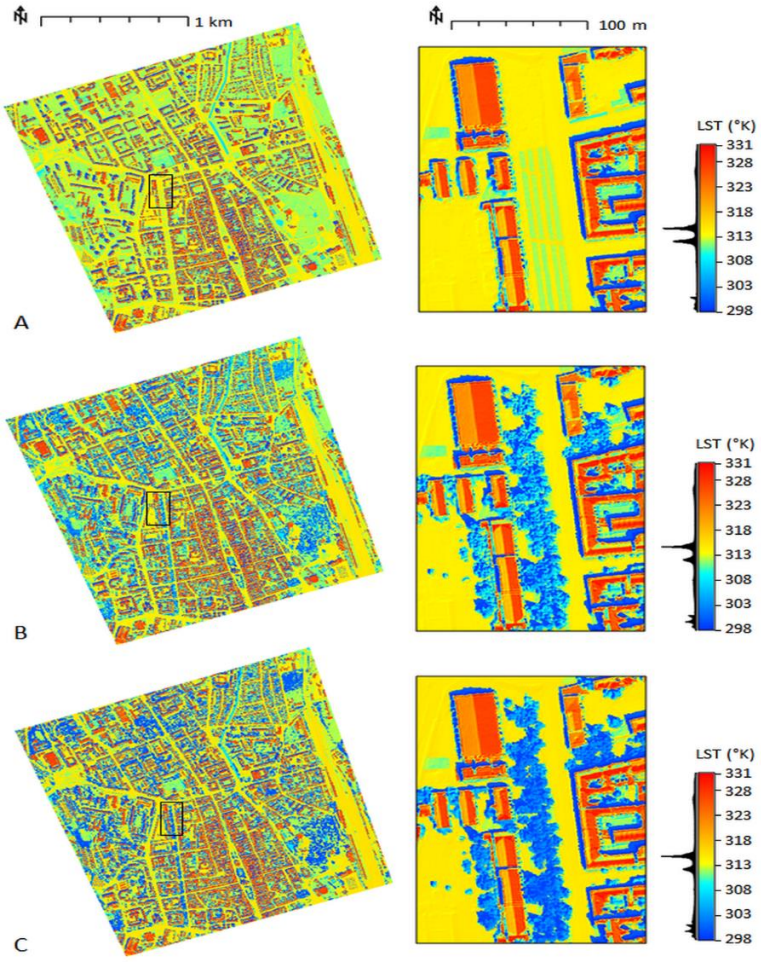

Figure 5.5. *Modelled land surface temperature in degrees Kelvin for the entire study area and the smaller site in the black outline as (A) without vegetation, (B) with non-transparent trees, (C) with transparent trees* [8].

The project achieved results that can be directly incorporated in the smart management of any city in Slovakia, China for elsewhere for mitigating overheating, flash flooding, traffic noise modeling or identifying suitable building facades for smart photovoltaic installations or improvement of wireless internet or smart navigation, taking advantage of the modern methods of ground surveying and remote sensing.

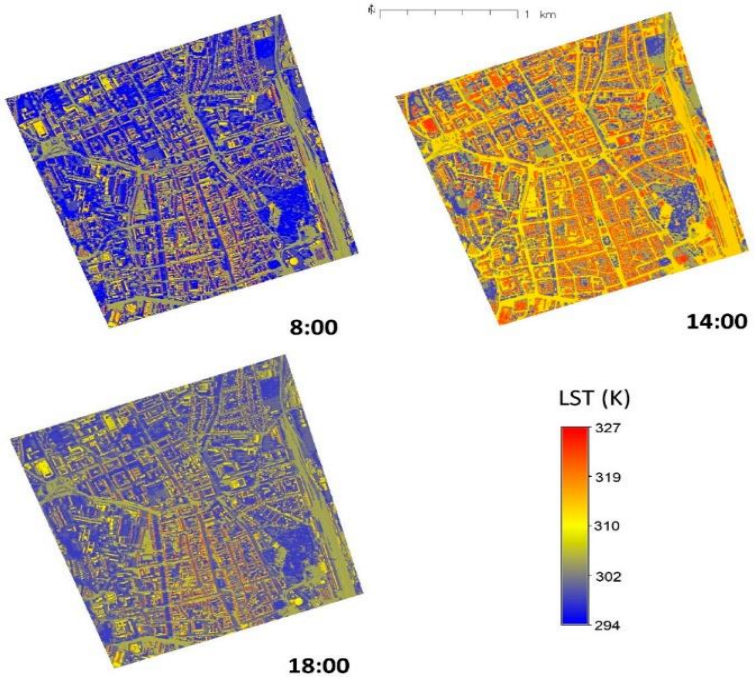

Figure 5.6. *Simulated land surface temperatures (LSTs) with heat storage at 8:00, 14:00 and 18:00 on 25 June 2020* [7].

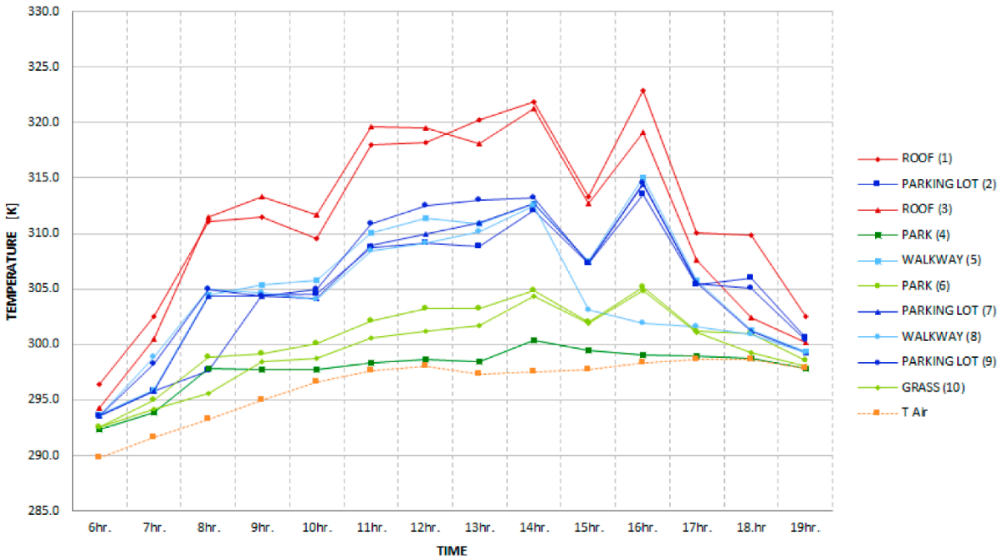

Figure 5.7. *Simulated LSTs with heat storage effects in 10 selected locations in the study area on 25 June 2020* [7].

Project: ***APVV-18-0044: Solar potential in urban areas and its application to the Smart City concept***

The use of solar radiation in the urban environment is becoming increasingly important for the sustainable development of cities and human societies. Several factors influence the distribution of solar radiation in urban areas, including urban morphology and the physical properties of urban materials. Most of these factors can be modeled with a relatively high accuracy using 2D and 3D solar radiation models. In this paper, the r.sun and v.sun solar radiation models are used to calculate solar radiation for the city of Košice in Eastern Slovakia to assess the accuracy of both approaches for vertical surfaces frequently found in urban areas. The results were validated by pyranometer measurements. The results showed relatively good estimates by the 3D v.sun model and poor estimates by the 2D r.sun model. This can be attributed to an improper representation of vertical surfaces by a digital surface model, which has a strong impact on solar resource assessments. We found that 3D city models prepared in level of detail 2 (LoD2) are not always adequate in case of complex buildings with morphological structures, such as terraces. These cast shadows on facades especially when solar altitude is high and, thus, assessments, even by a 3D model, are inaccurate [9], Fig. 5.8.

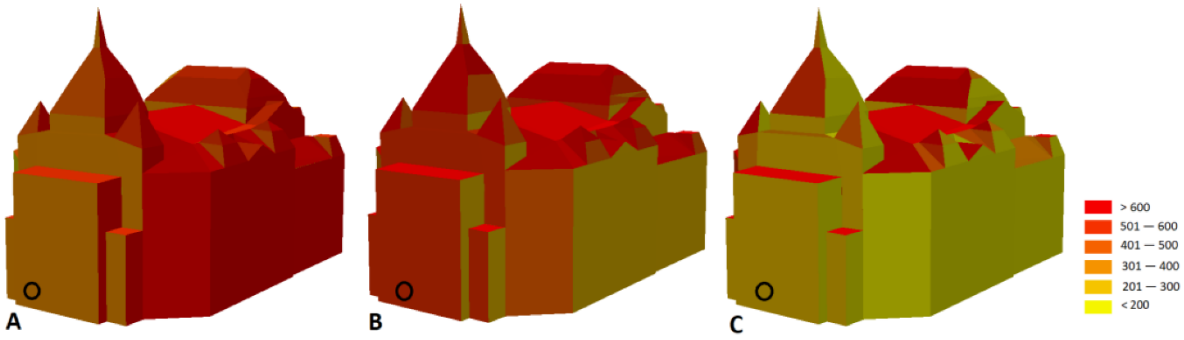

Figure 5.8. *Solar irradiance at the State Theatre on 23 June 2021 (W/m^2) at (**A**) 8:57 a.m., (**B**) 11:50 a.m., and (**C**) 3:31 p.m. The black circle represents the measurement location* [9].

Project: ***VEGA 1/0798/20: Synergistic use of multisource remote sensing data in Earth system research***

The aim of the project is to develop new methods of landscape mapping using synergies of a combination of several Earth-based remote sensing methods. The solution assumes data collection by means of laser scanning, passive multispectral and hyperspectral scanning and photogrammetry, in particular using the unique instrumentation and software equipment existing in the home institution, which is currently a state-of-the-art unpiloted and terrestrial remote technology. In the practical sense the practical level, the research focused on the use of the mentioned technologies and their synergic use for increasing the accuracy, detail and thus the interpretation power to improve understanding of selected natural phenomena and processes, such as landsliding, phenological phases and vegetation growth, identification of neotectonic features in land surface, land surface temperature modelling in the urban landscape using the high spatial, spectral and temporal resolution. For these tasks, new geomorphometric analysis methods with 2D and 3D data structures, multi-dimensional regression modelling and machine learning methods are proposed. In terms of understanding the complexity of the landscape, we developed approaches for integrating the multisource data with other types of field- and lab-based data. We used the concept of space-time and hyperspectral data cube for this task.

National Forest Centre Zvolen

Satellite-based observation of forest decline

The activities in 2020-2021 and this publication is the result of the project implementation: Centre of Excellence of Forest-based Industry, ITMS: 313011S735 supported by the Research & Development Operational Programme funded by the ERDF.

The satellite data and layers of forest damage classification from 2020 and 2021 were added into the web service STALES https://web.nlcsk.org/?page_id=17612. The system is proposed to inform forest owners and forest state administration about the actual condition of forest stands and its changes. So far the individual satellite images from 1990, 1996, 1998, 2000, 2003, 2006-2021 were mosaicked into nationwide mosaic, from which we derived forest damage to each of those years. The services are based on Landsat satellite images in spatial resolution of 30 × 30 meters and Sentinel data in resolution 10 × 10 m since 2016. Mosaics are created from the composition of Landsat (Sentinel) bands in false colours, i.e. Near-infrared, Mid-infrared and Red band.

Mapping applications are prepared so that the boundaries of forest districts are visible at the scale of 1:100 000 and the boundaries of forest compartments at the scale of 1:20 000. STALES service actually consists of 4 map applications: Map application 1 (currently under reconstruction) – visualization of satellite scenes and forest health condition; Map application 2 – a comparison of satellite scenes from different time periods (Fig. 5.9.); Map application 3 – dynamic visualization of actual and historical satellite scenes; Map application 4 – dynamic visualization of forest health condition (Fig. 5.10.).

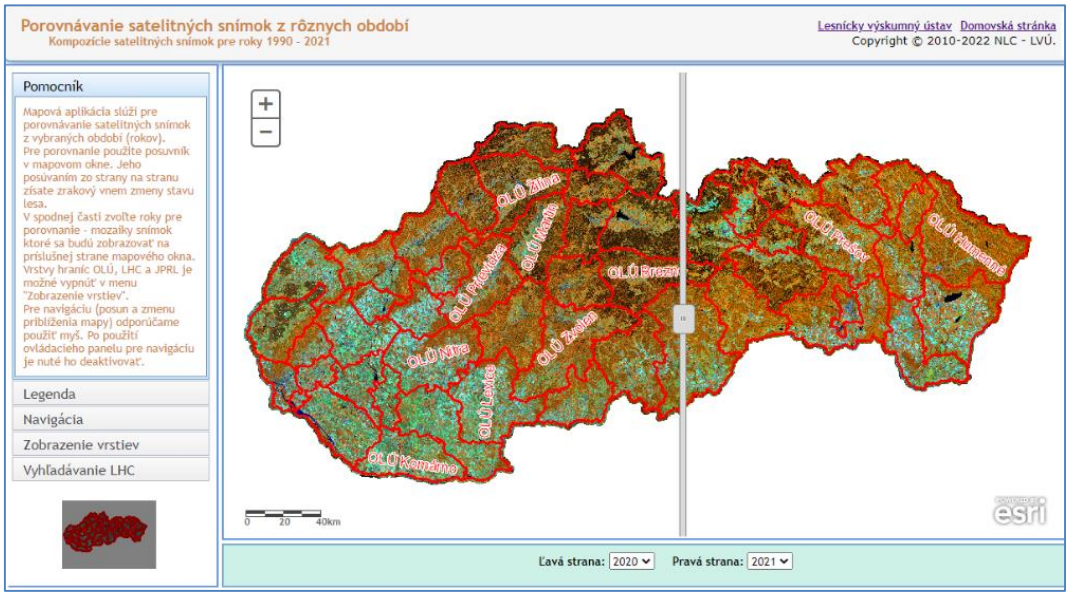

Figure 5.9. *Web service* http://www.nlcsk.sk/stales/stales_swipe_tool.html *– map application for comparison of satellite scenes from two different years according to selection.*

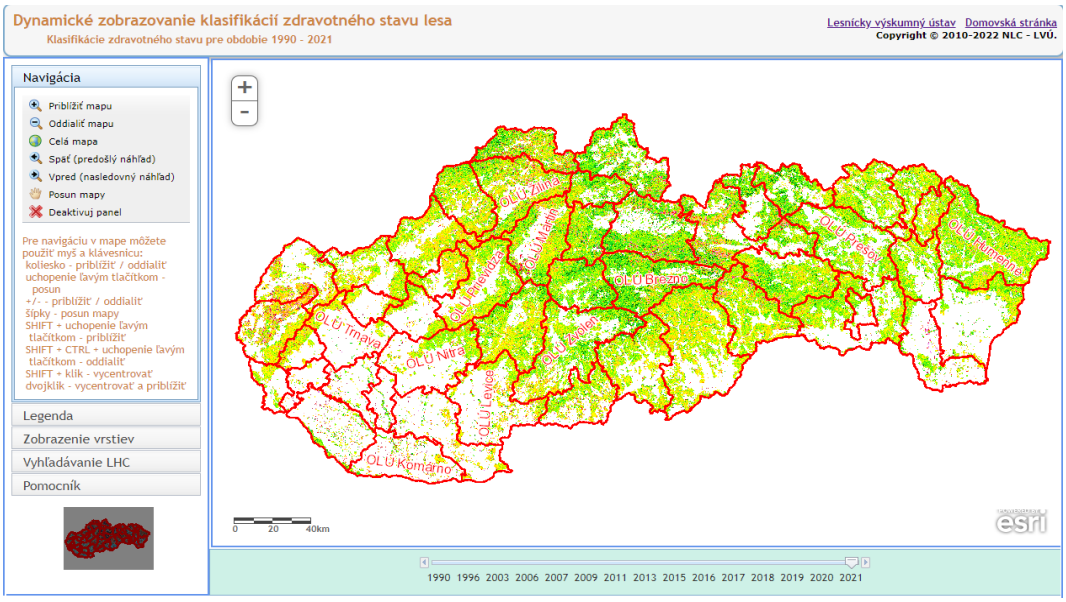

Figure 5.10. *Web service* http://www.nlcsk.sk/stales/klasdynam.html *– map application for dynamic visualization of forest health condition from 1990 to 2021.*

Biomass Mapping on Abandoned Agriculture Land

The activity focused on Above Ground Biomass (AGB) estimation on Abandoned Agricultural Land (AAL) by using radar data. Abandonment of land is a European problem and phenomenon when agricultural land is gradually overgrown with shrubs and forest. This wood biomass has not yet been systematically inventoried in Slovakia.

The first objective was to propose a method for AAL identification based on free data. We combined Sentinel-2 satellite images with data from the Land Parcel Identification System (LPIS) and the National Cadastre.

The second objective was to derive an allometric model for shrub AGB estimation on AAL Due to the lack of such models, we carried out a quantification of shrub AGB biomass on AAL sample plots.

The third objective was to separately analyse Sentinel-1 and -2 data, to test the backscattered amplitude and the interferometric coherence and their seasonal variation to determine the optimal period for AGB retrieval on AAL.

The fourth objective was to verify whether AGB estimation could be improved by integrated AGB regression models that combined radar and optical satellite data, multi-temporal data, polarimetric coherence and backscatter. The decision to apply empirical multiple regression models for AGB estimation came from their simplicity, comprehensibility and good performance, which are important for operational deployment.

Concept of Biomass Estimation on Abandoned Agricultural Land

A simplified flowchart of the concept of AGB estimation on AALis depicted on Fig. 5.11.

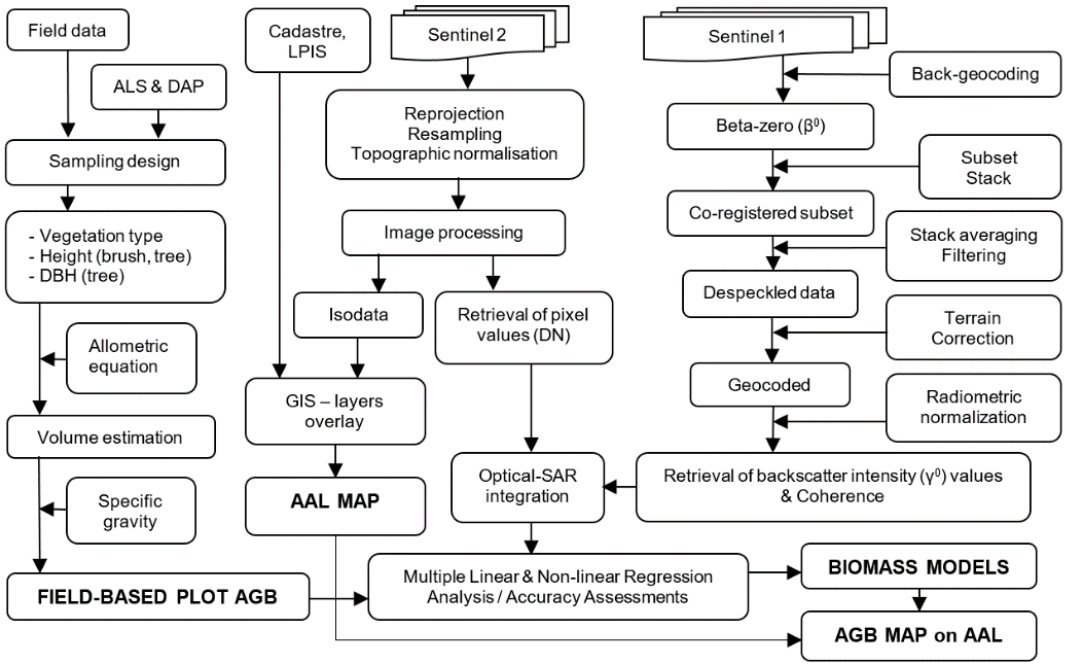

Figure 5.11. *Flowchart of the spatial identification and estimation of AGB on AAL. LPIS, Land Parcel Identification System; ALS, airborne laser scanning; DAP, digital aerial photography.*

AAL Identification

In spatially identifying AAL in the study area Víglaš we used a straightforward approach based on a combination of available cadastral data, LPIS and Sentinel-2 imagery.

The National Cadastre is a public land registry and information system containing, inter alia, geometric determinations and data about the types of land parcels. Cadastral parcels coded as arable land, permanent grassland (meadows and pastures) and orchards in the GIS vector format were used.

The Land Parcel Identification System (LPIS) is an integrated administrative and control information system based on photographs of agricultural parcels used to check payments made under the EU Common Agricultural Policy. The LPIS contains a vector layer of agricultural parcels and information about crop and land use, which are used on farmers' applications for subsidies. We assumed that such parcels represented actively managed agricultural land.

The LPIS vector boundaries of actively managed agricultural land (arable land, meadows and pastures) and cadastral parcels registered as agricultural land (of the same type) were overlaid to identify the land considered by LPIS as uncultivated. Those cadastral parcels that fell outside the LPIS blocks were considered as potentially abandoned agricultural land. Then we filtered out pixels under snow cover using Sentinel-2 imagery from the winter season; i.e., we masked arable land, meadows and pastures. Thus the remaining areas represented real AAL with woody vegetation.

Shrub Biomass Estimation

As regional biomass tables are not available for shrub vegetation, the allometric model for calculating the dry matter of the above-ground biomass of shrubs was derived based on the empirical material obtained from blackthorn stands in the study area Víglaš, which made up about 90% of all the bushes. The model was based on one independent variable (mean

height) and was expressed as the dry matter of the above-ground biomass per 1 m^2 at full canopy (Tab. 5.1.). The allometric equation was used to calculate the biomass: $m_{AGB} = b_0 h^{b1}$; where m is the weight of AGB in kilograms per m^2, h is mean height in metres, and b_0 and b_1 are regression coefficients.

Table 5.1. *Allometric model for quantifying above-ground woody biomass of shrubs on abandoned agricultural land*

Vegetation	Model	*n*	R^2	RMSE (%)	*p*-Value
Shrubs (blackthorn)	$m_{AGB} = 1.2417 \times h^{1.45361}$	20	0.81	23.9	<0.001

Predictor Variable Pre-Selection

The predictor variables are clustered into three groups: Sentinel-1 radar backscatter, Sentinel-1 coherence data and Sentinel-2 DN.

In the Sentinel-1 radar backscatter, the averages from the multi-temporal images from 2017 were calculated for leaf-on period; leaf-off period with snow; and leaf-off period without snow to reduce the speckle in the single images and to investigate the impact of the backscatter variation on the AGB estimation. The average $\gamma°_{VH}$ and $\gamma°_{VV}$ from a leaf-off period without snow cover were found to have the highest correlation with the AGB (r_{VH} = 0.79 and r_{VV} = 0.77). We included in the prediction model a variable calculated as the average of the ascending and descending passes. Averaging images from both tracks reduces the problems of artefacts caused by foreshortening and shadowing.

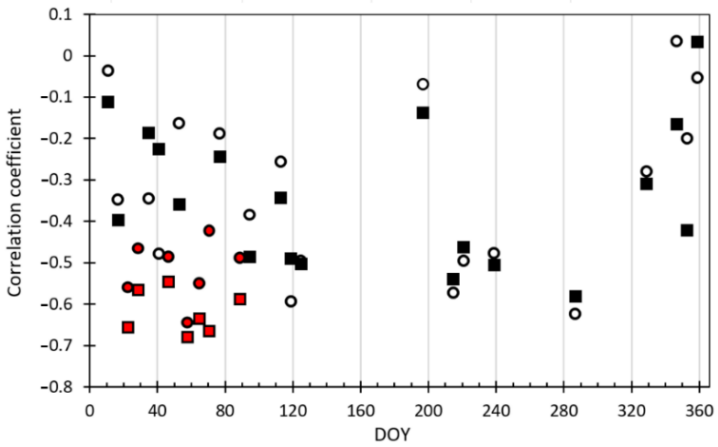

Figure 5.12. *Correlation coefficients between AGB and the coherence of VH (circle) and VV (square) polarisation during the year. DOY, day of year. The coherence pair temporal baseline is 6 days combining S-1A and S-1B images from 2017 . Red indicates the images used for the derivation of the average products. Correlations stronger than − 0.22 (−0.30) are significant at the 0.05 (0.01) level.*

Coherence data are the second group of variables significantly correlated with the AGB. The correlation coefficients between the AGB and the coherence are negative, as the coherence decreases with a higher AGB. Fig. 5.12. depicts the time series of the correlation coefficients between the AGB and VV and VH coherence during the year. The group with the highest correlations could be observed in the leaf-off period with snow cover (DOY 40 to 92), with the highest r_{VV} = −0.68 and r_{HV} = −0.64. Based on these findings, two prediction variables (Coh_{VV_avg} and Coh_{VH_avg}) were derived for the AGB estimation by averaging

the seven coherence pairs with the highest correlations from DOY 40 to 92. The correlation coefficient of the average coherence (r_{VV} = −0.77 and r_{HV} = −0.72) was higher than from the single pairs, and the average coherence was less affected by coherent noise. This confirms the importance of averaging coherent pairs.

In the case of Sentinel-2 DN values, the highest correlations with the AGB were observed for band B5 vegetation red edge (r_{B5} = −0.85) and band B4 red (r_{B4} = −0.76) from the top of the vegetation season (22 June 2017). In general, the red bands (B4 and B5) correlate higher than bands B8, near infrared (NIR), and B11, short-wave infrared (SWIR) (Tab. 5.2.).

Table 5.2. *Correlation coefficients between AGB and Sentinel-2 bands from 4 periods in descending order*

28 January 2017		29 March 2017		22 June 2016		30 September 2018	
Band	**r**	**Band**	**r**	**Band**	**r**	**Band**	**r**
B5	−0.65 ***	B4	−0.65 ***	B5	−0.85 ***	B4	−0.74 ***
B4	−0.64 ***	B11	−0.65 ***	B4	−0.76 ***	B5	−0.63 ***
B8	−0.57 ***	B5	−0.62 ***	B11	−0.47 ***	B11	−0.56 ***
B11	0.07°	B8	−0.49 ***	B8	0.01°	B8	0.44 +++

Performance of AGB Predictive Model

Considering the most correlated variables with AGB and removing the highly correlated predictors five variables were included for further analysis: $\gamma^{\circ}_{VH\_leaf\text{-}off}$ and $\gamma^{\circ}_{VV\_leaf\text{-}off}$ (average from ascending and descending images – Fig. 5.13a.), Coh_{VH_avg} and Coh_{VV_avg} (average of the seven highest correlations – Fig. 5.13b.) and $B5_{22vi}$ (Sentinel-2 B5 band from 22 June 2016 – Fig. 5.13c.).

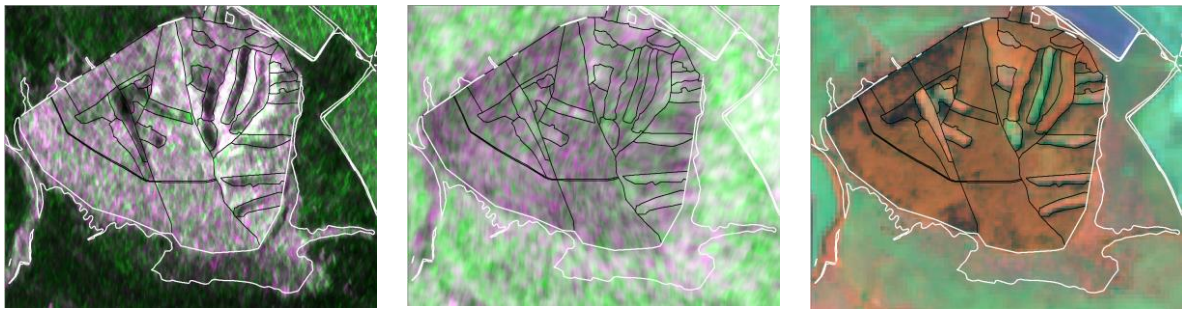

a) b) c)

Figure 5.13. *Lokality Chvojno in study area Víglaš:* ***a)*** *Composition of $\gamma^{\circ}_{VH\_leaf\text{-}off}$ and $\gamma^{\circ}_{VV\_leaf\text{-}off}$ (average from ascending and descending images) - black and green represent a lower, burgundy color a higher AGB;* ***b)*** *Coherence: composition of Coh_{VH_avg} a Coh_{VV_avg} (average of the seven highest correlations) - green color represents lower, grey-burgundy colors higher AGB;* ***c)*** *Composition of Sentinel-2 bands: B8/B11/B5 - green color represents lower, orange-brown color higher AGB.*

The Multiple linear regression (MR) model includes two additional terms, $Coh_{VH\_avg} \times B5_{22v}$ and $\gamma^{\circ}_{VV\_leaf\text{-}off}/B5_{22vi}$, as a common function of the predictive variables (Tab. 5.3.). Their

selection was based on the highest R^2 from all possible interactions derived by multiplying or dividing two predictive variables. Reference and estimated AGB is compared in Fig. 5.14a.

Table 5.3. *Significance of coefficient (predictors) in AGB models*

Model	$B5_{22vi}$	$\gamma^{\circ}_{VH\_leaf\text{-}off}$	$\gamma^{\circ}_{VV\_leaf\text{-}off}$	Coh_{VH_avg}	Coh_{VV_avg}	$Coh_{VH\_avg} * B5_{22vi}$	$\gamma^{\circ}_{VV\_leaf\text{-}off}/B5_{22vi}$
MR	***	*n.s.*	*n.s.*	***	*n.s.*	+++	+++

n.s., not significant; +++ highly significantly positive ($p < 0.001$); *** highly significantly negative ($p < 0{,}001$).

Dividing the reference AGB into three categories allows us to better understand the performance of the MR model (Fig. 5.14b.). The selected ranges approximately correspond with the AGB of shrubs (4–100 t.ha^{-1}), shrub–tree formations (100–200 t.ha^{-1}) and tree formations (200–350 t.ha^{-1}). The assessment was based on quantifying the root mean square error (RMSE), bias and random error within each range.

The accuracy analysis reveals that the model overestimates the AGB under ~200 t.ha^{-1} and underestimate above this level. The most considerable overestimation bias occurs in the AGB middle range between 100 and 200 t.ha^{-1} (Fig. 5.14. right). The RMSE (in absolute units t.ha^{-1}) increases with a higher AGB. On the contrary, relative RMSE and CV sharply decrease with a higher AGB. The random error (SE) is the dominant error source for all the ranges of AGB (Tab. 5.3., Fig. 5.14. right).

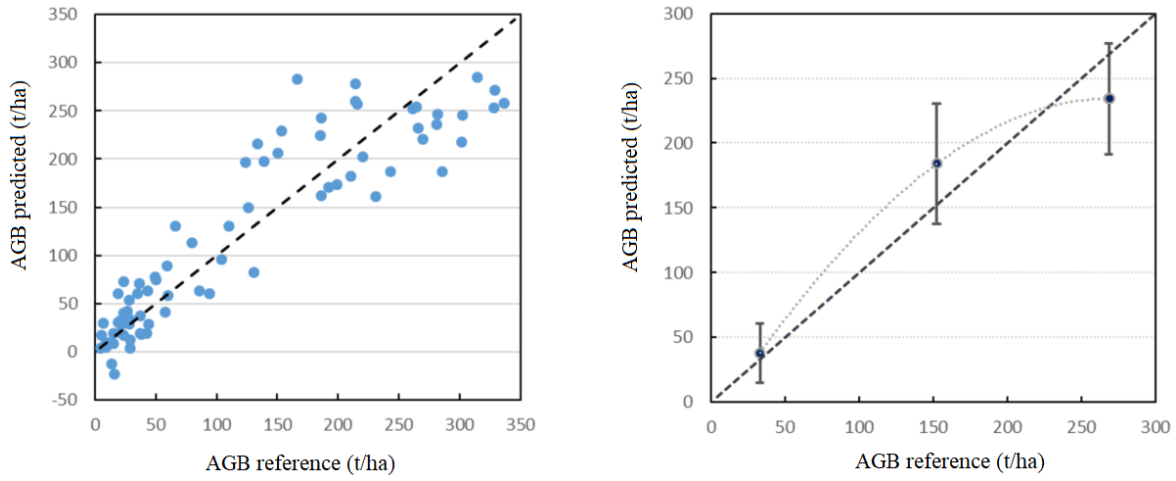

a) b)

Figure 5.14. Left: *Reference versus predicted AGB for Multiple regression (MR) model.* ***Right:*** *Comparison of the observed and predicted AGB averages per 3 reference AGB ranges: Error bars indicate a random error (SE) of the predicted AGB per reference AGB range. The dotted line indicates a fitting curve to calculated points (3rd order polynomial), and the dashed line corresponds to y = x line. If error bars do not overlap y = x line, bias is the dominant error in that AGB range.*

Table 5.4. *Accuracy of the model stratified by the reference AGB range: sample size (N), root mean square error (RMSE), relative RMSE (RMSE%), bias, standard deviation of the error (SE*

= Random error) and coefficient of variation (CV) of the error (when CV > 1, random error dominates; when CV < 1, bias dominates)

Model	Reference AGB (t.ha^{-1})	N	RMSE (t.ha^{-1})	RMSE %	BIAS (t.ha^{-1})	SE (t.ha^{-1})	CV
MR	0-100	42	23.7	70.5	5.1	22.7	4.5
	100-200	15	56.4	37.0	31.6	46.7	1.5
	200-350	20	55.0	20.5	-34.3	42.9	1.3
	Overall	**77**	**41.2**	**35.1**	**0.3**	**41.2**	**-**

AGB estimation on AAL in the study area of Forest managemnt unit Viglaš

The overall accuracy of the AAL map was verified on 127 randomly selected points and reached 89.8%, which confirms the potential for the operational deployment of the proposed method of AAL identification. In addition to 3214 hectares of forest land listed in the National Forestry Database for the Viglas forest management unit (FMU), we identified 992 hectares of shrub and tree formation on AAL. The total area covered by woody biomass is then 4206 hectares. Thus the proportion of AAL covered by woody biomass is 23.6% in the study area.

The estimated AGB was divided into nine categories in 50 t/ha step to clearly show its distribution on AAL (Tab. 5.5. and Fig. 5.15.).

Table 5.5. *Biomass estimation in Viglas according to MR model*

Class	Area		AGB	
t.ha^{-1}	ha	%	Tonne (t)	%
<0	47	5	0	0
0–50	194	20	4858	4
50–100	221	22	16,590	14
100–150	183	18	22,913	19
150–200	145	15	25,410	21
200–250	104	10	23,352	19
250–300	60	6	16,401	13
300–350	26	3	8479	7
350+	12	1	4343	3
	992	100	122,346	100

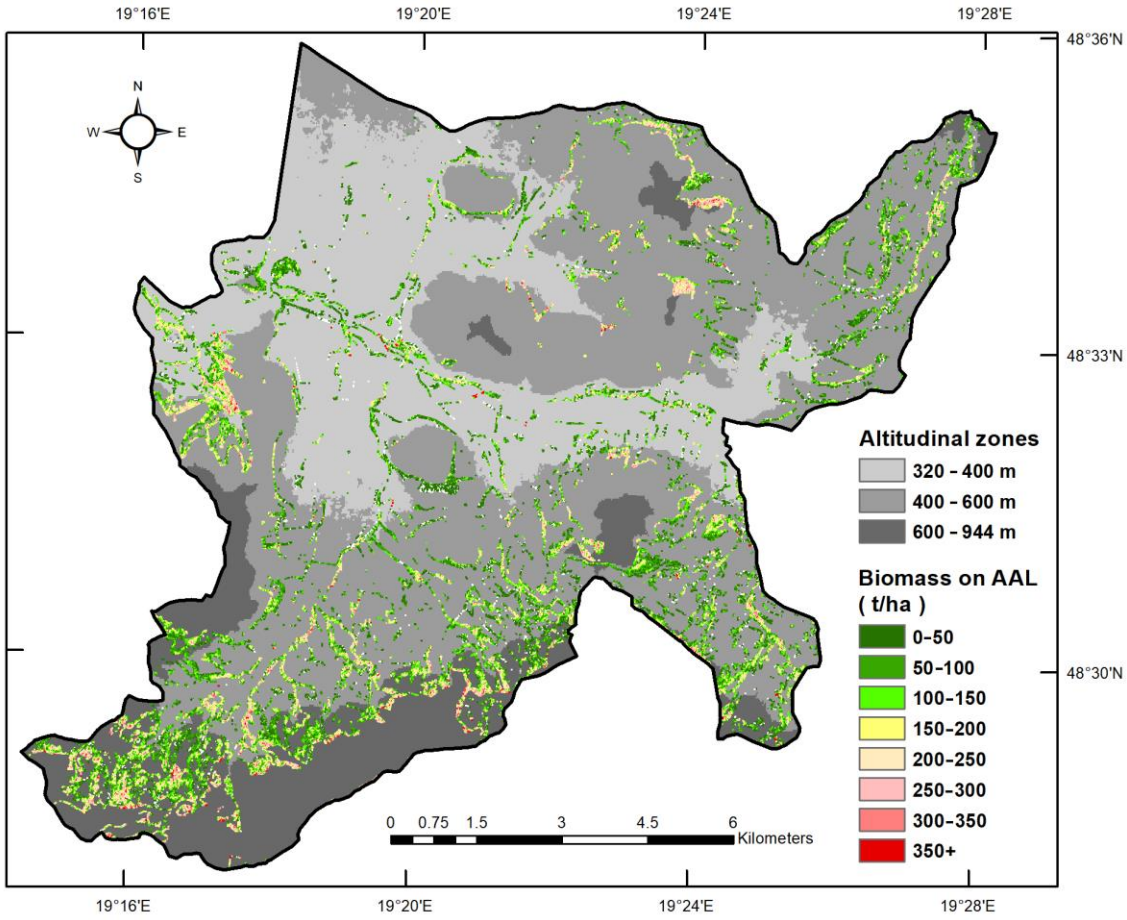

Figure 5.15. *Distribution of predicted above-ground biomass on abandoned agricultural land in the study area of FMU Viglas according to altitudinal zones (grey background colours). In order to enhance the visual perception, the number of pixels was magnified by a median filter with dimensions of 3 × 3 pixels.*

The estimated above-ground biomass on AAL was ~122,000 tons. The AGB on forest land is ~750,000 tons according to the National Forestry Database for the Viglas FMU. Total wood AGB is then ~872,000 tons in the whole area of the Viglas FMU. Thus the proportion of AGB on AAL is 14.0%, significantly less than the area proportion (23.6%). This indicates a lower mean AGB on AAL than on forest land. Indeed, the average AGB on AAL is 123 $t.ha^{-1}$, and on managed forest land it is 233 $t.ha^{-1}$.

The obtained results for wood AGB on AAL according to the area of individual classes show an uneven representation (Table 5.5.). The first three classes, with biomass from 0 to 150 $t.ha^{-1}$, represent up to 60% of the area. The occurrence of classes with AGB above 250 $t.ha^{-1}$ is only 10%. The predominance of low AGB classes indicates the dominance of shrub formations on AAL.

The spatial distribution of woody vegetation on AAL is uneven. The share of AAL increases with altitude and the distance from the populated part of the valley in the territory. The abandonment process is evident in the second and third altitudinal classes (Figure 5.15.).

In addition to the overgrowing of meadows and pastures, historical landscape elements like narrow-band fields, overgrown ramparts of collected stone are gradually disappearing under the influence of ongoing secondary succession. Summarising the acquired knowledge about the AGB, and its spatial distribution and shrub species composition, we can state that the situation of overgrowing areas is not satisfactory from either an economic or environmental point of view.

National Agricultural and Food Centre – Soil Science and Conservation Research Institute

Remote sensing control of area-based subsidies in agriculture

The subsidies play a key role in agriculture sector and contribute to the prosperity of agricultural subjects. The subsidies to agriculture sector represent major part of European budget and that is why there is taken an emphasis to the control.

During the years 2020 and 2021, the CwRS was no longer performed at the NPPC – VÚPOP, unlike previous years / periods.

Quality Assessment of Land Parcel Information System – QA LPIS (2020; 2021)

Land Parcel Identification System (LPIS) is the main component of Integrated Administration and Control System (IACS) for area based direct support. The purpose of LPIS is to implement the Common agricultural policy of the European Union (CAP EU) measures.

The quality assessment framework of LPIS is an integral part of LPIS management and upkeep processes and is also required by European legislation. EU member states are required to perform QA LPIS annually.

In this framework, the LPIS of a MS/Region is regarded as a system under test, which is composed of two major components: the local application schema and the data records stored in the system. The so called Executable Test Suite (ETS) targets at the data component by annually assessing conformity according to Article 6 of (EU) Regulation No 640/2014.

QA implementation is based on current satellite images taken in the year of review. Selected reference parcels by EC for QA LPIS were on SCRI vectorised on the background of current satellite images, provided by EC. Subsequently, they are compared with the valid state of the LPIS layer. The satellite images were overlaid with the digitized vectors showing the position of the parcels which were checked. The land use check was completed by Rapid field visits RFVs; directly in the field in cases of ambiguous situation on satellite images.

QA LPIS is realized through 9 quality elements, grouped into two conformance classes, as defined by the Regulation. Based on the item conformance verdicts issued for the various criteria during the item inspection, verdicts made on each conformance class. There are several reasons for errors. The two most common are operator error and outdated orthophotomaps/ land use changes.

The conformance class 1 means to *"assess the quality of LPIS"* and counts non-conforming items. Furthermore, counting items offers a straightforward entry for the LPIS upkeep processes. This counting of items includes the first three types of the quality elements (QE1, QE2 and QE3).

QE1 assesses the maximum eligible area of the system and evaluates 2 quality elements: QE1a absence of bias (i.e. accuracy) of the land represented in the LPIS as a whole, QE1b parcel level precision of the land represented in the LPIS as a whole – overestimation areas and underestimation areas.

QE2 assesses individual parcels with correctness issues and evaluates 3 quality elements: QE2a proportion of items with incorrectly recorded area or "contaminated" with ineligible features –error type Update – outdated orthophotomaps (Fig. 5.18.).

QE2b distribution of items, according to the correctness of the eligible area recorded and QE2c number of non-conforming reference parcels in LPIS with classification error –mistake/ error of operator (Fig. 5.19.).

QE3 shows number of reference parcels that have functional issues - "critical defects" (Fig. 5.17.).

Conformance class 2 is assessed under the last three elements (QE4, QE5 and QE6). QE4 categorization of the non-conformities, QE5 ratio of total declared area in relation to the total area recorded for the area conforming reference parcels and QE6 rate of non-conforming reference parcels due to undetected and unaccounted land cover change, as observed in ETS, accumulated over the years.

These 3 elements aim to *"identify possible weaknesses"* and this requires a broader system wide analysis, beyond the individual item or reference parcel. This is most obvious for QE4 which analyses the LPIS processes and design as factors for creating quality problems. For instance, a single, large parcel can be contaminated, can have critical defect (for example, multi-parcel), and can have its land wrongly classified. Although this represents a single non-conforming item, it does reflect three different system weaknesses.

Quality assessment of the Slovak LPIS was realized in three zones for campaign year 2020 and in three zones for campaign year 2021 (Fig. 5.16.). VHR satellite imagery for each zone were delivered from JRC EC.

Site 2020 QA SK – 1 covers parts of Prešov, Bardejov and Svidník districts (EK provided World View 2 satellite image from 9th April 2020), zone is localised in East Slovakia. Site 2021 QA SK - 2 covers parts of Čadca, Kysucké Nové Mesto and Žilina districts (EK provided GEO EYE 1 satellite image from 8th April 2020, zone is localised in North Slovakia. Site 2021 QA SK – 3 covers part of Námestovo district in north part of Slovakia (EK provided World View 2 satellite image from 27th June 2020).

Site 2021 QA SK – 1 covers parts of Michalovce, Trebišov and Vranov nad Topľou districts (EK provided World View 2 satellite image from 9th April 2021), zone is localised in East Slovakia. Site 2021 QA SK – 2 covers parts of Rimavská Sobota, Lučenec and Poltár districts (EK provided GEO EYE 1 satellite image from 16th April 2021, zone is localised in South Slovakia. Site 2021 QA SK – 3 covers parts of Dunajská Streda and Galanta districts in west part of Slovakia (EK provided World View 2 satellite image from 3rd June 2021).

The Satellite images were georeferenced by SSCRI staff. Measured and archive control and check points were used. For all three zones the Quality checks of georefence were carried out and control protocol were elaborated.

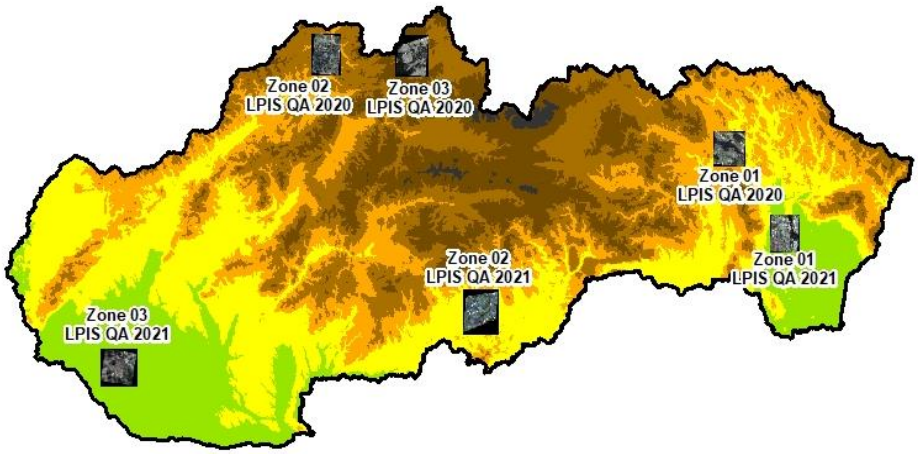

***Figure 5.16**. Localization of the controlled sites in QA LPIS 2020 and 2021.*

a) **b)**

Figure 5.17. *Example of case with identified critical defect: a) Invalid common RP boundary and b) Total absence of eligible features.*

Figure 5.18. *Example of the occurrence of non-agricultural land cover features on the reference parcels with causes "Update" – changes of the underlying land were not applied.*

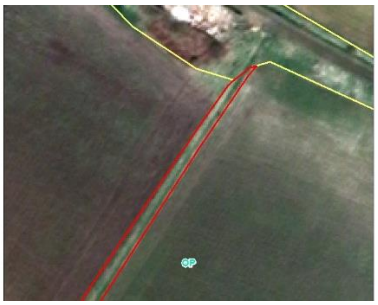

Figure 5.19. *Example of the occurrence of non-agricultural land cover features on the reference parcels with causes "Erroneous processing" – a mistake of LPIS operator.*

Remote sensing within crop yield and crop production forecasting (2020;2021)

Monitoring of Crop Conditions and Crop Monitoring

Regional monitoring of natural crop conditions aims to study the influence of weather (coupled with soil) on crop growth and crop development during current vegetation season.

NDVI (Normalized Difference Vegetation Index) are derived from NOAA's AVHRR sensor. The NDVI Vegetation Index, characterizes the total biomass state (volume and vitality), the higher the NDVI value, the more biomass is developed (characterized by a higher content of chlorophyll in plants and hence a more potent photosynthesis).

Development of the NDVI vegetation index in 2021 and its comparison with the situation in 2020 and long term average is documented on Fig. 5.20.

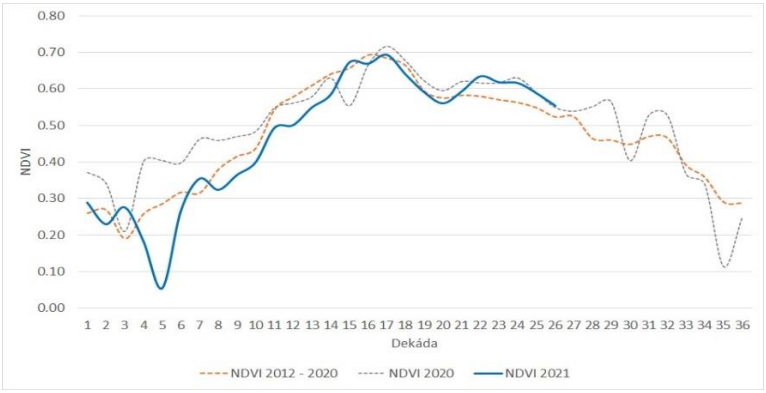

Figure 5.20. *Development of the NDVI vegetation index in 2021 and its comparison with the situation in 2020 and long term average, data source: NPPC – VÚPOP.*

Crop yield forecasting

The aim of the crop yield and crop production forecasting is to provide the most likely, scientific, and as precise as possible independent forecast for main agricultural crop yields for Ministry of Agriculture and Rural Development of the Slovak Republic and for the public.

National Crop Yield and Crop Production Forecasting System has been created on SSCRI and is based on three different principles which are applied to specify vegetation indexes as biomass development stage and biomass development:

- Remote Sensing method – method of interpretation of vegetation indicators (as NDVI or DMP – Dry matter development) from satellite images (mainly from low resolution satellite sensors as NOAA AVHRR and SPOT Vegetation satellite system);
- Bio-physical modeling (WOFOST model) and simulation of vegetation indexes (mainly TWSO – Total Dry Weight of Storage Organs and TAGP – Total Above Ground Production). In WOFOST, weather and phenological data, soil hydro-physical data and crop physiological data are utilized as model key inputs;
- Integrated assessment method, which means the implementation of specific meteorological and vegetation indicators in the statistical analysis, assesses the impact of weather on the projected harvest. Integrated estimate summarizes a wider range of disparate indicators and indices that are currently for the purposes of forecasting yields and consequently the production of crops used.

The crop yield and crop production forecasting is carried out for main agricultural crops – winter wheat, spring barley, oil seed rape, grain maize, sugar beet, sunflower and potatoes. The forecasts are reported six times per year – in the half of May, June and July for "winter and spring crops" and in the end of July, August and September for "summer crops". The forecast results are interpreted at national level as well as at NUTS3 and NUTS4 level. The example of crop yield forecasting in 2021 can be seen in the Fig. 5.21a. and 5.21b.

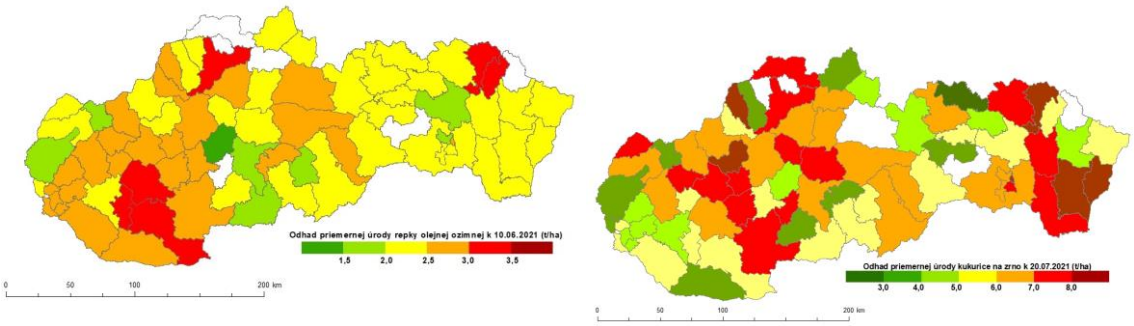

a b

Figure 5.21. *Example of crop yield forecasting with remote sensing in first decade of June in 2021 for rape (a) and in the second decade of July for maize (b).*

Verification of high resolution layer – "HRL" permanent grasslands for the reference year 2018

Verification of High Resolution Layer (HRL) of Small woody feature, Permanent Grassland and Permanent grassland changes was conducted on NPPC – VUPOP during years 2020 and 2021 according to the current methodology. „Guidelines for verification of High Resolution Layers produced by the CLMS (Copernicus Land Monitoring Service) as part of the 2018 reference year production. Verification of HRL Grassland - GRA and Grasssland changes - GRAC took place in 2020. The third layer of HRL – Small Woody Features – SWF was verified in 2021. SWF layer is new product based on VHR data, mapping small patchy and linear woody features. In 2021 a complete report was submitted for verification of HRL layers of GRA; GRAC and SWF too.

Copernicus, is the European Programme for the establishment of a European capacity for Earth Observation. The EEA has been delegated the implementation of the pan-European and local components of the Copernicus Land monitoring service. The objective of the Copernicus land monitoring service is to provide users in the field of environment and other terrestrial applications with information based on space data combined with other sources.

The clustomer in Slovakia was the Slovak Environmental Agency, Banská Bystrica, based on the requirements of the European Environmental Agency – EEA. Thematic accuracy assessment of the HRL Grassland layer is the goal of verification. The HRL layers are provided by EEA to NPPC through contract with Slovak Environmental Agency.

The HRLs are part of the land use/land cover mapping component of the Copernicus Land Monitoring Service (CLMS), serving a broad user community from European public bodies to Member States and regional environmental authorities, as well as the value-adding sector. They provide support to various environmental policies and political decision-making, and significantly contribute to assessing Europe's current environmental status and monitoring changes over time. Pan-European High Resolution Layers (HRL) provide information on specific land cover characteristics, and are complementary to land cover / land use mapping such as in the CORINE land cover (CLC) datasets.

HRL layers are produced primarily from Sentinels. The pan-European HRL 2018 SWF layer is available at 5 m and 100 m resolution (HRL GRA 10 m and 100 m and GRAC 10 m resolutions).

Verification was done by three methods: 1. a general overview of HRL data quality; 2. Verification using the "Look and Feel" method (for the recommended strata and two types of errors Comission and Omission) and 3. Quantitative verification.

Commission error is defined as the area classified erroneously as belonging to the HRL class.

Omission error is defined as the area classified erroneously as NOT belonging to the HRL class.

Type of "Omission error" – is documented on Fig. 5.22. SWF Omission error - Isolated/scattered patches of trees, an example from the east part of Slovakia- In this case, there was also probably a shift of whole SWF polygon to the north compared to the verification layer and orthophotomap.

Example of Comission error – is showed on Fig. 5.23. SWF Commission error – Linear hedgerows and scrubs, an example from the south west part of Slovakia. In this case, was SWF classified on the grassland without bushes and trees compared the situation on the orthophotomap.

Verification was carried out visually in GIS environment interpretation and comparison HRL based satellite layers with orthophotos and with thematic GIS layers generated from the LPIS, biotops of natural and semi-natural grassland and ZB GIS.

Figure 5.22. *SWF Omission error – Isolated/scattered patches of trees. An example from the east part of Slovakia.*

Figure 5.23. *SWF Commission error – Linear hedgerows and scrubs, an example from the south west part of Slovakia.*

Generally, we conclude that the layers HRL is not well classified, but much better than the HRL layer of 2015 reference year production.

Time series of satellite images would help to improve the accuracy of HRLs in future.

Ministry of Environment of the Slovak Republic (MOE SR)

Activities of the MOE SR were concentrated on the work involved with the Copernicus programe: Copernicus programe is the European programe for Earth Observation. The Programe entered its full operational stage in the year 2014. The work on the EU level was concentrated on cooperation with the Copernicus Committee, Copernicus Security board and Copernicus User forum and commenting on the EU level the technical and legislative documents regarding the Programe.

Cooperation with the European Space Agency (ESA) was limited due the fact that the Slovak Republic is not full member of ESA yet. However in 2020 Slovakia started process to became ESA Associated member state. Slovakia is going to become ESA Associated member state at august 2022. Slovakia is actively participating in Plan for European cooperating States (PECS). At the national level the Slovak national Copernicus working group continued its operation with the aim to coordinate Copernicus related activities on the national level and dissemination of information related to Copernicus programe. In 2021 new national Copernicus portal was published with information on Copernicus programe and data access. National satellite Copernicus imagery portal is still in development and MOE SR distributes the Sentinel satellite images for the Slovak Republic on demand. Compared to previous period user uptake and usage of the Copernicus data has growing trend but is still relatively low compared to neighboring EU countries. Several public government organizations and private companies are actively using Copernicus spatial data. MOE SR successfully collaborated with Slovak investment and trade development agency on international Cassini Hackaton event. In the following years Slovakia plans to focus on user trainings in remote sensing and Programe information dissemination.

Pavol Jozef Šafárik University in Košice is member of Copernicus Academy network and is actively using Copernicus programe spatial data in its courses and lectures. Private company InSAR is successfully operate as member of Copernicus Relays network, promoting the information about programe and data usage to public and professional through workshops, courses and conference. Two annual Hackathons were organized in Bratislava with successful use of the Copernicus data by the participants to develop application prototypes.

Slovak Environmental Agency (SEA) in Banská Bystrica

Activities of the SEA were concentrated on the work involved with the ***Copernicus*** programe and unmanned fixed wing UAVs survey for Regulations of Green Infrastructure Design (in Slovak MUSES – miestny systém ekologickej stability).

Copernicus programe is the European programe for Earth Observation. The Programe entered its full operational stage in the year 2014. The work on the EU level was concentrated on cooperation with the Copernicus Committee, Copernicus Security board, Copernicus User forum and Copernicus Ground segment task force and commenting on the EU level the technical and legislative documents regarding the Programe. Cooperation with the European Space Agency is limited due the fact that the Slovak Republic is not full member of ESA yet. Cooperation with the European Environment Agency (EEA) was concentrated on implementation of the CORINE Land Cover (CLC) 2018 and High Resolution Layer (HRL) products as a part of the Copernicus Land observation service.

Copernicus Land Monitoring

SEA joined the activities in project Copernicus Local Land monitoring services under Framework Contract EEA/IDM/R0/16/009/Slovakia. The contract between SEA and EEA was signed on 8 June 2017 and project tasks were implemented from autumn 2017 till the end of 2021. The project flagship was CLC2018, the fifth CLC inventory in Europe. The final integrated European results is available since late 2018.
Next tasks were finalized in 2020-2021 by SAE:

- Post-production verification of the High Resolution Layers (HRL) for the 2018 reference year (Imperviousness, Dominant Leave Type, Grasslands, Small woody features Water and Wetness) with participation of *National Forest Centre* and *National food and agriculture center*.
- Support and testing of future CLC+
- CLC+ Backbone Raster verification (reference year 2018)
- Refinement of land use inventory for Slovakia (based on national resources only)
- Creation of simplified LULUCF LUA layer for CLC+ verification purposes

UAV surveys

From April 2020 SAE could use UAV devices for capturing data used for Regulations of Green Infrastructure Design. First testing flights were held from September 2020. For surveying there is one fixed wing UAV and one multicopter. 5 different cameras (visible, IR, thermos, hyperspec, 3D visible) available. In 2021 several hundreds of images were acquired in 5 locations. Precision test, and several case study analyses was realized. In 2022 number of mapping locations probably increases to several tenth.

References:

[1] BARKA, I – BUCHA, T.: (2021). Satelitné monitorovanie zdravotného stavu lesov Slovenska (Satellite monitoring of the health status of forest in Slovakia). In. Tóthová, S., Gergeľ, T., (eds): *Zborník odborných prác z konferencie – LignoSilva,* Zvolen 28. 9. 2021. Zvolen: NLC, pp. 84-92.

[2] BUCHA, T. – PAPČO, J. – SAČKOV, I. – PAJTÍK, J. – SEDLIAK, M. – BARKA, I. – FERANEC, J.: (2021). Woody Above – Ground Biomass Estimation on Abandoned Agriculture Land Using Sentinel-1 and Sentinel-2 Data. *Remote Sensing,* 13, 2488, 1-24.

[3] FEDOR, T. – HOFIERKA, J.: (2021). Increasing the accuracy of the WRF-ARW numerical weather prediction model using Corine Land Cover and JAXA data. *Geographia Cassoviensis*, 15, 218-232.

[4] FERANEC, J.: (2020). Prístupová cesta Slovenskej republiky do Európskej vesmírnej agentúry (Accession of the Slovak Republic to the European Space Agency). In Luby, Š., Peťko, B. (eds.). *Slovenské vesmírne odysey (Slovak Space Odysseys): (spomienky a prognózy pri príležitosti 20. výročia slovenského letu na stanicu Mir – memories and forecasts on the occasion of the 20th anniversary of the Slovak flight to Mir station) (in Slovak)*, pp. 89-102. Bratislava: Veda.

[5] FULMEKOVÁ, Z. – ZVERKOVÁ, A. – SKALSKÝ, R. – SVIČEK, M. – KUSÝ, D.: (2021). *Application and updating of the national agro-meteorological modeling system to estimate crop production and crop yield (SK_CGMS).* Final report to solving tasks under the contract with MPRV for the year 2021. SSCRI Bratislava, 35 pp.

[6] GOGA, T. – SZATMÁRI, D. – FERANEC, J. – PAPČO, J.: (2020). Abandoned Agricultural Land Identification Using Object-based Approach and Sentinel Data in the Danubian Lowland, Slovakia. *The International Archives of the Photogrammetry, Remote Sensing and Spatial Information Science* – ISPRS Archives, Vol. 43-B3, 1539-1545.

[7] HOFIERKA, J. – GALLAY, M. – ONAČILLOVÁ, K. – HOFIERKA, J. Jr.: (2020). Physically-based land surface temperature modeling in urban areas using a 3-D city model and multispectral satellite data. *Urban Climate,* 31, 100566.

[8] HOFIERKA, J. – BOGĽARSKÝ, J. – KOLEČANSKÝ, Š. – ENDEROVA, A.: (2020). Modeling Diurnal Changes in Land Surface Temperature in Urban Areas under Cloudy Conditions. *ISPRS Int. J. Geo-Inf.*, 9, 534.

[9] KOLEČANSKÝ, Š. – HOFIERKA, J. – BOGĽARSKÝ, J. – ŠUPINSKÝ, J.: (2021). Comparing 2D and 3D Solar Radiation Modeling in Urban Areas. *Energies,* 14 (24), 8364.

[10] SAČKOV, I. – BARKA, I. – BUCHA, T.: (2020). Mapping Aboveground Woody Biomass on Abandoned Agricultural Land Based on Airborne Laser Scanning Data. *Remote Sensing,* 12, 4189.

[11] SVIČEK, M. – PÁLKA, B. – PÁLKOVÁ, S. – HUTÁR, V. – ZVERKOVÁ, A.: (2021). Post-production verification of High Resolution Layers for the 2018 reference year HRL 2018 look & feel verification report for GRAC – Grassland Change. *Portfólio aktivít európskeho projektu „Copernicus Local Land Monitoring Services"*. Banská Bystrica: Slovenská agentúra životného prostredia, 15 pp.

[12] SZATMÁRI, D. – FERANEC, J. – GOGA, T. – RUSNÁK, M. – KOPECKÁ, M. – OŤAHEĽ, J.: (2021). The Role of Field Survey in the Identification of Farmland Abandonment in Slovakia Using Sentinel-2 Data. *Canadian Journal of Remote Sensing*, 47, 4, 569-587.

[13] ŠUPINSKÝ, J. – GALLAY, M. – HOFIERKA, J. – BOGĽARSKÝ, J.: (2021). Krajina na dotyk: nové formy vizualizácie a interakcie s geopriestorovými dátami (Tangible landscape: new forms of visualizationand geospatial data interaction). *Kartografické listy / Cartographic Letters*, 29(2), 60-70.

[14] TIAN, Y. – BIAN, Z. – LEI, S. – JI, C. – ZHAO, Y. – ZHANG, S. – DUAN, L. – SEDLÁK V.: (2021). A process-oriented method for rapid acquisition of canopy height model from RGB point cloud in Semi-arid region. *IEEE Journal of Selected Topics in Applied Earth Observations and Remote Sensing*, 14, 12187-12198.

[15] YU, Z. – ZHANG, Q. – ZHANG, Y. – ZHENG, N. – SEDLÁK, V.: (2021). Singular value decomposition-based iterative robust cubature Kalman filtering and its application for integrated global positioning system/strapdown inertial navigation system navigation. *IET Radar, Sonar and Navigation*, 15, 12, 1727-1735.

6. SPACE METEOROLOGY

J. Kaňák, Ľ. Okon, L. Méri, M. Jurašek

6.1 Preparation for processing and usage of new imagery data from Meteosat third generation satellites, including Flexible Combined Imager and Lightning Imager instruments

6.1.1 New EUMETSAT satellites

EUMETSAT satellite programs are split into current (operational) and future satellite series. For operational usage in Slovak Hydrometeorological Institute, current satellites we use regularly in real-time or near real-time for weather analyses and forecasts, for monitoring of severe weather and its impact on economic and everyday life. Meteosat Second Generation (MSG) satellites EUMETSAT will replace them with Meteosat Third Generation (MTG) in the end of 2022. Satellite with the instruments is shown in Figure 6.1. Therefore all users and mainly national meteorological services must be prepared to switch from MSG to MTG data, imagery and products. This requires enhancing reception chain for satellite data, increase data transmission widths, processing and computing capabilities and the application software. There are ways that are more possible how to adapt the current capabilities for future effective usage of next generation satellite data. Some of them is the heritage and skills already existing in SHMÚ, some are part of upgrades and new developments of the software for processing and visualization of satellite data.

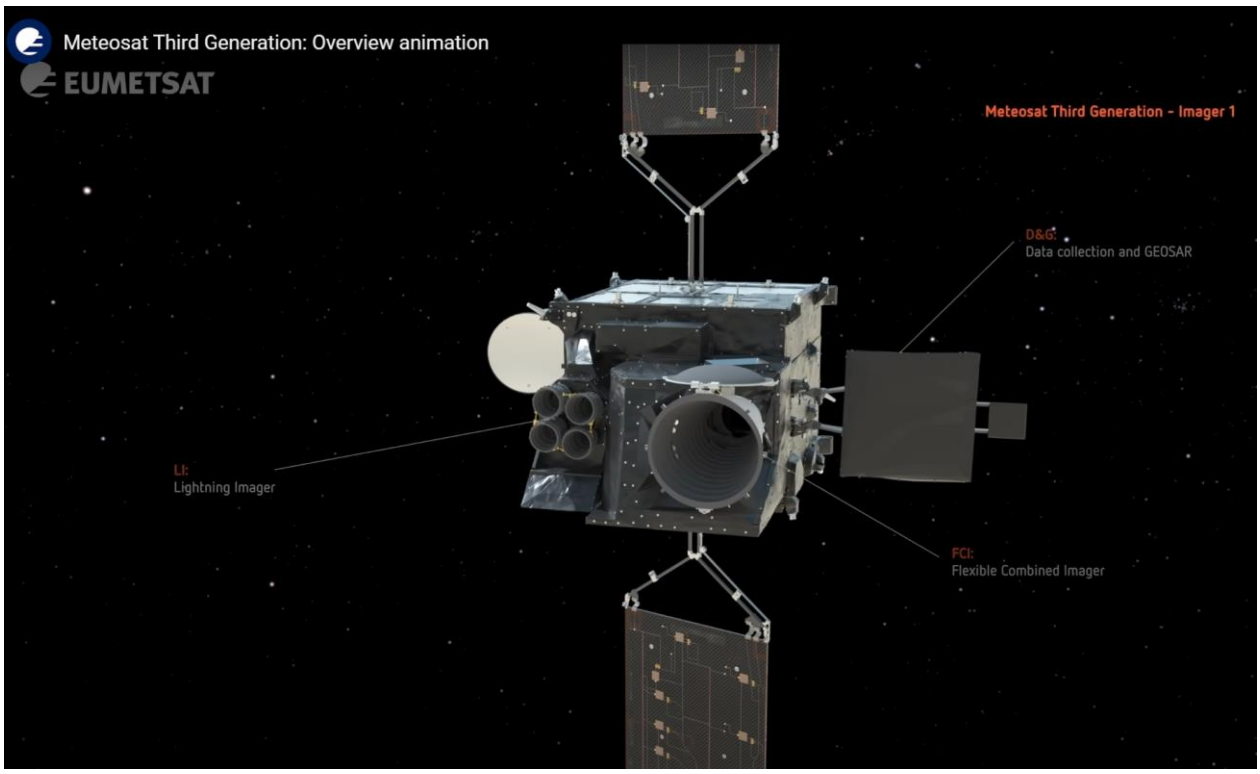

Figure 6.1. *MTG-I1 satellite and its instruments.*
Source: https://www.youtube.com/watch?v=LQ3xHJasKK8

6.1.2 MTG Lightning Imager Simulated Level 2 products: experience in Test Data processing and visualization.

This study we performed in a cooperation of NIMH (National Institute of Meteorology and Hydrology) Bulgaria and SHMI (Slovak Hydrometeorological Institute) with the aim of familiarization with the MTG Lightning Imager (LI) Data in three steps:

- Processing of LI Level 2 Test Data,
- Reporting faced problem in LI Level 2 Test Data processing,
- Visualizations & mapping the LI detections over Meteosat Imagery produced by MSGProc Software developed and operationally used in SHMI.

LI Level 2 Test data were available as three categories: LGR files containing flash groups within a time window of 10 seconds, LFL files containing the properties of the flashes within the same time window, and AFR files containing the accumulated information over 30 seconds gridded in 2km geo-satellite view projection. We worked with the second and the third type of test data. Fata files were available in standard NetCDF format and we worked with HDFView-3.0-win10_64 software to familiarize with the data content. After this, we prepared C-shell scripts to use HDF5-1.8.5 library and created C-routines running under Linux for geolocation and visualization of the flashes over the satellite imagery.

Final work was devoted to the interpretation of flash test-data originated from ground-based detections but in mode of satellite-ingested data sets. Main aim we fulfilled – to confirm that test-data are correctly encoding, geographically located and properly visualized over the real satellite scenes. Examples of visualization we provide in Figures 6.2. and 6.3.

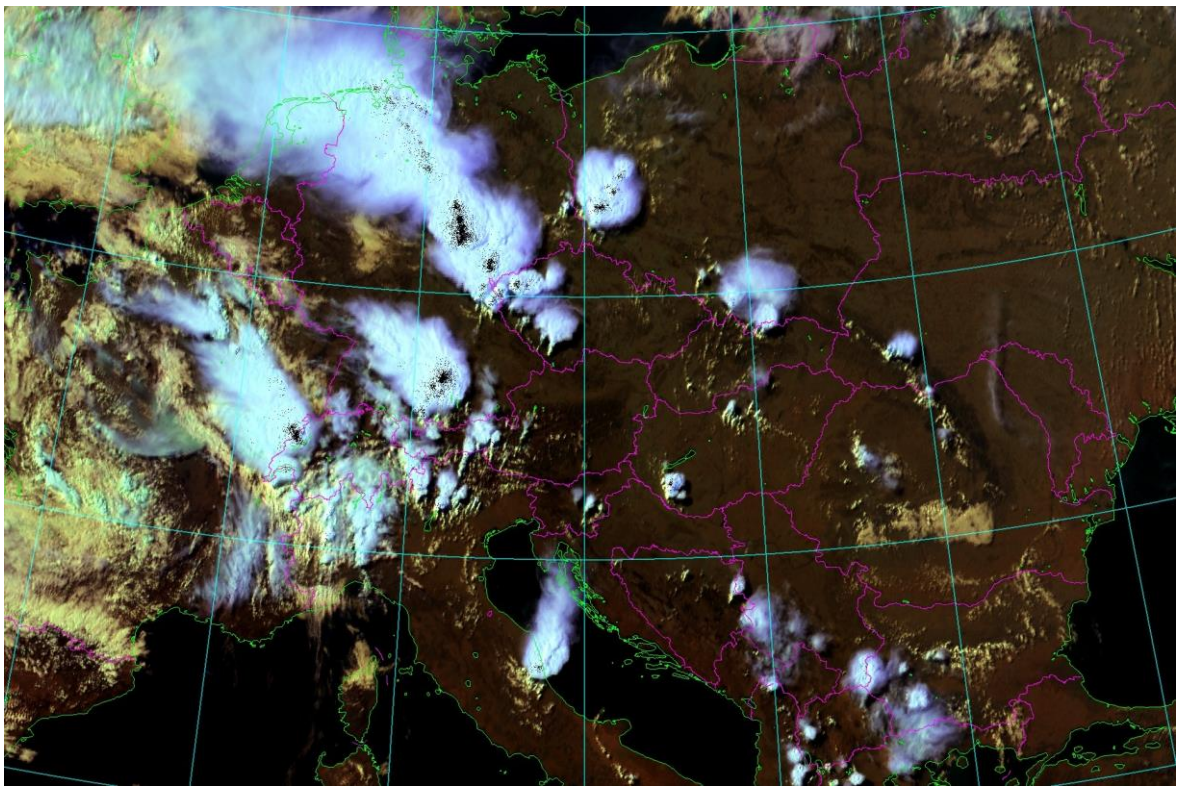

Figure 6.2. *Localization of flashes over storm clouds in single black-points interpretation. MSG HRV 20.6.2013 15:30UTC*

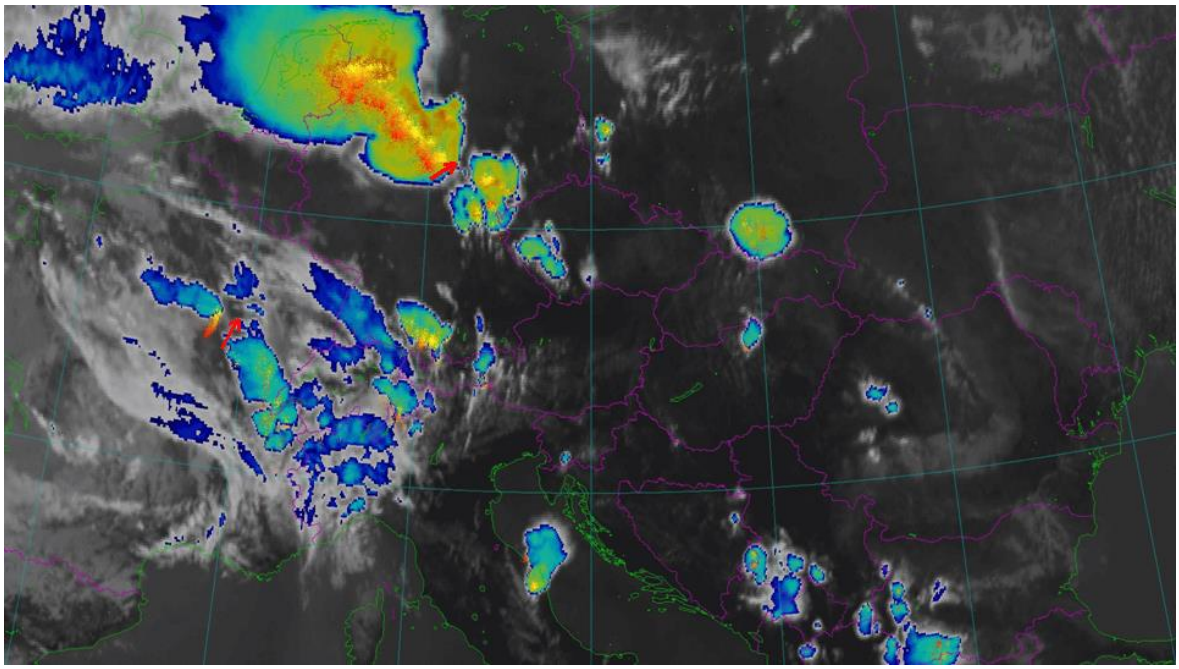

Figure 6.3. *Enhanced IR MSG RSS 20.6.2013 15:30UTC and 60-minutes flashes accumulations colorized from red (the oldest) to yellow (the newest). Red arrows indicate the movement of the lightning activity related to the storms development.*

6.1.3 Investigation of possibilities of dual satellite observations with new generation of geostationary satellites

Dual satellite observations are possible when two identical geostationary satellites are operating from positions distant at least 10, maximum 75 degrees in longitude. In case of European MSG satellites it is 41.5 degrees between Meteosat-8 and Meteosat-11, in case of NASA GOES satellites it is 62 degrees.

Thanks to the preparation of software for MTG satellites, which can be used just as well for GOES satellites, which are already operational, we have done several studies of stereoscopic cloud imaging at a higher resolution of 2 km. The aim was to verify that stereoscopy works not only with black-and-white single-channel images, but also with multi-channel color RGB images. We tested several RGB products listed here:

a) 24hMicrophiscs
b) Airmass
c) CloudPhase
d) CloudTypes
e) DailyCloudPhase_Distinction
f) DayMicrophysical
g) DaySolar
h) FireTemperature
i) NaturalColors
j) NaturalColorsWhite
k) NaturalTrueColors
l) Night
m) NightLowClouds
n) NightMicrophysical
o) VIS-IR
p) VolcanicAsh

As result from this study, Optimized Color Anaglyph method is the best, but also Full Color Anaglyph method can provide satisfactory results. However, these methods do not work in general, only for selected RGB products, where red component is not dominant, because red component transforms into black when anaglyph algorithm is applied. We learned from the comparison of standard and anaglyph RGB images following:

- Red color is reduced significantly because of anaglyph's algorithm, therefor clouds displaying at standard RGB in red, appear black in anaglyph,
- Some RGBs appear similar in anaglyphs, namely Natural colors, Natural white, True colors group, Cloud phase, Day solar, VIS-IR, Volcanic ash,
- 3D cloud height perception helps user to recognize more clearly between snow, low level clouds, fog in contrast with high thick cirrus clouds,
- 3D cloud height perception helps to recognize storm top features and better localize anvil cirrus clouds extension.

Figures 6.4. and 6.5. demonstrate the result of RGB Cloud Types product created from GOES-16 ABI instrument and combined into anaglyph using the same product generated form GOES-17 ABI instrument. Both satellites must measure at the same time for correct stereographic effect. We classify cloud types in this satellite scene and following categories were recognized:

1. Land surface
2. Land surface covered by snow
3. Thin high-level clouds with ice particles
4. Low level clouds
5. Glaciating clouds
6. Thin mid-level clouds with water droplets
7. Water surface
8. Thick high level clouds with ice particles
9. Thin mid-level clouds with water droplets

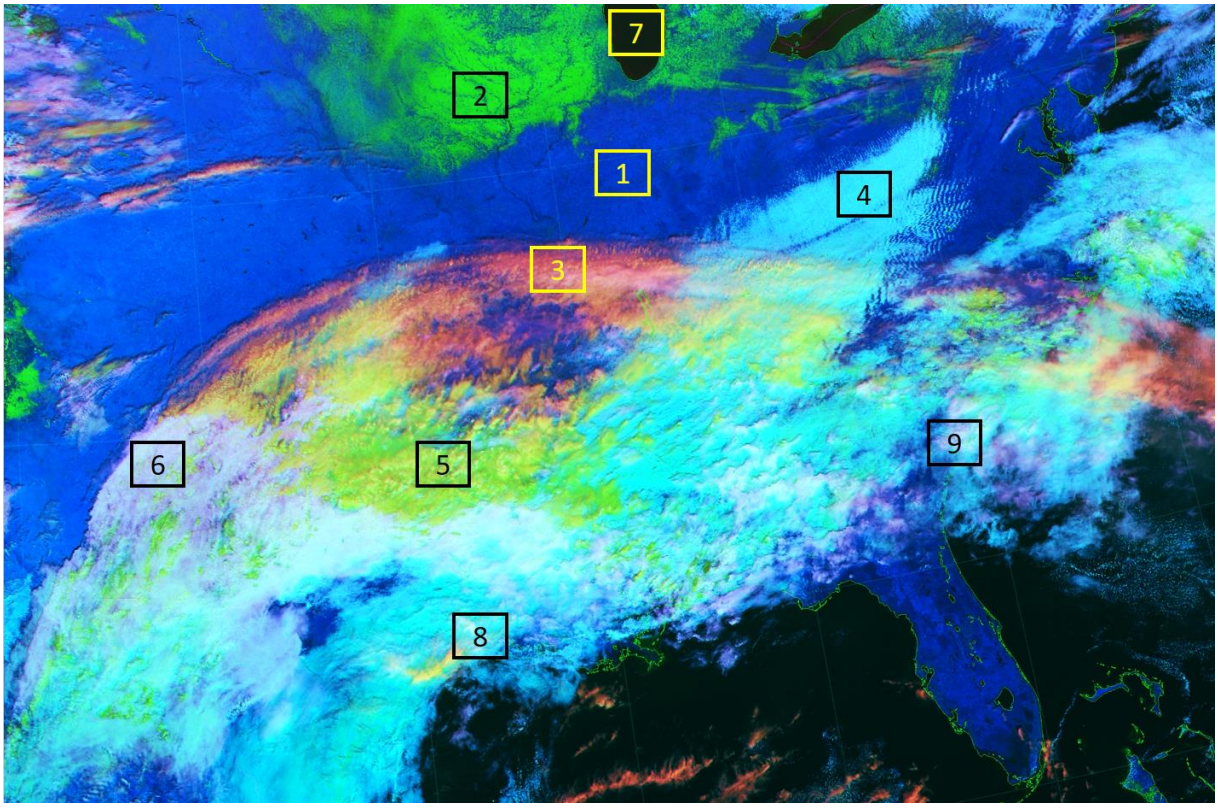

Figure 6.4. *RGB Cloud Types product from GOES-16 satellite.*

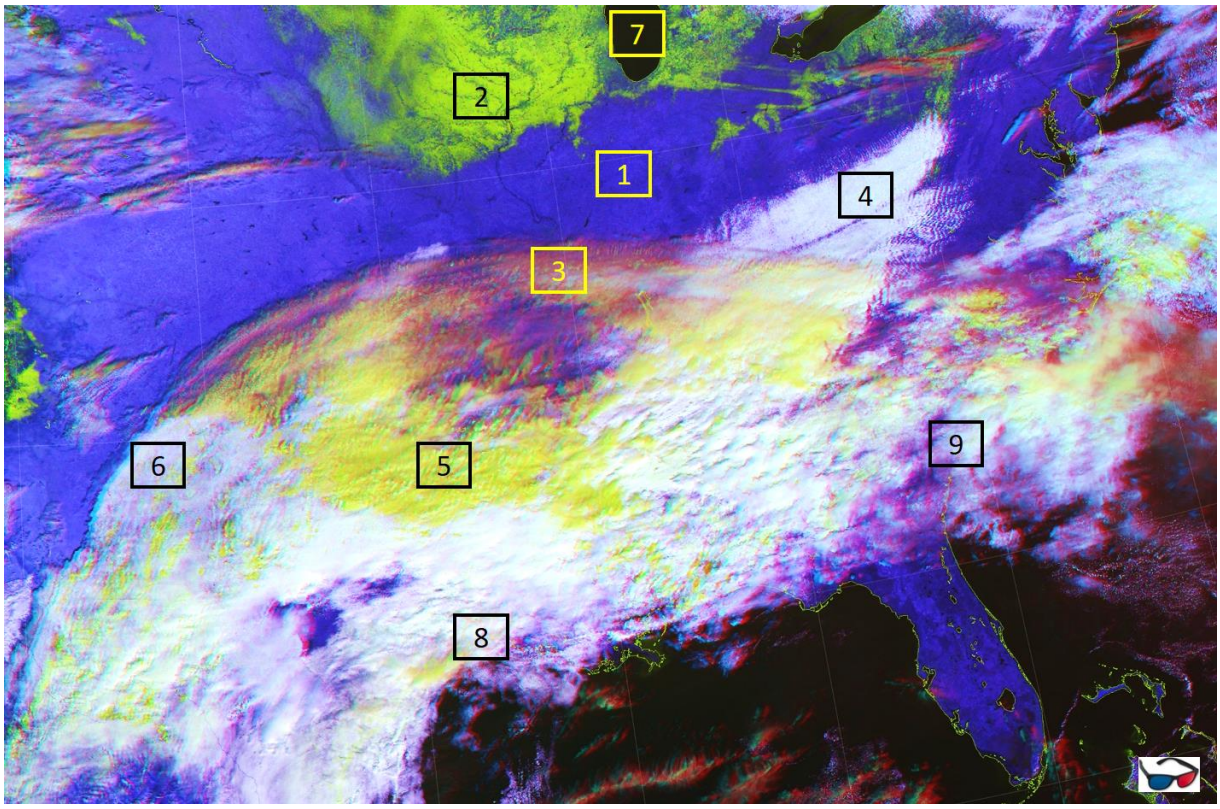

Figure 6.5. *Stereoscopic (anaglyph) RGB Cloud Types product from GOES-16 satellite.*

Categories numbers in the boxes over the image indicate the location of each classified cloud category.

Comparing Figures 6.4. and 6.5. we can state following:

Figure 6.4. contains data only from single satellite and help users to recognize cloud types by different colors. Information about cloud top height must be deducted from conceptual or NWP models and from previous working skills. Figure 6.5. contains data from dual satellite view integrated into RGB product and overlapped parallax shifts of clouds, which directly relates to cloud top height. Partial losses of colors and necessity of special glasses (anaglyph) can be considered as disadvantage. However, availability of this kind of information in near-real time can be useful to help users in quick decision-making activities. Operational graphical display systems are usually not ready to provide such operational types of information, so they remain only in the experimental testing phase.

6.2 New unified common code developed at SHMI in 2021 for validation of latest satellite precipitation products

6.2.1 H-SAF precipitation products quality assessment and meteorological applications

Traditionally, SHMI is participating on validation program of EUMETSAT HSAF project and every year we perform comparison of HSAF precipitation products against measurements of Slovak radar network. In 2021, EUMETSAT HSAF prepared new collection of products, namely H60, H61, H64, H67 and H68. All these products are new versions of previous products, providing instantaneous and accumulated precipitation fields, but region and/or data formats developers upgraded to the more general new standards of gridded meteorological data. For

these reasons old version of Unified Common Code (UCC) software was no more compatible with new products. We performed set of instantaneous changes of UCC codes and adopted compatible with new products. This work we done in extremely short time and tested by other members of HSAF team. After successful testing new version of UCC, we distributed software package to all members of HSAF consortium for yearly validation work. This task was important milestone of the project in its third continuation phase period called CDOP3 (2017-2022).

In the end of 2021 also user training was organized by HSAF and presentation provided to users can be accessed at EUMETrain web page: http://eumetrain.org/resources/precipitation_ew2020_s5a.html.

Quality assessment of the product is crucial before product will be used because:

- Validation methodology is complex and requires work with data,
- Detailed description users can find in PUM (Products User's Manual).

Users are encouraged to ask for data and products to be:

- Implemented in NHMS operational processing chains,
- Available for operational qualitative and quantitative usage.

6.3 Satellite products at SHMÚ and their potential in monitoring precipitation and drought

6.3.1 EUMETSAT HSAF and SHMÚ cooperation

Primary satellite data, especially images from the Meteosat satellite of processing level L1.5, have been receive and used at SHMÚ for a long time, especially in operational mode in the Department of Meteorological Forecasts and Alerts in the form of animations of color composite images. Data processed into higher-level products are still use less frequently, especially in the context of processing by NWC SAF software, or directly by SAF products received by the EUMETCast Satellite receiving system. Such products include the hydrology support products of the EUMETSAT H SAF (Hydrological Satellite Application Facility). SHMÚ, as a member of the consortium, has long been involved in the task of validation of products for precipitation detection and hydrological applications of these products. We present to the professional public operational satellite products for precipitation detection, the procedure for their validation and a case study presenting the use of these products in evaluating the long-term accumulated precipitation. Accumulated precipitation can be useful to monitor periods of droughts with precipitation deficits and surpluses. The ambition of this work is to show future users of satellite data that satellite products of a higher level of processing have the potential for climatological studies. A significant increase in this potential is expected in the near future thanks to the launch of the new generation of MTG (third generation Meteosat) and EPS-SG (second-generation European Polar System) satellites. Current measurements based on microwave SSM /AMSU-A/B instruments and Instruments, as we schematically show in Figures 6.6. and 6.7.

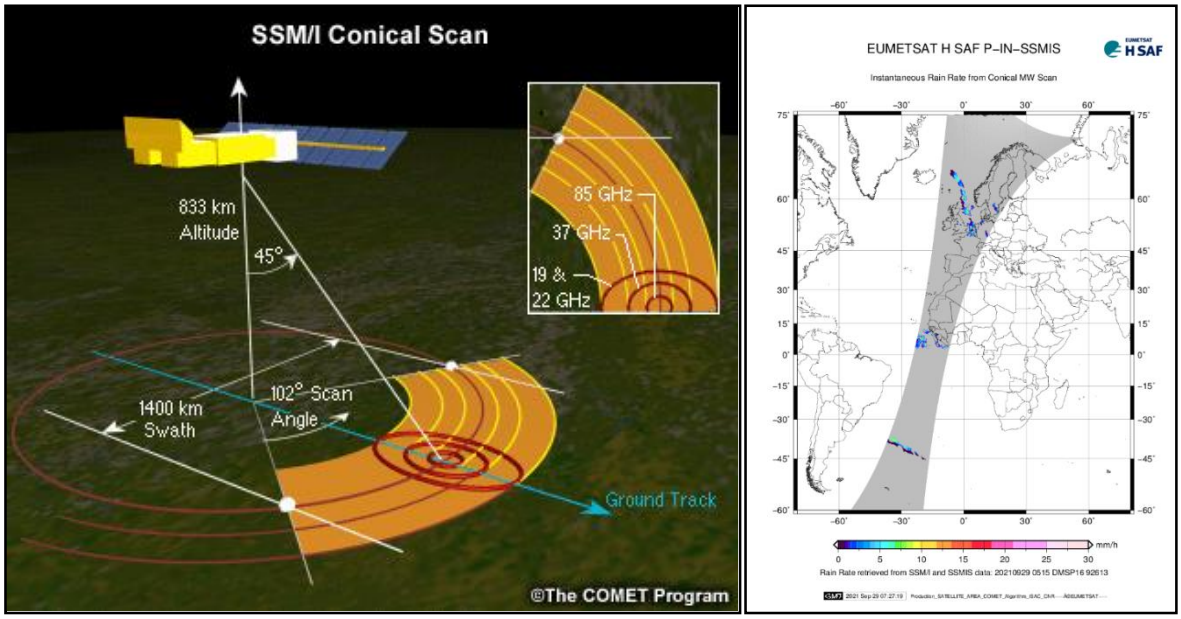

Figure 6.6. *Left – Geometry of conical scanning for SSMIS, source https://www.comet.ucar.edu/. Right – example of the P-IN-SSMIS product.*

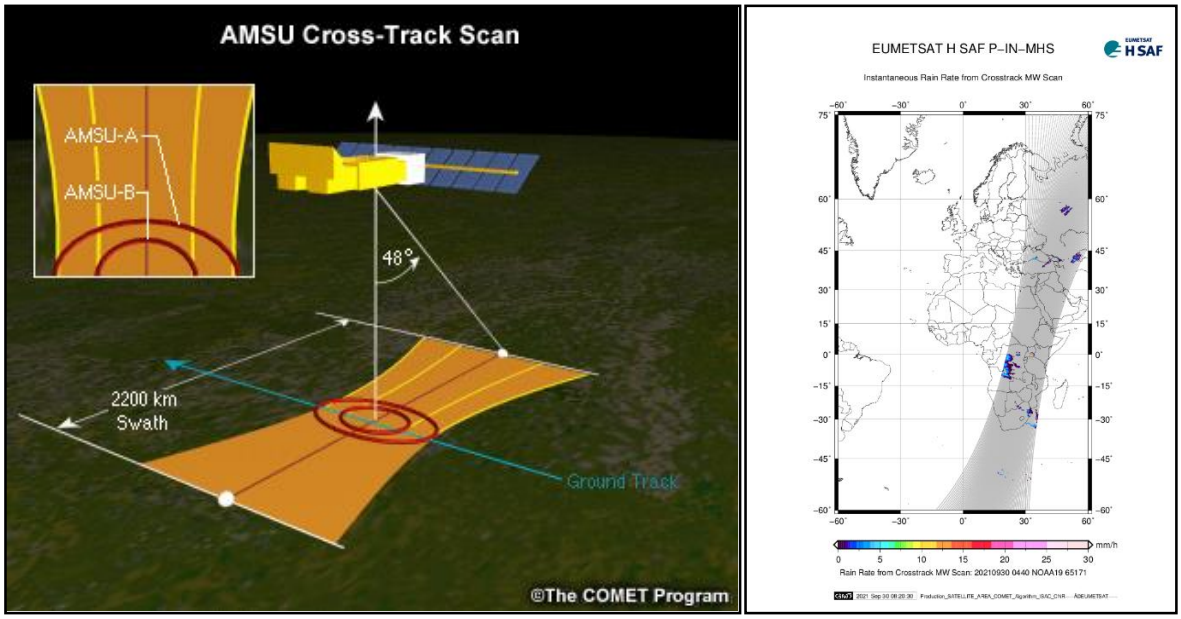

Figure 6.7. *Left – Viewing geometry of cross-track scanning radiometer AMSU-A, right – example of the P-IN-MHS product.*

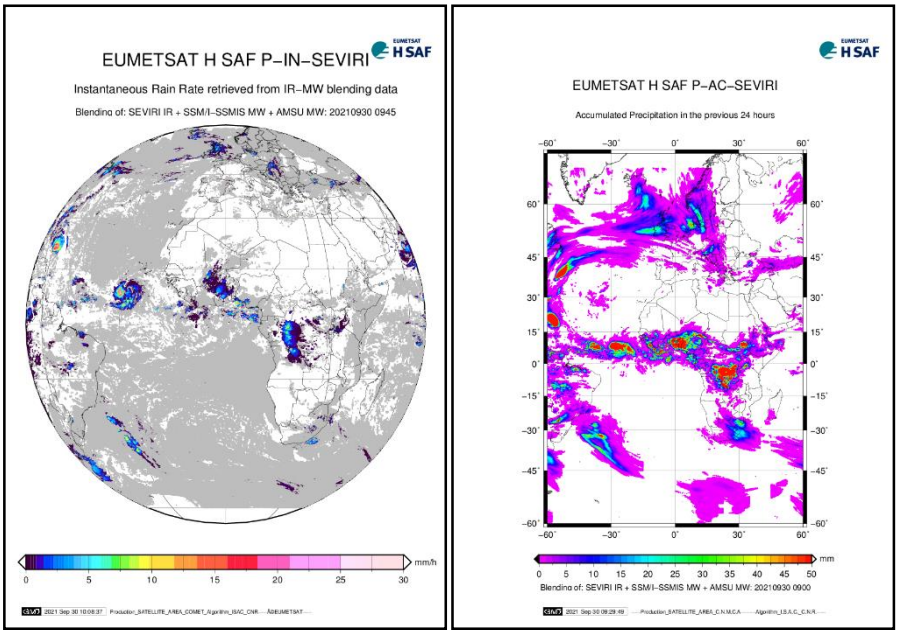

Figure 6.8. *Example of the P-IN-SEVIRI (left) and P-AC-SEVIRI (right) product, used in our study to monitor long-term drought periods over selected regions.*

6.3.2 Preparation of data for comparison

SHMÚ database – 24-hour rain totals:

- We checked the availability of data in the period 2012-2020 and selected only stations without gaps (9 years)
- To improve basins coverage by rain gauges we decided to use also gauges closed to the basin
- We calculated the average value of the totals over the basin for 9 years for each day of the year
- We obtained a long-term precipitation average as a replacement of the climatological standard (Hereinafter referred to as CS)

HSAF database – 24-hour rain totals:

- H05 data previous versions (before 2012) were considered inconsistent for further use we have available 9 years of data covering continuously this period,
- Therefore our decision to work with the years from 2012 to 2020,
- Advantage – we could use already pre-processed satellite data thanks to previous validation and hydro validation activities,
- We obtained a long-term precipitation average as a replacement for the climatological standard (CS),
- We used satellite products declared as “operational products” only.

The mentioned CSs for individual river basins from rain gauges and satellite data are naturally not identical. The differences result from different precipitation measurement methodologies – direct point versus distance measurements of radiances and the application of complex algorithms to satellite data. The results of the comparison will be demonstrated in the Hron basin and are shown in the following slides.

Question/task: Can we find a correction that shifts the gray curve in Figure 6.9. (long-term mean of H05) to the blue curve (long-term mean of rain gauges)?

Objective: When finding a correction, it is possible to adjust the yellow curve in Figure 6.10. so that it is in the best possible match with the orange curve (accumulated rain 2020-H05 versus 2020-rain gauges). Corrections we derived from the difference between long-term average of ground-measured rain measurements and long-term average of satellite-based rain estimations.

6.3.3 Results and way forward

We performed similar tests of correction for 5 sub-regions in Slovakia, which differ in size and local climatological specifications. The best results we obtained for bigger regions (Nitra and Hron rivers sub catchments). Seasonal variations, which disturb yearly rain accumulations, can be also corrected, but the year must be split into shorter periods. This is what we plan to investigate in near future. Currently we can say that in general long-term precipitation averages of ground truth and satellite estimations are in good coincident and can help to correct shorter time-series of satellite data. Because for correct determination the beginning and the end the drought period according to the satellite H05 product it is only possible after their correction with rain gauges. The estimation of the start and end of the drought period using corrected satellite data we demonstrate on Figure 6.11. Calculating surplus and deficit of rain over certain area from daily accumulation is practically impossible from uncorrected data (orange line), but after correction (grey line) it is comparable to rain gauge ground measurements (yellow line). Corrected satellite data are the corresponding to correct cross-section of zero-level of rain accumulation status, which are indicating the beginning and duration of drought periods.

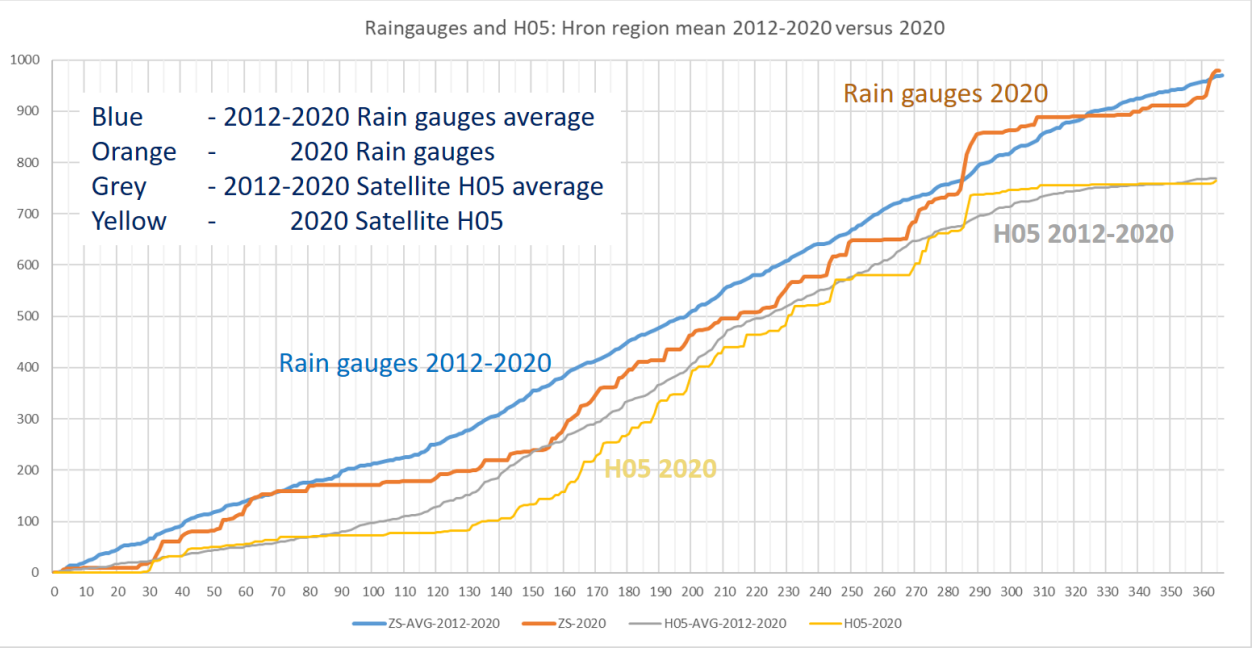

Figure 6.9. *Non-corrected satellite precipitation accumulations (yellow line) shows growing differences over the year 2020.*

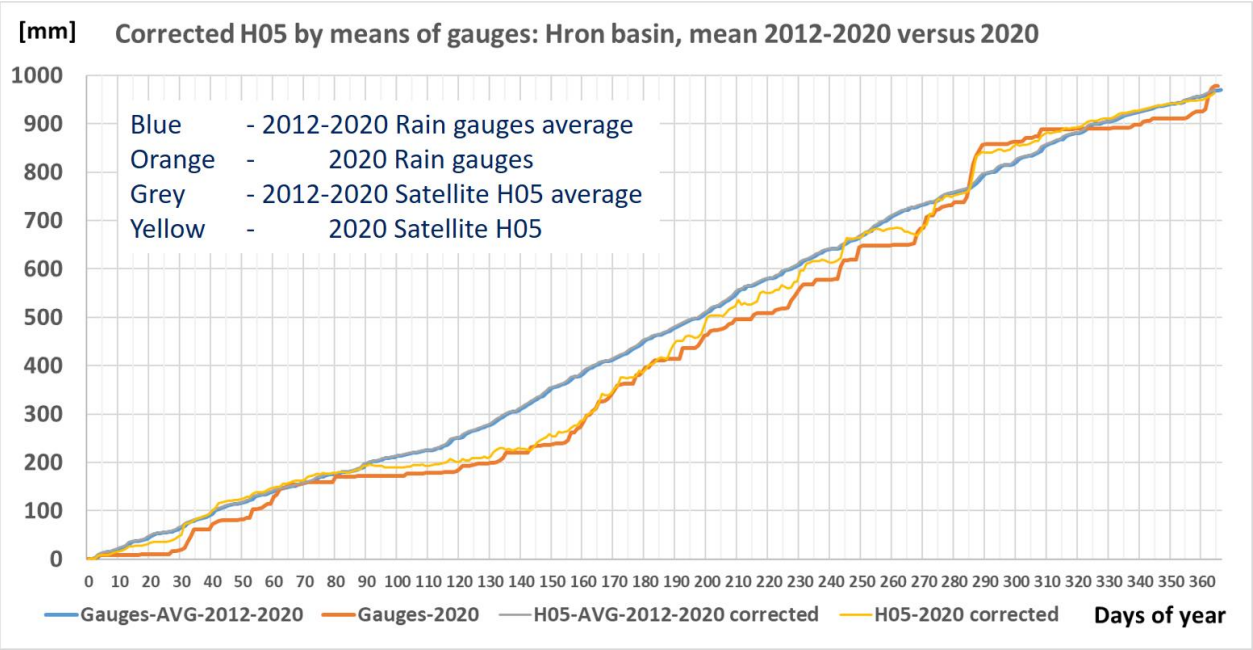

Figure 6.10. *Corrected satellite precipitation accumulations (yellow line) fit the ground-measured precipitation (orange line) over the year 2020.*

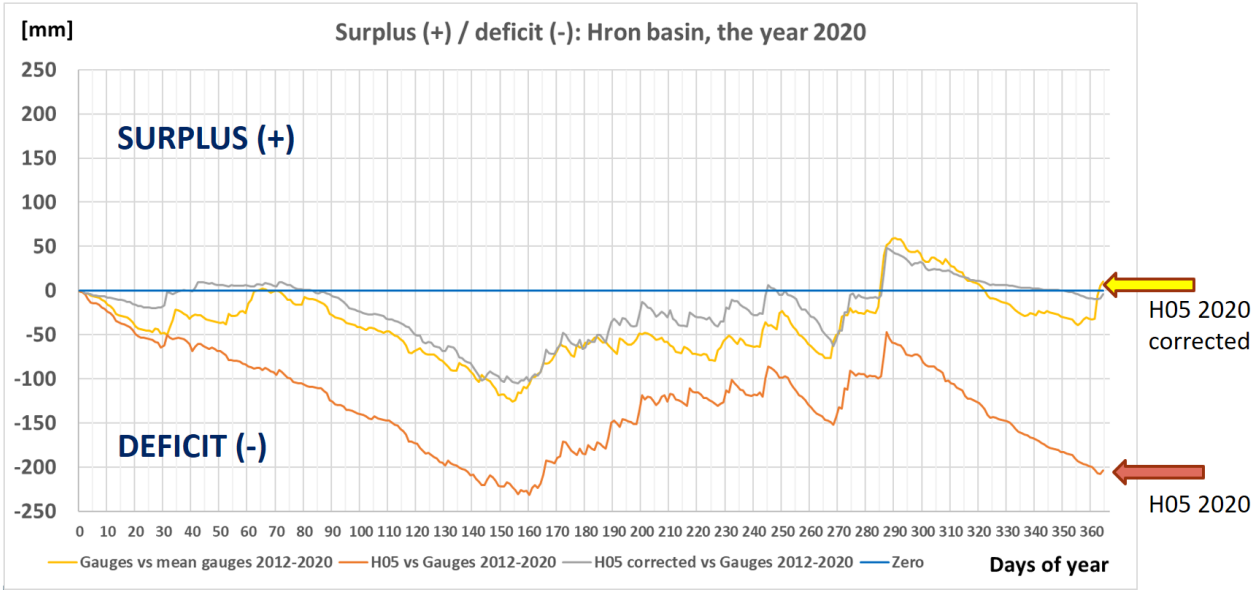

Figure 6.11. *Surplus and deficit of rain over certain area from daily accumulation is practically impossible from uncorrected data (orange line), but after correction (grey line). Corrected satellite data are the corresponding to correct cross-section of zero-level of rain accumulation.*

References:

[1] KAŇÁK, J. – OKON, Ľ. – PETRACCA, M. – PUCA, S.: H-SAF precipitation products quality assessment and meteorological applications. Lecture for EUMeTrain Precipitation Week Online Workshop 2020: http://eumetrain.org/events/precipitation_week_2020.html

[2] KAŇÁK, J.: Three years of dual MSG image data from operational, user and scientific perspective: possibilities and limitations. Presentation for EUMETSAT Convection Working Group meeting 6 – 8 April 2021. Online presentation.

[3] GEORGIEV Ch. – KAŇÁK, J. – KULISHEV, A.: MTG Lightning Imager Simulated Level 2 products: experience in Test Data processing and visualization. EUMETSAT Meteorological Satellite Conference. Special Session, 22 September 2021. Online.

[4] KAŇÁK, J.: Investigation of possibilities of dual satellite observations with new generation of geostationary satellites. EUMETSAT MTG-3T Workshop 2021, 8-11 March 2021. Online presentation.

[5] KAŇÁK, J. – OKON, Ľ. – MADARA, M. – JURAŠEK, M. – MÉRI, L. – HRUŠKOVÁ, K. – ZVOLENSKÝ, M.: Satelitné produkty na SHMÚ s potenciálom monitoringu zrážok a sucha. Meteorologický časopis/Meteorological Journal, Slovenský hydrometeorologický ústav, Bratislava. December 2021. Ročník 24 – čislo 2/Volume 24 – Number 2. Jeséniova 17, P.O.Box 15, 833 15 Bratislava 37, IČO 00 156 884, R. č. MK SR: 3268/09, ISSN 1335-339X. https://www.shmu.sk/File/ExtraFiles/MET_CASOPIS/1641565957_MC_2021-2.pdf

7. INSTITUTIONS INVOLVED IN SPACE RESEARCH

Members of the National Committee of COSPAR with e-mail addresses.

The website of NC is http://nccospar.saske.sk.

Astronomical Institute (AI)
Slovak Academy of Sciences (SAS)
Stará Lesná
059 60 Tatranská Lomnica
J. Rybák (choc@ta3.sk, NC member)

Faculty of Mathematics, Physics and Informatics (FMPI)
Comenius University
Mlynská dolina
842 15 Bratislava
J. Masarik (Jozef.Masarik@fmph.uniba.sk, NC member)

National Forest Centre
T.G. Masaryka 22
960 92 Zvolen
contact: T. Bucha (bucha@nlcsk.org)

Earth Science Institute (ESI)
Slovak Academy of Sciences (SAS)
Dúbravská cesta 9
840 05 Bratislava
M. Revallo (milos.revallo@savba.sk, Secretary of NC)

Institute of Animal Biochemistry and Genetics CBs
Slovak Academy of Sciences (SAS)
Dúbravská cesta 9
840 05 Bratislava

Biomedical Research Center of the Slovak Academy of Sciences (SAS)
Institute of Experimental Endocrinology (IEE)
Dúbravská cesta 9
845 05 Bratislava

Institute of Experimental Physics (IEP)
Slovak Academy of Sciences (SAS)
Watsonova 47
040 01 Košice
P. Bobík (bobik@saske.sk, NC member)

Institute of Geography (IG)
Slovak Academy of Sciences (SAS)
Štefánikova 49
814 73 Bratislava
J. Feranec (feranec@savba.sk, Vice-Chair of NC)

Institute of Materials and Machine Mechanics
Slovak Academy of Sciences (SAS)
Dúbravská cesta 9/6319
840 05 Bratislava
J. Lapin (juraj.lapin@savba.sk, NC member)

Institute of Measurement Science (IMS)
Slovak Academy of Sciences (SAS)
Dúbravská 9
842 19 Bratislava
contact: I. Frollo (frollo@savba.sk)

Institute of Normal and Pathological Physiology (INPP)
Slovak Academy of Sciences (SAS)
Sienkiewiczova 1
813 71 Bratislava
contact: F. Hlavačka (Frantisek.Hlavacka@savba.sk)

Slovak Central Observatory (SCO)
Komárňanská 137
947 01 Hurbanovo
I. Dorotovič (ivan.dorotovic@suh.sk, Chair of NC, Representative of Slovak NC to COSPAR)

Ministry of Environment of the Slovak Republic
Tajovského 28
975 90 Banská Bystrica
contact: J. Nováček (jozef.novacek@enviro.gov.sk)

Slovak Hydrometeorological Institute
Jeséniova 17
833 15 Bratislava
contact: J. Kaňák (jan.kanak@shmu.sk, NC member)

Slovak Organization for Space Activities (SOSA)
Ilkovičova 3 (FEI STU)
812 19 Bratislava
contact: M. Musilová (michaela.musilova@stuba.sk, NC member)

National Agricultural and Food Centre
Soil Science and Conservation Research Institute
Trenčianska 55
821 09 Bratislava
contact: M. Sviček (michal.svicek@nppc.sk)

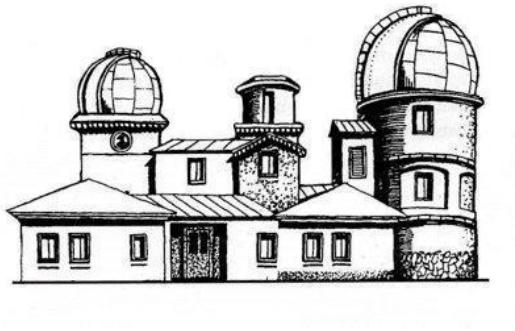

Space Research in Slovakia 2020 – 2021
National Committee of COSPAR in Slovak Republic
Slovak Academy of Sciences

Editors: Ivan Dorotovič and Ján Feranec

Published by the Slovak Central Observatory, Hurbanovo, April 2022
Responsible representative: Marián Vidovenec, Director General

ISBN: 978-80-89998-24-1